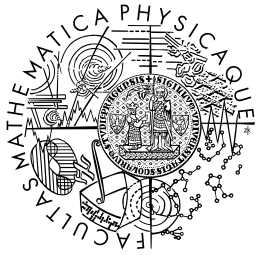

FACULTY
OF MATHEMATICS
AND PHYSICS
Charles University

DOCTORAL THESIS

Barbora Bezděková

Propagation and transfer of electromagnetic radiation in refractive and dispersive media in relativistic spacetimes

Institute of Theoretical Physics

Supervisor of the doctoral thesis:	prof. RNDr. Jiří Bičák, DrSc., dr. h. c.; doc. Mgr. David Heyrovský, Ph.D.
Study programme:	Theoretical Physics, Astronomy and Astrophysics
Study branch:	Physics

Prague 2024

I declare that I carried out this doctoral thesis independently, and only with the cited sources, literature and other professional sources. It has not been used to obtain another or the same degree.

I understand that my work relates to the rights and obligations under the Act No. 121/2000 Sb., the Copyright Act, as amended, in particular the fact that the Charles University has the right to conclude a license agreement on the use of this work as a school work pursuant to Section 60 subsection 1 of the Copyright Act.

In Prague 17 May 2024 .....

Author's signature

Do you know the laws of the heavens? Can you set their dominion over the earth?[1]
Jób 38,33

[1]Víš, jaké jsou řády nebes? Ty jsi je ustanovil, aby dozírala na zemi?

Let me first thank my family, especially my parents, for their support of my career, although it is not always easy for them to let me go. I am also thankful to many people who have continuously assured me about the relevance of my work, even in a much broader context than through academia.

I would like to thank the co-authors of papers which were used as a basis of this thesis. Namely, I am grateful to prof. Volker Perlick for his openness to my ideas and willingness to search for fundamental results, as general as possible. I thank doc. Vladimír Balek for his endless patience with answering my punctilious comments to his calculations. I appreciate the offer made by Oleg Tsupko to work together and to study problems that had not been considered before. I am glad that I got an opportunity to look at the same problem from a completely different point of view thanks to the approach applied by Christian Pfeifer.

I thank my consultant doc. Petr Hadrava for reading the Introduction and providing useful comments.

I acknowledge the reading of my thesis and acceptance of me as a student by doc. David Heyrovský. I am glad that I did not have to struggle too much with searching for a new supervisor.

However, my biggest gratitude belongs to the late prof. Jiří Bičák, my Supervisor, who led a substantial part of my work, who was always there to listen to me and support me, and who taught me many things, not necessarily only about physics. There is a lot I should have thanked him for earlier, but failed to do so. The only point I want to express here is my thankfulness for the opportunity he gave to a foolish girl, while others turned her down.

Dovolte mi v prvé řadě poděkovat mojí rodině, především mým rodičům, za jejich podporu v mojí práci, ačkoliv pro ně není vždycky snadné nechat mě jít. Jsem také velmi vděčná mnoha dalším lidem, kteří mě neustále přesvědčují o významu mojí práce, a to v mnohem větším rozsahu než pouze v akademickém kontextu.

Ráda bych poděkovala všem spoluautorům článků, které posloužily jako základ pro tuto práci. Jmenovitě děkuji prof. Volkeru Perlickovi za jeho otevřenost k mým nápadům a ochotu k nalezení co nejobecnějších možných výsledků. Děkuji doc. Vladimíru Balekovi za jeho neutuchající trpělivost při odpovídání na moje pendantské komentáře k jeho výpočtům. Vážím si nabídky Olega Tsupka ke společné práci o problémech, které se do té doby v literatuře neuvažovaly. Jsem ráda, že jsem dostala příležitost podívat se na stále stejnou problematiku z úplně jiné strany díky přístupu, který zvolil Christian Pfeifer.

Děkuji svému konzultantovi doc. Petru Hadravovi za přečtení úvodu mojí práce a za jeho věcné připomínky.

Vážím si přečtení mojí práce a přijetí mě za svého studenta doc. Davidem Heyrovským. Vybojovali jsme to oba a já jsem moc ráda, že jsem se hledáním nového vedoucího nemusela trápit příliš.

Moje největší poděkování nicméně patří prof. Jiřímu Bičákovi, mému Vedoucímu, který vedl podstatnou část mojí práce, byl tu vždy pro mě, aby mi nasouchal a podpořil mě, a naučil mě spoustu věcí, ne nutně jenom o fyzice. Je toho mnoho, za co jsem mu měla poděkovat, ale neudělala jsem to. To jediné, co chci na tomto místě vyjádřit, je moje vděčnost za to, že dal příležitost ztřeštěné holce, nad kterou všichni ostatní zlomili hůl.

Title: Propagation and transfer of electromagnetic radiation in refractive and dispersive media in relativistic spacetimes

Author: Barbora Bezděková

Institute: Institute of Theoretical Physics

Supervisor: prof. RNDr. Jiří Bičák, DrSc., dr. h. c.; doc. Mgr. David Heyrovský, Ph.D., Institute of Theoretical Physics

Abstract: Light rays propagating around a compact gravitating object in a dispersive and refractive medium have been frequently studied analytically during recent years. Their description in the geometrical optics approximation is very appropriately performed in the Hamiltonian formalism. Despite the apparent simplifications, systems typically analysed in the field are rather simple. The thesis presents results based on this formalism aimed to extend the current typical applications. First, a general axially symmetric object is considered and a generalized Carter constant for cold plasma is derived. Next, general expressions characterizing the basic properties of light propagation, such as the photon region or the deflection angle, are derived. Ray trajectories in the vicinity of objects described both by the Kerr and Hartle-Thorne metrics are discussed. A refractive and dispersive medium characterised either by radial or rotational motion is considered and the deflection angles around a spherically symmetric object are calculated. A perturbative approach to the moving medium is further presented in two distinctive ways. Light rays defined by their impact parameters are also studied in terms of the allowed regions around a Kerr black hole.

Keywords: relativistic spacetimes, geometrical optics, plasma, refractive and dispersive media

Contents

Introduction

A lot has been written about the effects of gravity on light rays. This is due to the fact that it represents both one of the basic predictions of general relativity and a powerful tool how to extend our knowledge about the Universe.

Although it became almost notoriously known that in vacuum the ray with impact parameter b propagating in the vicinity of a gravitating object with mass M is deflected by the angle

$$\alpha = \frac{4GM}{c^2 b},$$

where c denotes the speed of light and G is the gravitational constant, studies of light propagation in the vicinity of various astrophysical objects still reveal many unanticipated facts. Note that this formula is obtained in the linearized regime of the Schwarzschild metric, i.e., in the simplest case possible, but it is good enough to beat the Newtonian prediction.

During recent decades many new measurement techniques have been devised and enabled completely new ways how to observe the Universe. Along with better measurements also more detailed analytic descriptions of the systems are needed. This is also the case of light propagation.

In fact, light waves traveling across the Universe, no matter whether they span over distances near or far, are driven by several competing factors. It is not only the gravitational field of objects the light is passing by, interactions with a medium through which it propagates are also substantial. Then, in calculations presented in this thesis aiming to describe real astrophysical systems it has to be assumed that ultimate light trajectories are given by a composition of effects caused by gravitation, refraction, and dispersion.

In real astrophysical applications, the medium through which light propagates is typically plasma – the so-called fourth state of matter with many unintuitive properties. In comparison with the vacuum case the deviation of light rays is somewhat different than one would naively expect. This is shown in this thesis as well. It should be mentioned that plasma in the investigated systems can take many realistic types. When propagating around compact gravitating objects, plasma is usually in the form of a hot ($\sim 10^8$ K) accretion disc, while around less extreme objects it is believed that cold plasma occurs.

It has to be recalled that effects on light rays caused by the plasma presence are often negligible. However, there is a strong dependence on the wave frequency and the impact starts to be significant in the radio band. Moreover, if the wave propagates in a dense atmosphere, refraction cannot be disregarded either.

Analytic description of both the gravitational field and the medium of refractive and dispersive properties acting on the light trajectories is much easier when the Hamiltonian formalism is used. This approach was originally introduced by J. L. Synge in his book Relativity: The General Theory [Synge, 1960], where the basic Hamiltonian was derived in the geometrical optics approximation. Since then, it has been applied in many studies. These works are often focused on calculations of the deflection angle in a cold plasma around a specific gravitating object and on the description of other parameters related to light bending.

This work follows the previously obtained results and provides new applications of the formalism with a special scope on problems which are typically not

considered in the literature. It can thus bring new legitimate aspects in the field. However, it somewhat exceeds this approach since it also contains results related with the topic in a broader sense (especially the last chapter).

Throughout the text, I tend to call a gravitating object around which the light bends as "a black hole", while the formalism is more generic. It does not have to be necessarily the most extreme gravitating compact source, but any object of a sufficiently large gravitating field, e.g., a star. Except in the case of specific examples, the term "black hole" is used only as a formal descriptor in the text, keeping in mind that it is completely unimportant whether the object has a horizon or not.

The thesis consists of six chapters. In Chapter 1 the formalism applied in the rest of the thesis is introduced. Some recent findings related to the topic are also summarised there. Chapter 2 presents several general relations derived for an axially symmetric stationary spacetime surrounded by a medium of refractive and dispersive properties. In Chapter 3 the formulae obtained in Chapter 2 are applied to specific systems and their validity is demonstrated. Chapter 4 is focused on the calculation of the deflection angle around a spherically symmetric object in a moving medium defined in two specific situations. Chapter 5 presents a completely different approach to study the light rays in a cold plasma around an object described by the Kerr metric, in terms of allowed regions for rays. Technical details related to the construction of the accessible and forbidden regions are provided in Chapter 6.

The notation of indices throughout the thesis is $i, j = 1, 2, 3$; $\alpha, \beta = 0, 1, 2, 3$. Unless specified otherwise, it is assumed that $G = c = 1$ and the signature reads $(-, +, +, +)$.

1. The Hamiltonian Formalism for Ray Propagation in Relativistic Spacetimes

This chapter is dedicated to the theoretical description of the formalism which is applied in the majority of the thesis. Since there is a lot of detailed literature about this topic, it is not intended to provide a complete summary of all of them. Complementary to that, the Hamiltonian formalism adjusted for a description of light trajectories influenced simultaneously by the medium and gravitational field is set into a broader context of a more general theory and also main terms frequently applied in this context are thoroughly introduced. Moreover, the intention was also to discuss the relevant parameters from a different perspective than usual and to highlight some typically overlooked aspects of the theory. First, the geometrical optics approximation is introduced, as it is the main assumption under which the work is performed.

1.1 Geometrical Optics Limit

Relativistic geometrical optics seen as an approximation of the Maxwell equations formulated in the covariant form is typically adapted for a non-dispersive isotropic medium, but it can serve well also in dispersive and anisotropic media if certain conditions hold in the instantaneous local Lorentz rest frame of such medium. These conditions are [Bičák and Hadrava, 1975]

- typical wavelength λ_t of considered waves is short in comparison with the typical scales on which the properties of the medium (i.e., the refractive index, the velocity) vary,
- the waves are locally monochromatic, i.e., the variation scales of wave properties (the amplitude, wavelength, polarization) are large in comparison with λ_t,
- the characteristic curvature radius of the spacetime is much larger than λ_t,
- the medium varies negligibly over one typical wave period.

As it basically relies on a comparison of two characteristic scales in the system, geometrical optics is also sometimes called *two-scale method* and it corresponds to approximate solutions based on the WKB methods [see, Breuer and Ehlers, 1980, 1981].

This approximation allows one to study the motion of photon particles in terms of *rays*, interpreted as worldlines of the light signals. In this approach there are thus three basic assumptions [Anile and Pantano, 1979]

- an existence of rays, a congruence of curves, is guaranteed,
- conservation equations of field square amplitudes along the rays exist,

- a transport equation for the polarization vector of the field along the ray can be derived.

To describe the geometrical optics approximation more rigorously, following Breuer and Ehlers [1980, 1981], let me introduce a linear differential operator which is a function of some real parameter ε, namely

$$D(\varepsilon) = \sum_{j=0}^{p} \varepsilon^j \sum_{k=0}^{j} A_k^{j-k}. \tag{1.1}$$

Matrix A_k^r is of dimension $(m \times m)$ and its elements are forms of degree r in the partial differential operators $\partial/\partial x^a$, where $a = 1, ..., n$. Their coefficients are smooth, real, and functions of $x \in \mathbb{R}^n$. Because $D(\varepsilon)$ maps $\mathbb{R}^m$ functions on $\mathbb{R}^n$ onto functions of the same kind, relation

$$D(\varepsilon) \cdot U(\varepsilon) = 0 \tag{1.2}$$

represents a linear, homogeneous partial differential equation of order p which additionally depends on some parameter ε. This expression is solved via an m-vector U on $\mathbb{R}^n$. The analysed relations are complex in general, but they are effectively real in the given application.

An asymptotic form of solution U can be written as

$$U(x, \varepsilon) = \mathrm{e}^{(i/\varepsilon)S(x)} V(x, \varepsilon) \overset{\varepsilon \to 0}{\approx} \mathrm{e}^{(i/\varepsilon)S(x)} \sum_{n=0}^{\infty} \left(\frac{\varepsilon}{i}\right)^n V_n(x), \tag{1.3}$$

where S denotes the eikonal, which is generally a complex function, while amplitudes V, V_n are from $\mathbb{C}^m$, defined on $\mathbb{R}^n$. The next question is how to find S and V_n in the limit $\varepsilon \to 0$ (which effectively corresponds to the geometrical optics approximation). The gradient operator d, written as

$$d = (\partial/\partial x^1, ..., \partial/\partial x^n), \tag{1.4}$$

can be applied in the identity

$$\mathrm{e}^{-(i/\varepsilon)S(x)} d \mathrm{e}^{(i/\varepsilon)S(x)} = d + \left(\frac{i}{\varepsilon}\right) dS \tag{1.5}$$

which transforms equation $D(\mathrm{e}^{(i/\varepsilon)S} V) = 0$ into $L \cdot V = 0$, where

$$L(\varepsilon) = \mathrm{e}^{-(i/\varepsilon)S(x)} D(\varepsilon) \mathrm{e}^{(i/\varepsilon)S(x)}. \tag{1.6}$$

Note that $L(\varepsilon)$ contains also wave covector dS. Using the identity for d in the definition of $D(\varepsilon)$ leads to

$$L(\varepsilon) = \sum_{j=0}^{p} \varepsilon^j L_j, \tag{1.7}$$

where differential operator L_j is of order j. Moreover, the form of L_0 can be derived when $i\partial S/\partial x^a$ is plugged in $\sum_{l=0}^{p} A_0^l$ instead of $\partial/\partial x^a$. Then, operator L_0 is a complex $(m \times m)$ matrix even when $D(\varepsilon)$ contains real coefficients, functions of x^a and polynomially of $\partial S/\partial x^a$.

Applying the identity (1.5) in the relation $D(\varepsilon) \cdot U(\varepsilon) = 0$ with approximate solution for $\varepsilon \to 0$ returns

$$\sum_{j=0}^{p} \varepsilon^j L_j \cdot \sum_{n=0}^{\infty} \left(\frac{\varepsilon}{i}\right)^n V_n(x) \sim 0. \tag{1.8}$$

The zeroth-order solution reads

$$L_0 \cdot V_0 = 0, \tag{1.9}$$

which effectively requires

$$\det(L_0) = 0. \tag{1.10}$$

This is a polynomial of degree mp in $\partial S/\partial x^a$ with real coefficients depending on x^a, while L_0 can be complex. It is called the *dispersion relation* and it specifies a principal variety in $\mathbb{R}^{2n}$ of generally many branches, the cotangent bundle of $\mathbb{R}^n$. Moreover, since it is a partial differential equation of the first order of degree mp in S, it represents the eikonal equation as well.

Taking a real factor of the polynomial $\det(L_0)$ associated with one or more branches of the principal variety as $\mathcal{H}(x, dS)$, the eikonal equation can also be written as

$$\mathcal{H}(x, dS) = 0, \tag{1.11}$$

solutions of which are from $\mathbb{R}^{2n}$ and have to satisfy the canonical equations

$$\dot{x} = \frac{\partial \mathcal{H}}{\partial (dS)}, \quad \dot{dS} = -\frac{\partial \mathcal{H}}{\partial x}. \tag{1.12}$$

The projections of characteristic strips in $\mathbb{R}^{2n}$ where the solutions given by the canonical equations hold onto $\mathbb{R}^n$ are called *rays*. Infinitesimal parts on the ray where $S = const.$ are given by values of dS. Moreover, the dispersion relation and canonical equations lead to the ray velocity with respect to any observer to be the phase velocity, if $\dot{x} \neq 0$ on the ray.

In the lowest-order approximation, where $U^{(0)}$ can be found from

$$U^{(0)} = \mathrm{e}^{(i/\varepsilon)S} V_0, \tag{1.13}$$

the deviation between the exact solution U and the approximate one is given by

$$|U - U^{(0)}| = \mathcal{O}(\varepsilon). \tag{1.14}$$

It is hence seen that ε governs the accuracy of the obtained solutions and moreover, the described approach indeed represents an approximation method.

To provide a more physical context, in typical applications which are discussed below, it holds $p = 3$, $m = 3$, $n = 4$. In this case, the solution U can be interpreted as plane, monochromatic waves which, under the assumption $\varepsilon \ll 1$, can be expressed as

$$\hat{a}(x, \varepsilon) \overset{\varepsilon \to 0}{\approx} \mathrm{e}^{(i/\varepsilon)S(x)} \sum_{n=0}^{\infty} \left(\frac{\varepsilon}{i}\right)^n \hat{a}_n(x). \tag{1.15}$$

The asymptotes $\hat{a}_n(x)$ have to be defined such that the linear approximation is still legitimate, i.e., they have to be sufficiently small.

In the complementary view, there are two scales, say λ_t and L_t, corresponding to the scale of the typical wavelength and background variations, respectively. Then, parameter ε is defined as $\varepsilon = \lambda_t/L_t$. The limit $\varepsilon \to 0$ can thus be performed in two separate ways:

(i) $\lambda_t \to 0$,

(ii) $L_t \to \infty$.

In the case (i), the background scale L_t is fixed and all terms in the dispersion relation are of the same order in ε. Moreover, it is typically assumed that $L_t = 1$ and thus $\varepsilon = \lambda_t$. In contrast to that, case (ii) suggests to fix λ_t instead, which leads to different powers of ε in individual terms of the dispersion relation. Setting $\lambda_t = 1$ gives $\varepsilon = L_t^{-1}$ and the corresponding dispersion relation may be expressed in terms of dimensionless covariant directional derivative given by $L_t\nabla$.

Although both approaches (i) and (ii) are based on the same assumptions and are valid in the scope of the geometrical optics, the difference between them lies in the domain of validity. In the case (i), the wave itself is approximated in the given domain along with fixed inhomogeneity and the corresponding accuracy increases with decreasing wavelength. However, a range of original wavelengths is kept in the case (ii) and it is the spacetime which is approximated in order to improve the description and reach smaller inhomogeneity. The latter method is hence more suitable for describing the effect of matter on waves, e.g., dispersion, as it is already included in the lowest order approximation. This is not true for case (i). Choice of an appropriate approximation has to be set numerically from the realistic values of relevant parameters in given physical systems. Due to unknown error estimates for particular cases in corresponding systems it is not always possible to decide unambiguously which approach is more suitable. However, when dealing with the light propagation in a medium, main interest lies in studying the dispersion effects and case (ii) is hence typically chosen.

1.2 Rays and Waves in the Hamiltonian Theory

To provide a slightly different, but still useful, insight into the topic, rays and waves are studied from the perspective of the Hamiltonian formalism in this section. It is useful to look at the Hamiltonian presented in the following section from a more general perspective which is the main aim of the following paragraphs. There are two different ways how to introduce the Hamiltonian, and since these involve specific features in relativistic physics, it seems useful to introduce the formalism from this broader point of view. Both descriptions were originally presented by Synge [1960].

General theory

Initially, the existence of a spacetime metric $g_{\alpha\beta}$ is not assumed. In this more general description only a Hamiltonian surface Σ is required, situated in an 8-dimensional space with for now unspecified coordinates (x^α, y_α). A 7-dimensional subspace is described by an equation in the form

$$\mathcal{H}(x, y) = 0. \tag{1.16}$$

Note that it is Σ which is defined, not $\mathcal{H}(x,y)$. As the surface Σ can be associated with a large variety of functions $\mathcal{H}(x,y)$, there is some kind of freedom which of them will be chosen to represent Σ. Regardless of the exact choice, it still holds that a displacement $(\delta x^\alpha, \delta y_\alpha)$ is part of Σ iff

$$\frac{\partial \mathcal{H}}{\partial x^\alpha}\delta x^\alpha + \frac{\partial \mathcal{H}}{\partial y_\alpha}\delta y_\alpha = 0. \tag{1.17}$$

It leads to the conclusion that the expressions $\frac{\partial \mathcal{H}}{\partial x^\alpha}$, $\frac{\partial \mathcal{H}}{\partial y_\alpha}$ must reach definite values at given points of Σ.

Let me consider an integral along an arbitrary curve σ in Σ as

$$I = \int (y_\alpha dx^\alpha - l\mathcal{H}ds). \tag{1.18}$$

It is assumed that there is an additional varied curve on Σ given by running parameter s fixed at the same ending points as σ and $l(s)$ represents a Lagrange multiplier. It is a so-called side condition given by the second term in I. For such an integral the extremals are relevant, and hence its variation in the form $\delta I = 0$ is required. A standard variational calculation returns

$$\delta I = [y_\alpha \delta x^\alpha] + \int \left(\delta y_\alpha dx^\alpha - \delta x^\alpha dy_\alpha - \mathcal{H}\delta l ds - l\frac{\partial \mathcal{H}}{\partial x^\alpha}\delta x^\alpha ds - l\frac{\partial \mathcal{H}}{\partial y_\alpha}\delta y_\alpha ds \right). \tag{1.19}$$

From the condition $\delta I = 0$ for any δx^α, δy_α, and δl, with restriction $\delta x^\alpha = 0$ at both ends of σ, one gets

$$\frac{dx^\alpha}{ds} = l\frac{\partial \mathcal{H}}{\partial y_\alpha}, \quad \frac{dy_\alpha}{ds} = -l\frac{\partial \mathcal{H}}{\partial x^\alpha}, \quad \mathcal{H} = 0. \tag{1.20}$$

The Lagrange multiplier $l(s)$ remains ambiguous, but for a given $\mathcal{H}$ it is possible to choose s such that the extremal equations take the Hamiltonian, or canonical, form, i.e.,

$$\frac{dx^\alpha}{ds} = \frac{\partial \mathcal{H}}{\partial y_\alpha}, \quad \frac{dy_\alpha}{ds} = -\frac{\partial \mathcal{H}}{\partial x^\alpha}. \tag{1.21}$$

The constraint $\mathcal{H}(x,y) = 0$ is necessary to determine the extremal by values of (x^α, y_α) when $s = 0$.

A different interpretation of points x^α and y_α can be also applied, taking now as a starting object a 4-dimensional spacetime with coordinates x^α. The Hamiltonian surface Σ is then not characterized as a 7-dimensional subspace, but rather as a set of 3-dimensional spaces of y associated with each point of the spacetime. Additionally, there is again the equation $\mathcal{H}(x,y) = 0$ with x^α fixed, associated with the given space of y, which effectively forces to consider this space as 4-dimensional. Since coordinates in the space of y are y_α and to keep the description invariant under any transformations of x coordinates in the given spacetime, then $y_\alpha dx^\alpha$ has to be invariant. This necessarily leads to the fact that y_α transforms like a covariant vector and it justifies the introduction of y coordinates with subscript indices, contrary to x coordinates.

In this geometrical interpretation the curve to be extremalized is $x^\alpha = x^\alpha(s)$, associated with a vector field $y_\alpha = y_\alpha(s)$. Although it is the same geometrical

construct as before, its understanding is different, putting more emphasis on the points of spacetime given by sets of x. Hence, if there exists an extremal between two points $A(x')$ and $B(x)$, it can be written as

$$S(x', x) = S(A, B) = \int_A^B y_\alpha dx^\alpha. \tag{1.22}$$

Note that this integral is also known as the Hamilton principal or characteristic function. Variation of this function gives

$$\delta S = y_\alpha \delta x^\alpha - y'_\alpha \delta x'^\alpha. \tag{1.23}$$

Since differentials δx^α and $\delta x'^\alpha$ are again arbitrary, this returns two equations

$$\frac{\partial S}{\partial x^\alpha} = y_\alpha, \quad \frac{\partial S}{\partial x'^\alpha} = -y'_\alpha. \tag{1.24}$$

A corresponding substitution into $\mathcal{H}(x, y) = 0$ leads to the form

$$\mathcal{H}\left(x, \frac{\partial S}{\partial x}\right) = 0, \tag{1.25}$$

which is the well known Hamilton-Jacobi equation. Notice that an analogous equation holds also for (x', y').

A set of extremals in the given spacetime forms a (simply connected) domain $\mathbb{D}$ of an arbitrary dimension – typically two, three, or four. In $\mathbb{D}$ there is a vector field y_α given by the extremals. Moreover, circulation along an arbitrary closed curve defined as

$$\oint_C y_\alpha dx^\alpha \tag{1.26}$$

can be introduced in $\mathbb{D}$. If circulations along all closed curves in $\mathbb{D}$ are equal to zero, the extremals form a coherent system. Such extremals are called *rays*.

In a coherent system, where A is a fixed point in $\mathbb{D}$ and point B from $\mathbb{D}$ varies, the integral

$$I(A, B) = \int_A^B y_\alpha dx^\alpha \tag{1.27}$$

is independent of the integration path. With constant $\tilde{b}$, the relation

$$I(A, B) = \tilde{b} \tag{1.28}$$

restricts B to a subspace in $\mathbb{D}$ which can be denoted as a *wave*. A set of waves given by changing $\tilde{b}$ does not depend on A. In other words, integrals of the total differential equation $y_\alpha dx^\alpha = 0$ are waves. It is important to mention that this equation is integrable, as the only relevant system is coherent. Rays and waves are thus defined by a set of extremals *only* from coherent systems. Both the simplest and the most general examples of coherent systems are discussed below.

The simplest coherent system can be constructed from a set of extremals starting at fixed A and forming $\mathbb{D}$. Then, for the principal function $S(A, B)$ and for a closed curve C in $\mathbb{D}$ one gets

$$\oint_C y_\alpha dx^\alpha = \oint_C dS = 0. \tag{1.29}$$

Thus, it can be seen that the system is coherent. The waves associated with this system are given by

$$S(A, B) = const., \tag{1.30}$$

where B generally varies. Since $I(A, B)$ in the coherent system is only a function of B (point A is fixed), S can be called a *one-point* principal function and the wave equation can be written as

$$S(x) = const. \tag{1.31}$$

The most general coherent system is constructed when a subspace W of arbitrary dimension in the spacetime is considered and a vector field y_α on it is chosen, such that

$$\mathcal{H}(x', y') = 0, \quad y'_\alpha \delta x'^\alpha = \delta S'. \tag{1.32}$$

It is assumed that the function S on W is positioned at (x'^α, y'_α). The given relations are required for every displacement $\delta x'^\alpha$ on W.

Then, all possible extremals are led from points at W with initial values (x'^α, y'_α). In the domain covered by the given extremals an arbitrary point $B(x)$ can be associated with the function

$$S(x) = \int_A^B y_\alpha dx^\alpha + S'(A). \tag{1.33}$$

The integral is computed along the extremal. At point A the extremal aiming to B leaves subspace W. Variation of B yields

$$\delta S(x) = y_\alpha \delta x^\alpha - y'_\alpha \delta x'^\alpha + \delta S' = y_\alpha \delta x^\alpha, \tag{1.34}$$

where the differential condition given above for y_α was applied. The obtained relation corresponds to a differential in the domain of extremals, and the circulation hence vanishes. Thus, the extremals form a coherent system of rays, where waves are given by $S(x) = const.$ and $S(x)$ is the one-point principal function.

It was shown that the general Hamiltonian approach relies on an existence of a surface Σ along with the corresponding equation $\mathcal{H}(x, y) = 0$. Additionally, when a Riemannian spacetime with a metric $g_{\alpha\beta}$ is assumed, there are two kinds of fundamental curves – geodesics and the Hamiltonian extremals. However, no direct relation between the two can be determined. This can be performed in terms of geometrical optics, where the Hamiltonian extremals are interpreted as optical rays and geodesics do not play a significant role. More details about this aspect are provided below.

Riemannian spacetime

The theory for rays and waves can also be constructed in the Riemannian spacetime with the exclusive usage of tensor $g_{\alpha\beta}$. This can be derived when for the Hamiltonian surface Σ the equation $\mathcal{H}(x, y)$ is expressed in the form

$$\mathcal{H}(x, y) = \mathcal{H}_1(x, y)\mathcal{H}_2(x, y)\mathcal{H}_3(x, y) = 0, \tag{1.35}$$

where

$$\mathcal{H}_1(x, y) = g^{\alpha\beta} y_\alpha y_\beta, \quad \mathcal{H}_2(x, y) = g^{\alpha\beta} y_\alpha y_\beta + 1, \quad \mathcal{H}_3(x, y) = g^{\alpha\beta} y_\alpha y_\beta - 1. \tag{1.36}$$

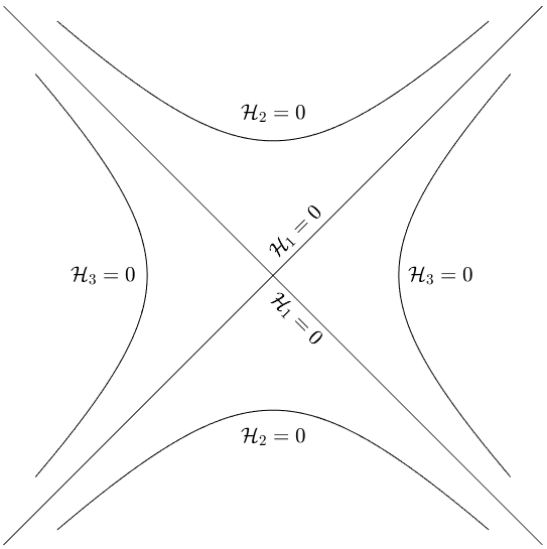

Figure 1.1: Hamiltonian surfaces in the Riemannian spacetime (adapted from Synge [1960]).

A subspace of three dimensions where x are fixed and $g^{\alpha\beta}$ are constants is thus split into sheets, where either $\mathcal{H}_1$, $\mathcal{H}_2$, or $\mathcal{H}_3$ equals zero (see Fig. 1.1). Vector y must reach its extremal value on one of these sheets.

From the Lagrange formulation given above the corresponding equations for extremals read

$$\frac{dx^\alpha}{ds} = lg^{\alpha\beta}y_\beta, \quad \frac{dy_\alpha}{ds} = -lg^{\beta\gamma}{}_{,\alpha}y_\beta y_\gamma, \tag{1.37}$$

and because l is a scalar function, changing the parameter s can lead to the equations

$$\frac{dx^\alpha}{ds} = g^{\alpha\beta}y_\beta, \quad \frac{dy_\alpha}{ds} = -\frac{1}{2}g^{\beta\gamma}{}_{,\alpha}y_\beta y_\gamma. \tag{1.38}$$

Due to that the following holds:

$$g_{\alpha\beta}\frac{dx^\alpha}{ds}\frac{dx^\beta}{ds} = g^{\alpha\beta}y_\alpha y_\beta \begin{cases} = 0 & \text{for } \mathcal{H}_1 = 0, \\ = -1 & \text{for } \mathcal{H}_2 = 0, \\ = 1 & \text{for } \mathcal{H}_3 = 0. \end{cases} \tag{1.39}$$

It can hence be seen that the Hamiltonian extremals *are* geodesics, namely null ones for $\mathcal{H}_1 = 0$, timelike for $\mathcal{H}_2 = 0$, and spacelike for $\mathcal{H}_3 = 0$. Note that this is generally not the case when a medium is present, which is discussed in detail in the following section.

From the obtained relations the Hamilton principal function can be written as

$$S(A,B) = \int_A^B y_\alpha dx^\alpha = \int_A^B g^{\alpha\beta}y_\alpha y_\beta ds = \iota\int_A^B ds, \tag{1.40}$$

where $\iota = \{0, -1, 1\}$ for null, timelike, and spacelike geodesics, respectively.

The first canonical equation presented above can be used to express

$$y_\alpha = g_{\alpha\beta}\frac{dx^\beta}{ds}. \tag{1.41}$$

From $y_\alpha \delta x^\alpha = 0$ one can show further for null rays that

$$y_\alpha \frac{dx^\alpha}{ds} = g_{\alpha\beta}\frac{dx^\alpha}{ds}\frac{dx^\beta}{ds} = 0 \tag{1.42}$$

which demonstrates that in this class rays both are orthogonal to waves and lie in them, while in the remaining cases rays are solely orthogonal to waves.

Similarly to the previous approach, a coherent system can be constructed, setting the subspace W and the corresponding function S'. In the case when W

is only one point of the spacetime, S' is constant, so that $\delta S'$ vanishes, and solely the condition $\mathcal{H}(x', y') = 0$ has to be solved. In order to satisfy that, vector y_α has to be taken such that its end point lies on either $\mathcal{H}_1 = 0$, $\mathcal{H}_2 = 0$, or $\mathcal{H}_3 = 0$. Hence, these extremals are either null, timelike, or spacelike geodesics, respectively.

Especially in the case of null geodesics one gets $y_\alpha dx^\alpha = 0$ along the rays, which returns $S(x) = S' = const.$ However, waves alone are defined by the condition $S(x) = const.$ and the null geodesics originating at point W thus form a single wave, a null surface corresponding to the null cone. For timelike and spacelike geodesics waves are obtained by considering constant elements along the rays, forming hyperboloids. These curves effectively correspond to those presented in Fig. 1.1.

When W is a timelike curve given by the relation $x'^\alpha = x'^\alpha(p)$, where parameter p remains constant along the ray, the function $S'(p)$ and the vector y'_α have to obey

$$\mathcal{H}(x', y') = 0, \quad y'_\alpha \frac{dx'^\alpha}{dp} = \frac{dS'}{dp}. \tag{1.43}$$

The latter expression corresponds to a flat 3-subspace which breaks the surfaces of $\mathcal{H}$ into sheets, where suitable y exists. When only intersections of the 3-subspace with $\mathcal{H}_1 = 0$ are assumed, one gets a system of null rays and waves. For the option $S' = const.$ there exists no y with extremal given from $\mathcal{H}_1 = 0$, such that the second equation given above holds. It is worth mentioning that this conclusion corresponds to the fact that any null vector is not orthogonal to a timelike vector.

1.3 Synge's Formalism

The pioneering work in analytical calculations of light propagation in a medium around a compact gravitating source was performed by Synge [1960]. Although this work might seem a little old fashioned, it experiences a huge revival, which is supported also by more than 1 000 citations within last 10 years.

To give a more physical essence to the relevant variables, the canonical quantities are further denoted as x^α and p_α. Meaning of the spacetime coordinates for the former set is maintained, while the latter one is discussed more in detail below.

To describe the ray propagation through a refractive, dispersive medium characterized by refractive index n and 4-velocity V^α, the corresponding Hamiltonian takes the form

$$\mathcal{H}(x^\alpha, p_\alpha) = \frac{1}{2}\left[g^{\beta\delta} p_\beta p_\delta - (n^2 - 1)(p_\gamma V^\gamma)^2\right]. \tag{1.44}$$

The spacetime metric $g^{\beta\delta}$ characterizes a gravitating object, while n and V^α define the medium which surrounds it. Furthermore, the dependence of photon frequency $\omega(x^\alpha)$ as measured by an observer at rest with respect to the medium at point x^α is derived from

$$\omega(x^\alpha) = -p_\gamma V^\gamma. \tag{1.45}$$

Both the wave phase speed and $\omega(x^\alpha)$ are assumed to be measured in the rest frame of the medium.

In accordance with classical optics, the medium can be described in terms of the refractive index and its other properties via the medium equation, which in this case takes the form

$$n^2 = 1 + \frac{p_\alpha p^\alpha}{(p_\beta V^\beta)^2}. \tag{1.46}$$

Note that this expression is based on the relation between the wave phase velocity v_{ph} for which $n = v_{ph}^{-1}$. Moreover, the definition (1.46) relies on the fact that the specific form of the refractive index is given by the medium description known from outside and in this sense it enters the medium equation as a known quantity. Note that (1.46) can be also applied to derive the Hamiltonian (1.44).

As discussed in previous sections, a substantial constraint laid on the Hamiltonian is $\mathcal{H}(x^\alpha, p_\alpha) = 0$. In a more physical context it corresponds to energy conservation in the system which restricts the initial values, while it is sustained by the canonical equations.

The covariant component p_α, regarded as fundamental in $\mathcal{H}(x^\alpha, p_\alpha)$, is the frequency 4-vector which is typically treated as a 4-momentum component of a photon. However, it should be mentioned that photons in plasma are usually considered as "phenomenological", meaning that the derivation of their 4-momentum from the quantum theory of the electromagnetic field in a medium is not unique. Moreover, unlike photons in vacuum, their 4-momentum in an arbitrary medium is neither tangent to the photon worldline, nor parallel-transported along it [Bičák and Hadrava, 1975]. However, the most intuitive way how to define p_α is such that the corresponding photons can be directly related with photons associated with wave packets in a given medium. In this sense rays discussed in terms of geometrical optics and throughout this thesis represent the "history" of photons. For more details about this description, see Bičák and Hadrava [1975].

Using the Hamiltonian (1.44), we get the equations of motion (canonical equations) in the form

$$\frac{dx^\alpha}{ds} = \frac{\partial \mathcal{H}}{\partial p_\alpha}, \quad \frac{dp_\alpha}{ds} = -\frac{\partial \mathcal{H}}{\partial x^\alpha}. \tag{1.47}$$

It is necessary to mention explicitly that although sometimes stated in the literature, s is generally *not* an affine parameter. This is due to the inhomogeneity caused by the plasma which prevents s from following the affine reparametrisation. However, if (1.47) imply geodesic, then s is an affine parameter in the equation of the geodesic. Additionally, note that dispersion effects here naturally enter the equations of motion because n is in this case a function of ω which is from (1.45) a known function of p_α.

As discussed above, a known definition of n determined from other parts of physics such as plasma theory can be applied to the formalism to study light propagation within such a medium. For instance, in the cold plasma approximation the Hamiltonian takes the form[1]

$$\mathcal{H}(x^\alpha, p_\alpha) = \frac{1}{2}\left[g^{\beta\delta} p_\beta p_\delta + \omega_p^2(x^\alpha)\right], \tag{1.48}$$

where ω_p is the electron plasma frequency, related to the electron number density N_e through

$$\omega_p^2(x^\alpha) = \frac{e^2 N_e(x^\alpha)}{\epsilon_0 m_e}. \tag{1.49}$$

[1]For details on deriving this relation from (1.44), see Chapter 4.

Parameters e, ϵ_0, and m_e represent the electron charge, vacuum permittivity, and the electron mass, respectively.

Note that the derivation of Hamiltonian (1.48) can be also performed in full generality, based on Maxwell's equations, the equation of motion for the electron fluid, electron charge conservation equation and normalisation of 4-velocity. This calculation can be found in Perlick [2000]. Notice that this relation can be used only for light propagation in a non-magnetized plasma.

A more general approach was performed by Breuer and Ehlers [1980, 1981], where the case of a magnetized cold plasma was studied. The corresponding Hamiltonian can then be expressed as

$$\begin{aligned}\mathcal{H}(x^\alpha, p_\alpha) = \omega_0^2(\omega_0^2 - \omega_p^2)(\omega_0^2 - \vec{k}^2 - \omega_p^2)^2 \\ - (\omega_0^2 - \vec{k}^2)[\omega_0^2\vec{\omega}_L^2(\omega_0^2 - \vec{k}^2 - \omega_p^2) + \omega_p^2(\vec{\omega}_L \cdot \vec{k})^2],\end{aligned} \tag{1.50}$$

where k^i is the wave 3-vector (i.e., $p^2 = \vec{k}^2 - \omega_0^2$), and ω_L^i is the Larmor angular velocity defined as $\vec{\omega}_L = (-e/m_e)\vec{B}$.

If $\vec{B} = 0$, one gets

$$\mathcal{H}(x^\alpha, p_\alpha) \sim -\omega_0^2 + \vec{k}^2 + \omega_p^2 = p^2 + \omega_p^2 = g^{\beta\delta}p_\beta p_\delta + \omega_p^2,$$

and this expression corresponds to (1.48) defined without a magnetic field.

Note that although there is a significant importance of a description which includes the magnetic field, besides Breuer and Ehlers [1980, 1981] only Broderick and Blandford [2003] seriously studied such systems. This tends to be a serious issue when speaking about applications to real physical systems. For this reason, one of the future research directions in this field should definitely be focused on this topic.

1.4 Applications of Synge's Formalism

As mentioned in the previous section, many works based on Synge's approach have been published during the last several years. At this stage it might be useful to provide a brief overview of the main findings presented in these studies. Thus, it can easily be seen how results presented in this thesis contribute to the current state of the field.

One of the earliest studies developing the formalism of Synge was probably the one by Bičák and Hadrava [1975], where more astrophysical context was provided. Furthermore, an extensive description of this subject, in a broader range, was provided in a monograph by Perlick [2000]. Among others, the deflection angle around a Kerr black hole in a cold plasma was given there.

Recent attention to the Synge approach probably started with papers by Bisnovatyi-Kogan and Tsupko [2009, 2010], where light deflection was studied in the weak-field approximation and a cold plasma was assumed. The Schwarzschild metric was used to define the gravitating object and plasma was considered both homogeneous and non-homogeneous. The main conclusion of these studies was that a plasma effect on light deflection occurs even in a homogeneous medium. The deflection angle around a slowly rotating object in a cold plasma in the weak-field limit was studied by Morozova et al. [2013]. In the corresponding systems,

Bisnovatyi-Kogan and Tsupko [2010] and Morozova et al. [2013] also described possible effects on gravitational lensing in terms of image magnification.

A strong gravitational field of a Schwarzschild black hole along with a homogeneous cold plasma were assumed for calculating the deflection angle by Tsupko and Bisnovatyi-Kogan [2013]. Relativistic images were also studied within this work, which includes derivation of their angular positions and magnifications.

Ray tracing of light in the vicinity of a Schwarzschild black hole in plasma was investigated in a series of papers by Rogers [2015, 2017a,b]. Several profiles of plasma density were assumed and its relevance in comparison to the gravitational effects was analysed. Moreover, the dependence of photon trajectories on frequency was discussed in detail.

On the contrary to the spherically symmetric spacetime, practically the only axially symmetric spacetime almost exclusively studied is the Kerr case. Light propagation in the Kerr metric in the presence of a cold plasma was studied in detail by Perlick and Tsupko [2017, 2024]. The main result of the work by Perlick and Tsupko [2017] is a general formula for the plasma electron frequency which satisfies the separability conditions for the Hamilton-Jacobi equation that are necessary to completely solve the problem. Furthermore, the black hole shadow, the deflection angle, and different types of orbits were discussed in this study. The continuation of the research on this topic in Perlick and Tsupko [2024] is devoted to more specific types of photon orbits, resulting in additional effects not observed in vacuum. The deflection angle in the weak deflection limit up to the second order is also presented by the authors.

Application of the Synge Hamiltonian to the Robertson-Walker spacetime was performed in Schulze-Koops et al. [2017]. The findings show that possible cosmological redshift and distance measurement fluctuations due to plasma are small, but they lead to measurable values in the radio frequency band. Note that light propagation in a plasma in the Friedmann universe was studied already by Bičák and Hadrava [1975].

The deflection angle for a stationary spacetime in a cold plasma in the weak-field limit was calculated by Crisnejo et al. [2019]. Contrary to the studies presented so far, a technique based on the Gauss-Bonnet theorem was applied in this work. The orbit equation in the equatorial plane was presented and terms of the deflection angle up to the third order in the weak-field approximation were obtained.

Dispersion effects caused by the presence of a plasma on the light rays around a Kerr black hole were analysed by Kimpson et al. [2019a]. Implications for observations of pulsar rays bent near the galactic center were discussed. Kimpson et al. [2019b] followed this setting and investigated possible ways how to test general relativity in the given framework. This can be obtained in terms of the time-frequency signal which can be directly measured. The study suggests which factors are relevant in order to calculate the time-frequency dependence in order to compare them with observations.

Light propagation around a Kerr black hole surrounded by a cold plasma of various profiles was described by Sárený and Balek [2019]. Moreover, star distribution functions defined as the angular dependence of the density of background star images were introduced. Examples for vacuum and a few plasma distributions were plotted and discussed.

A detailed analysis of the light-deflection angle around a spherically symmetric spacetime surrounded by a general dispersive medium characterised by its refractive index was given by Tsupko [2021]. The derived general formula was applied to particular media and corrections to the vacuum case were discussed. Note that in these calculations the medium was assumed to be static.

Following the preceding discussions, some recent works considered more specific systems. Matsuno [2021] calculated the deflection angle around a gravitating object characterized by the Kaluza-Klein metric immersed in a cold plasma. The ray behaviour around a neutron star given by a spherically symmetric metric in a cold plasma was analysed by Briozzo and Gallo [2023].

Another feature frequently studied in this field is the so-called black hole shadow. The shadow occurs due to the presence of an event horizon which is magnified by the gravitating effects of the black hole. As a result, the shadow is much larger than the event horizon itself. The form of a shadow of an arbitrary spherically symmetric black hole embedded in a cold plasma was calculated in Perlick et al. [2015]. Note that a useful general form of a spherically symmetric gravitating object which was further applied in other studies was probably originally introduced in this work.

Some recent works calculating the black hole shadow in a plasma are, e.g., Badía and Eiroa [2023], Briozzo et al. [2023], Zhang et al. [2023], Kobialko et al. [2024]. A detailed review of analytical results related to the black hole shadows was presented by Perlick and Tsupko [2022].

Several works focused on gravitational lensing problems also assume the presence of a plasma. Er and Mao [2014] considered two astrophysically motivated forms of the lensing objects and studied gravitational lensing in the presence of a cold plasma. They assumed that the lens can be either a spiral or elliptical galaxy, defined the respective plasma density in such a galaxy and analyzed various parameters of strong lensing, such as the magnification, time delay, image positions, etc. This study argued that the effect of plasma depends on the galaxy redshift, as the ionized gas gets denser. Moreover, the presence of a plasma causes a change between the image positions in different frequency bands which can be applied to determine the plasma density of the lens galaxy. Er and Mao [2022] analyzed effects of a plasma in the lensing galaxy on strongly lensed fast radio bursts. They found the plasma effect to be apparent especially for low radio frequencies and proposed that the detection of lensed fast radio bursts could constrain both the mass and the plasma distributions in the lens. The effects of plasma on microlensing were investigated by Tsupko and Bisnovatyi-Kogan [2020] and the time delay due to plasma was discussed by Bisnovatyi-Kogan and Tsupko [2023]. Sun et al. [2023] considered a system composed of a star, its stellar wind, and a planet and analysed additional lensing effects due to the plasma.

A majority of studies based on the Synge formalism hence assume as a medium surrounding the gravitating object a cold non-magnetized plasma. It is the simplest plasma approximation with unexpected properties and astrophysical applications (see Section 4.1). However, in real physical systems it is not the only one. Furthermore, the gravitating object is usually assumed to be either spherically symmetric (Schwarzschild) or an axially symmetric Kerr black holes. For investigations of the validity of the description by the Kerr metric, a more general approach should be taken. This is typically not the case.

2. Light Propagation in a General Axially Symmetric Stationary Spacetime

In most of the studies based on Synge's approach [e.g., Rogers, 2017a, Tsupko, 2021, Briozzo and Gallo, 2023], spherically symmetric spacetimes were considered. In some other works [e.g., Morozova et al., 2013, Liu et al., 2017, Perlick and Tsupko, 2017], the Kerr metric was considered. However, none of them assumed a general axially symmetric spacetime, similarly as it was performed for a general spherically symmetric spacetime in Perlick et al. [2015]. Before analyzing the light deflection, we study a system with an axially symmetric object surrounded by a cold plasma and find general conditions for both the spacetime and the plasma which guarantee that the equations describing the light propagation are integrable. Results presented in this and the following chapter were published in Bezděková et al. [2022], Bezděková and Bičák [2023].

2.1 The Generalized Carter Constant

Due to conventional notation, let me assume that an axially symmetric stationary metric is defined in coordinates $(t, \varphi, r, \vartheta)$, and the metric coefficients are only functions of r and ϑ. They are independent of t and φ, as we assume the existence of two Killing vectors which are related to these coordinates. In order to study the deflection angle, it is necessary to derive an integrable system which requires the existence of a (generalized) Carter constant [Carter, 1968]. For this reason, one has to find conditions under which the existence of the Carter constant is guaranteed. As it is demonstrated further, this is closely related to the separability of the Hamilton-Jacobi equation for light rays in a plasma in a given spacetime.

The separability of the Hamilton-Jacobi equation is an entirely local property and for this reason, the specific physical interpretation of the coordinates is quite irrelevant. This means that whether t runs over all $\mathbb{R}$ and φ runs between 0 and 2π is in fact not important. From this point of view, the assumed coordinate system is not necessarily restricted, but coordinates are required to guarantee an existence of two commuting Killing vector fields that span timelike surfaces. This coordinate system is further denoted as $(t, \varphi, r, \vartheta)$ (due to its natural and usual understanding), but the coordinates can be basically arbitrary. Let me further mention that standard spherical coordinates – these typically denoted as $(t, \varphi, r, \vartheta)$ – can be inappropriate for finding the Carter constant, while defining the desired symmetries in another system can be much more convenient. This fact is discussed further in Section 3.1.

The separation of the Hamilton-Jacobi equation is possible if and only if the plasma density is independent of t and φ, or more generally, of the coordinates which do not occur in the metric coefficients. Moreover, since the possible separation depends on the chosen coordinate system, if the Hamilton-Jacobi equation separates, then it separates in a coordinate system in which the metric coefficients

g_{tr}, $g_{t\vartheta}$, $g_{\varphi r}$, $g_{\varphi\vartheta}$, and $g_{r\vartheta}$ vanish. Hence, the axially symmetric stationary metric can be written in a general form as

$$ds^2 = -A(r,\vartheta)dt^2 + B(r,\vartheta)dr^2 + 2P(r,\vartheta)dtd\varphi + D(r,\vartheta)d\vartheta^2 + C(r,\vartheta)d\varphi^2\,. \quad (2.1)$$

As outlined above, there are two Killing vector fields $\partial/\partial t$ and $\partial/\partial\varphi$ which span timelike surfaces. Meeting this condition requires $AC + P^2 > 0$, $B > 0$, and $D > 0$.

In addition to the dependence on coordinates, the metric coefficients can be in principle functions of arbitrary many parameters. As an example, in the Kerr metric there are two additional parameters – the mass M and the spin a. However, from the perspective of the equations of motion these are solely parameters (constants), and it is hence not necessary to state them explicitly in order to find the complete solution.

Non-vanishing terms of the inverse metric to (2.1) are

$$\begin{aligned} g^{rr} &= \frac{1}{B(r,\vartheta)}, \quad g^{\vartheta\vartheta} = \frac{1}{D(r,\vartheta)}, \quad g^{\varphi\varphi} = \frac{A(r,\vartheta)}{A(r,\vartheta)C(r,\vartheta) + P^2(r,\vartheta)}, \\ g^{tt} &= \frac{-C(r,\vartheta)}{A(r,\vartheta)C(r,\vartheta) + P^2(r,\vartheta)}, \quad g^{t\varphi} = \frac{P(r,\vartheta)}{A(r,\vartheta)C(r,\vartheta) + P^2(r,\vartheta)}. \end{aligned} \quad (2.2)$$

Since the separation can be performed only if the plasma frequency $\omega_p^2(x^\alpha)$ is solely a function of coordinates r and ϑ, let me set $\omega_p^2(r,\vartheta)$. Hence, when a spacetime is defined by the metric (2.1), the Hamiltonian (1.48) can be written as

$$\begin{aligned} \mathcal{H}(x^\alpha, p_\alpha) = \frac{1}{2}\Bigg[&\frac{p_r^2}{B(r,\vartheta)} + \frac{p_\vartheta^2}{D(r,\vartheta)} + \frac{p_\varphi^2 A(r,\vartheta)}{A(r,\vartheta)C(r,\vartheta) + P^2(r,\vartheta)} \\ &- \frac{p_t^2 C(r,\vartheta)}{A(r,\vartheta)C(r,\vartheta) + P^2(r,\vartheta)} + \frac{2p_t p_\varphi P(r,\vartheta)}{A(r,\vartheta)C(r,\vartheta) + P^2(r,\vartheta)} + \omega_p^2(r,\vartheta)\Bigg]. \end{aligned} \quad (2.3)$$

One can directly infer that p_t and p_φ are constants of motion because it is clearly seen that $\frac{\partial\mathcal{H}}{\partial t} = 0$ and $\frac{\partial\mathcal{H}}{\partial\varphi} = 0$. In an asymptotically flat spacetime, the constant $-p_t$ has a direct physical meaning for a ray reaching infinity, i.e., the frequency measured by a stationary observer at infinity [see, e.g., Perlick and Tsupko, 2017]. For emphasizing direct connection to its physical meaning, let me denote $-p_t$ as ω_0. Two more constants of motion in the system are still needed. One of them is the Hamiltonian itself, since $\mathcal{H}(x^\alpha, p_\alpha) = 0$. In order to derive the Hamilton-Jacobi equation, the Hamiltonian is typically expressed as a function of x^α and $\frac{\partial S}{\partial x^\alpha}$ rather than of x^α and p_α. For this reason, let me introduce the action S which can be written in a separated form as

$$S(t,\varphi,r,\vartheta) = -\omega_0 t + p_\varphi\varphi + S_r(r) + S_\vartheta(\vartheta). \quad (2.4)$$

The Hamilton-Jacobi equation is then derived from

$$0 = \mathcal{H}\Big(x^\alpha, \frac{\partial S}{\partial x^\beta}\Big), \quad (2.5)$$

which leads to the form

$$\begin{aligned} 0 = &\frac{1}{B(r,\vartheta)}\left(\frac{dS_r(r)}{dr}\right)^2 + \frac{1}{D(r,\vartheta)}\left(\frac{dS_\vartheta(\vartheta)}{d\vartheta}\right)^2 + \frac{p_\varphi^2 A(r,\vartheta)}{A(r,\vartheta)C(r,\vartheta) + P^2(r,\vartheta)} \\ &- \frac{\omega_0^2 C(r,\vartheta)}{A(r,\vartheta)C(r,\vartheta) + P^2(r,\vartheta)} - \frac{2\omega_0 p_\varphi P(r,\vartheta)}{A(r,\vartheta)C(r,\vartheta) + P^2(r,\vartheta)} + \omega_p^2(r,\vartheta). \end{aligned} \quad (2.6)$$

Note that this condition holds for arbitrary p_φ and ω_0. Thus, to find the separability conditions the only freedom is to multiply the equation by an arbitrary non-zero function $F(r,\vartheta)$, i.e.,

$$0 = \frac{F(r,\vartheta)}{B(r,\vartheta)}\left(\frac{dS_r(r)}{dr}\right)^2 + \frac{F(r,\vartheta)}{D(r,\vartheta)}\left(\frac{dS_\vartheta(\vartheta)}{d\vartheta}\right)^2 + F(r,\vartheta)\omega_p^2(r,\vartheta) \tag{2.7}$$
$$+ \frac{F(r,\vartheta)}{A(r,\vartheta)C(r,\vartheta)+P^2(r,\vartheta)}\left[p_\varphi^2 A(r,\vartheta) - \omega_0^2 C(r,\vartheta) - 2\omega_0 p_\varphi P(r,\vartheta)\right].$$

Equation (2.7) is regarded as separable if and only if its individual terms are either a function of r alone or a function of ϑ alone for arbitrary p_φ and ω_0. Terms independent of p_φ and ω_0 will be discussed first. The functions $dS_r(r)/dr$ and $dS_\vartheta(\vartheta)/d\vartheta$ are generally non-zero for light rays; separability can be achieved if

$$\frac{F(r,\vartheta)}{B(r,\vartheta)} \equiv \mathcal{F}(r) \quad \text{and} \quad \frac{F(r,\vartheta)}{D(r,\vartheta)} \equiv \mathcal{G}(\vartheta), \tag{2.8}$$

which gives

$$\frac{B(r,\vartheta)}{D(r,\vartheta)} = \frac{\mathcal{G}(\vartheta)}{\mathcal{F}(r)}. \tag{2.9}$$

This is the first necessary condition for separability which has been found. If the quotient of functions $B(r,\vartheta)$ and $D(r,\vartheta)$ is not in the form given by (2.9), one knows that separability cannot be achieved. Moreover, this is true for light rays moving both in vacuum and in a medium of any plasma density. Additionally, if condition (2.9) holds, the function $F(r,\vartheta)$ can be found either from the first or equivalently from the second equation in (2.8). The function $F(r,\vartheta)$ can be defined unambiguously up to a non-zero constant factor which can exist because $\mathcal{G}(\vartheta)$ and $\mathcal{F}(r)$ are unique up to a common non-zero constant factor. Furthermore, the function $F(r,\vartheta)$ is defined solely by the metric coefficients, i.e., it is independent of the plasma. From the requirement given above that $B(r,\vartheta)$ and $D(r,\vartheta)$ are positive, it is also obvious that $\mathcal{F}(r)$ and $\mathcal{G}(\vartheta)$ have to be both positive and $F(r,\vartheta)$ is hence positive, too and it is further secured that it has no zeros.

Applying conditions (2.8) in the Hamilton-Jacobi equation (2.6) returns

$$0 = \mathcal{F}(r)\left(\frac{dS_r(r)}{dr}\right)^2 + \mathcal{G}(\vartheta)\left(\frac{dS_\vartheta(\vartheta)}{d\vartheta}\right)^2 + F(r,\vartheta)\omega_p^2(r,\vartheta) \tag{2.10}$$
$$+ \frac{F(r,\vartheta)}{A(r,\vartheta)C(r,\vartheta)+P^2(r,\vartheta)}\left(p_\varphi^2 A(r,\vartheta) - \omega_0^2 C(r,\vartheta) - 2\omega_0 p_\varphi P(r,\vartheta)\right).$$

One more term independent of p_φ and ω_0 is the term with plasma frequency $\omega_p^2(r,\vartheta)$. In order to satisfy its separable character, it has to be the general form

$$\omega_p^2(r,\vartheta) = \frac{f_r(r) + f_\vartheta(\vartheta)}{F(r,\vartheta)}, \tag{2.11}$$

where $f_r(r)$ and $f_\vartheta(\vartheta)$ are arbitrary functions of r and ϑ, respectively. In this condition, it is obvious that the function $F(r,\vartheta)$ introduced in the previous step has to be non-zero, and it is determined uniquely, up to a constant factor, by the metric alone without any relation to the plasma frequency itself.

Let us now look at the terms from (2.10) proportional to p_φ^2, ω_0^2, and $p_\varphi\omega_0$, respectively. There has to be an additional condition set on $A(r,\vartheta)$, $C(r,\vartheta)$, and $P(r,\vartheta)$ in order to satisfy the separability which reads

$$\frac{F(r,\vartheta)}{A(r,\vartheta)C(r,\vartheta)+P^2(r,\vartheta)}X(r,\vartheta)=X_r(r)+X_\vartheta(\vartheta), \tag{2.12}$$

where X stands for A, C, or P.

If all separability conditions discussed above are satisfied, (2.7) can be rewritten as

$$\begin{aligned}&\mathcal{F}(r)\left(\frac{dS_r(r)}{dr}\right)^2+f_r(r)+p_\varphi^2A_r(r)-\omega_0^2C_r(r)-2\omega_0p_\varphi P_r(r)= \\ &-\mathcal{G}(\vartheta)\left(\frac{dS_\vartheta(\vartheta)}{d\vartheta}\right)^2-f_\vartheta(\vartheta)-p_\varphi^2A_\vartheta(\vartheta)+\omega_0^2C_\vartheta(\vartheta)+2\omega_0p_\varphi P_\vartheta(\vartheta)\equiv-\mathcal{K}.\end{aligned} \tag{2.13}$$

The Hamilton-Jacobi equation expressed in the form given above allows one to introduce the parameter $\mathcal{K}$ independent of both r and ϑ, i.e., a new constant of motion. Hence, the parameter $\mathcal{K}$ will be called the (generalized) Carter constant below.

Let me further make two crucial observations. It is important to realize that if the Hamilton-Jacobi equation for light rays does not separate in vacuum for the given spacetime, it does not separate for light rays in plasma either, whatever the plasma density is, i.e., plasma itself cannot cure possible non-separability stemming from the spacetime definition. On the other hand, if the Hamilton-Jacobi equation for light rays separates in vacuum, there exists a range of plasma densities, defined by condition (2.11), where $F(r,\vartheta)$ is given by the metric, but functions $f_r(r)$ and $f_\vartheta(\vartheta)$ are arbitrary, defined to separate for light rays in the plasma as well.

The Carter constant found in (2.13) is associated with a conformal Killing tensor field both in vacuum and in plasma. To show this, recall that definition (2.13) sets the Carter constant only on the hypersurface $\mathcal{H}=0$. The Carter constant can be defined over the entire cotangent bundle (x^α,p_α), but one has to introduce

$$\mathcal{K}(x^\alpha,p_\beta)=K^{\mu\nu}(x^\alpha)p_\mu p_\nu-\frac{1}{2}f_r(r)+\frac{1}{2}f_\vartheta(\vartheta) \tag{2.14}$$

where

$$\begin{aligned}K^{\mu\nu}(x^\alpha)p_\mu p_\nu=&\frac{1}{2}\mathcal{G}(\vartheta)p_\vartheta^2-\frac{1}{2}\mathcal{F}(r)p_r^2+\frac{1}{2}\Big(A_\vartheta(\vartheta)-A_r(r)\Big)p_\varphi^2 \\ &-\frac{1}{2}\Big(C_\vartheta(\vartheta)-C_r(r)\Big)p_t^2+\Big(P_\vartheta(\vartheta)-P_r(r)\Big)p_\varphi p_t.\end{aligned} \tag{2.15}$$

A symmetric second-rank tensor field $K^{\mu\nu}(x^\alpha)$ depends on the metric coefficients, but not on the plasma density. When performing a straightforward calculation, one finds out that the function $\mathcal{K}(x^\alpha,p_\beta)$ can be expressed in two equivalent forms as

$$\mathcal{K}(x^\alpha,p_\beta)=-\mathcal{F}(r)p_r^2-A_r(r)p_\varphi^2+C_r(r)p_t^2-2P_r(r)p_\varphi p_t-f_r(r)+F(r,\vartheta)\mathcal{H}(x^\alpha,p_\beta)\,, \tag{2.16}$$

$$\mathcal{K}(x^\alpha, p_\beta) = \mathcal{G}(\vartheta)p_\vartheta^2 + A_\vartheta(\vartheta)p_\varphi^2 - C_\vartheta(\vartheta)p_t^2 + 2P_\vartheta(\vartheta)p_\varphi p_t + f_\vartheta(\vartheta) - F(r,\vartheta)\mathcal{H}(x^\alpha, p_\beta). \tag{2.17}$$

When assuming that $\mathcal{H} = 0$, i.e., under a specific choice of the hypersurface, expressions (2.16) and (2.17) lead to the function $\mathcal{K}$ defined by (2.14) of exactly the same form as the Carter constant introduced in (2.13).

Moreover, the Poisson bracket $\{\mathcal{K}, \mathcal{H}\}$ vanishes on the hypersurface $\mathcal{H} = 0$ because $\mathcal{K}$ is a constant of motion. This is true for arbitrary definitions of $f_r(r)$ and $f_\vartheta(\vartheta)$. Choice $f_r(r) = 0$ and $f_\vartheta(\vartheta) = 0$ returns the Poisson bracket in the form $\{K^{\mu\nu}(x^\alpha)p_\mu p_\nu, g^{\rho\sigma}(x^\beta)p_\rho p_\sigma\}$ which is zero on the hypersurface $g^{\rho\sigma}(x^\beta)p_\rho p_\sigma = 0$. Hence, $K^{\mu\nu}(x^\alpha)$ is a conformal Killing tensor field of the spacetime.

2.2 General Form of the Photon Region

After finding the necessary and sufficient conditions for the existence of the Carter constant and hence integrability of the equations of motion, the parameters relevant for the light description in the vicinity of an axially symmetric object in a plasma can be studied. One of them is the so-called photon region, i.e., the region where light rays move along a sphere with $r = const.$ defined in the Boyer-Lindquist coordinates. For the compactness of the expressions, let me further write A_r instead of $A_r(r)$ etc., bearing in mind that these functions are actually functions of the argument they carry as an index.

It is now useful to rewrite $\frac{dS_r}{dr}$ and $\frac{dS_\vartheta}{d\vartheta}$ in (2.13) by applying $\frac{dS_r}{dr} = p_r$ and $\frac{dS_\vartheta}{d\vartheta} = p_\vartheta$, respectively. From simple algebraic manipulations of (2.13) we derive

$$\mathcal{F}(r)p_r^2 = -\mathcal{K} - f_r - p_\varphi^2 A_r + \omega_0^2 C_r + 2\omega_0 p_\varphi P_r, \tag{2.18}$$

$$\mathcal{G}(\vartheta)p_\vartheta^2 = \mathcal{K} - f_\vartheta - p_\varphi^2 A_\vartheta + \omega_0^2 C_\vartheta + 2\omega_0 p_\varphi P_\vartheta. \tag{2.19}$$

Since the photon region is defined as a set of all light ray trajectories entirely present on the hypersurface $r = const.$, $\dot{r} = \ddot{r} = 0$ has to be satisfied along these rays. The dot means the derivative with respect to the curve parameter present in Hamilton's equations. These light rays will be further called "spherical" although r does not have to be necessarily a radius coordinate. The corresponding equations of motion are

$$\dot{r} = \frac{\partial \mathcal{H}}{\partial p_r} = \frac{p_r}{B(r,\vartheta)}, \quad \dot{\vartheta} = \frac{\partial \mathcal{H}}{\partial p_\vartheta} = \frac{p_\vartheta}{D(r,\vartheta)}. \tag{2.20}$$

They return

$$B^2(r,\vartheta)\mathcal{F}(r)\dot{r}^2 = -\mathcal{K} - f_r - p_\varphi^2 A_r + \omega_0^2 C_r + 2\omega_0 p_\varphi P_r, \tag{2.21}$$

and

$$D^2(r,\vartheta)\mathcal{G}(\vartheta)\dot{\vartheta}^2 = \mathcal{K} - f_\vartheta - p_\varphi^2 A_\vartheta + \omega_0^2 C_\vartheta + 2\omega_0 p_\varphi P_\vartheta. \tag{2.22}$$

Along an arbitrary spherical light ray there are two equations which have to hold and take the form

$$0 = -\mathcal{K} - f_r - p_\varphi^2 A_r + \omega_0^2 C_r + 2\omega_0 p_\varphi P_r \equiv R(r), \tag{2.23}$$

$$0 = -f_r' - p_\varphi^2 A_r' + \omega_0^2 C_r' + 2\omega_0 p_\varphi P_r' \equiv R'(r). \tag{2.24}$$

The derivative with respect to r is denoted by $'$. From these two equations it is possible to express, for every spherical light ray, the constants of motion $\mathcal{K}$ and p_φ. The general formulae take the form

$$p_\varphi = \frac{\omega_0 P_r'}{A_r'}\left(1 \pm \sqrt{1 - \frac{A_r'}{\omega_0^2 P_r'^2}\left(f_r' - \omega_0^2 C_r'\right)}\right), \tag{2.25}$$

$$\begin{aligned}\mathcal{K} =& \frac{A_r}{A_r'}\left(f_r' - \omega_0^2 C_r'\right) - f_r + \omega_0^2 C_r \\ &+ 2\frac{\omega_0^2 P_r'}{A_r'}\left(P_r - \frac{A_r P_r'}{A_r'}\right)\left(1 \pm \sqrt{1 - \frac{A_r'}{\omega_0^2 P_r'^2}\left(f_r' - \omega_0^2 C_r'\right)}\right).\end{aligned} \tag{2.26}$$

The remaining pair of the equations of motion reads

$$\dot{\varphi} = \frac{\partial \mathcal{H}}{\partial p_\varphi} = \frac{p_\varphi A(r,\vartheta)}{A(r,\vartheta)C(r,\vartheta) + P^2(r,\vartheta)} - \frac{\omega_0 P(r,\vartheta)}{A(r,\vartheta)C(r,\vartheta) + P^2(r,\vartheta)}, \tag{2.27}$$

$$\dot{t} = \frac{\partial \mathcal{H}}{\partial p_t} = \frac{\omega_0 C(r,\vartheta)}{A(r,\vartheta)C(r,\vartheta) + P^2(r,\vartheta)} + \frac{p_\varphi P(r,\vartheta)}{A(r,\vartheta)C(r,\vartheta) + P^2(r,\vartheta)}. \tag{2.28}$$

The inequality

$$\mathcal{K} - f_\vartheta \geq p_\varphi^2 A_\vartheta - \omega_0^2 C_\vartheta - 2\omega_0 p_\varphi P_\vartheta \tag{2.29}$$

has to be satisfied because the left-hand side of (2.22) cannot be negative. Expressions (2.25) and (2.26) can be further plugged into inequality (2.29) which gives the final formula

$$\begin{aligned}&\frac{A_r}{A_r'}\left(\frac{f_r'}{\omega_0^2} - C_r'\right) + C_r + 2\frac{P_r'}{A_r'}\left(P_r - \frac{A_r P_r'}{A_r'}\right)\left(1 \pm \sqrt{1 - \frac{A_r'}{P_r'^2}\left(\frac{f_r'}{\omega_0^2} - C_r'\right)}\right) - \frac{f_r}{\omega_0^2} \\ &\geq \frac{f_\vartheta}{\omega_0^2} - \frac{A_\vartheta}{A_r'}\left(\frac{f_r'}{\omega_0^2} - C_r'\right) - C_\vartheta + 2\frac{P_r'}{A_r'}\left(\frac{A_\vartheta P_r'}{A_r'} - P_\vartheta\right)\left(1 \pm \sqrt{1 - \frac{A_r'}{P_r'^2}\left(\frac{f_r'}{\omega_0^2} - C_r'\right)}\right).\end{aligned} \tag{2.30}$$

The inequality (2.30) establishes the photon region because a spherical light ray is present at every point (r,ϑ) where the given condition holds. Note that there can be up to two solutions corresponding to the plus or minus signs before the square root.

There are two kinds of spherical light rays – stable or unstable when regarding perturbations in the r-direction. Considerably significant are the unstable rays, for they can be used as limit trajectories of light rays that reach the photon region from infinity. A spherical light ray is unstable if

$$0 < R''(r) = -f_r'' - p_\varphi^2 A_r'' + \omega_0^2 C_r'' + 2\omega_0 p_\varphi P_r''. \tag{2.31}$$

2.3 Black Hole Shadow

Thanks to the separability of the Hamilton-Jacobi equation for light rays, it is possible to obtain the analytical formula for the boundary curve of the shadow. This will be done for the case when the defined spacetime describes a black hole,

with a general form given by (2.1), but the chosen procedure can be applied also to other compact objects, e.g., wormholes or neutron stars.

The shadow is typically calculated for an observer located at fixed coordinates (r_O, ϑ_O) outside the black hole horizon. To adequately describe the configuration of the system, a suitable orthonormal tetrad has to be introduced. It takes a general form

$$e_0 = Y_1\partial_t + Y_2\partial_\varphi|_{(r_O,\vartheta_O)}\,, \tag{2.32}$$

$$e_1 = \frac{1}{\sqrt{D(r,\vartheta)}}\partial_\vartheta\Big|_{(r_O,\vartheta_O)}\,, \tag{2.33}$$

$$e_2 = Y_3\partial_t + Y_4\partial_\varphi|_{(r_O,\vartheta_O)}\,, \tag{2.34}$$

$$e_3 = -\frac{1}{\sqrt{B(r,\vartheta)}}\partial_r\Big|_{(r_O,\vartheta_O)}\,. \tag{2.35}$$

The functions Y_1, Y_2, Y_3, Y_4 are defined by the orthonormality conditions $g(e_0,e_0) = -1$, $g(e_2,e_2) = 1$, $g(e_0,e_2) = 0$. Their specific forms have to be obtained individually for a given metric. Component e_0 can be treated as the 4-velocity of an observer. In full generality, the orthonormality conditions for the chosen form of the metric (2.1) are

$$-A(r,\vartheta)Y_1^2 + 2P(r,\vartheta)Y_1Y_2 + C(r,\vartheta)Y_2^2 = -1, \tag{2.36}$$

$$-A(r,\vartheta)Y_3^2 + 2P(r,\vartheta)Y_3Y_4 + C(r,\vartheta)Y_4^2 = 1, \tag{2.37}$$

$$-A(r,\vartheta)Y_1Y_3 + P(r,\vartheta)(Y_1Y_4 + Y_2Y_3) + C(r,\vartheta)Y_2Y_4 = 0. \tag{2.38}$$

Note that there are only three equations (2.36)–(2.38) for four unknown functions Y_1, Y_2, Y_3, Y_4. Due to that, one of the unknowns has to be chosen arbitrarily. Although this statement might seem to be rather artificial, it is only a consequence of the fact that any normalized timelike vector in the two-space spanned by ∂_t and ∂_φ can be chosen for the 4-velocity.

Furthermore, let me define the tangent vector to the light ray

$$\lambda(s) = (r(s), \vartheta(s), \varphi(s), t(s)). \tag{2.39}$$

It can be written as

$$\dot\lambda = \dot r\partial_r + \dot\vartheta\partial_\vartheta + \dot\varphi\partial_\varphi + \dot t\partial_t\,. \tag{2.40}$$

The dot again has the meaning of the derivative with respect to parameter s used in Hamilton's equations. Because this tangent vector can be defined at an arbitrary point, it can be in principle defined also at the point of the observer. At this position, the tangent vector takes the form

$$\dot\lambda = -\tilde\alpha e_0 + \tilde\beta(\sin\theta\cos\psi e_1 + \sin\theta\sin\psi e_2 + \cos\theta e_3)\big|_{(r_O,\vartheta_O)}\,. \tag{2.41}$$

The positive functions $\tilde\alpha$, $\tilde\beta$ will be defined below, while θ and ψ are the observer's celestial coordinates – the colatitude and the azimuthal angle, respectively. The Hamiltonian (1.48) gives the parametrization of light rays in the form $g(\dot\lambda,\dot\lambda) = -\omega_p^2$ and then

$$\tilde\alpha^2 - \tilde\beta^2 = \omega_p^2\big|_{(r_O,\vartheta_O)}\,. \tag{2.42}$$

Additionally, $\tilde{\alpha}$ is given by

$$\begin{aligned}\tilde{\alpha} = g(\dot{\lambda}, e_0) = g(\dot{\lambda}, Y_1\partial_t + Y_2\partial_\varphi) &= Y_1(\dot{t}g_{tt} + \dot{\varphi}g_{t\varphi}) + Y_2(\dot{t}g_{t\varphi} + \dot{\varphi}g_{\varphi\varphi}) \\ &= Y_1(-\omega_0) + Y_2 p_\varphi,\end{aligned} \tag{2.43}$$

and hence

$$\tilde{\beta} = \sqrt{\left(-Y_1\omega_0 + Y_2 p_\varphi\right)^2 - \omega_p^2}. \tag{2.44}$$

In agreement with previous definitions, the derived expressions have to be calculated at the point of the observer, i.e., at (r_O, ϑ_O). The condition $\tilde{\alpha} > 0$ governs the orientation of the light ray from observer's position into the past, which means that $\omega_0 = -p_t$ is negative.

As a further step, it is desirable to find a relation between the celestial coordinates θ, ψ and the constants of motion p_φ, $\mathcal{K}$. This can be performed when comparing the factors before ∂_r and ∂_φ in (2.40) and (2.41) with the usage of (2.32)–(2.35). This gives

$$\dot{r} = -\beta\cos\theta\frac{1}{\sqrt{B(r,\vartheta)}}, \tag{2.45}$$

$$\dot{\varphi} = -\tilde{\alpha}Y_2 + \tilde{\beta}\sin\theta\sin\psi Y_4. \tag{2.46}$$

In order to find the specific formulae for the given system, the expressions for the dotted variables (2.21), (2.22), (2.27), (2.28), and the factors $\tilde{\alpha}$, $\tilde{\beta}$ (2.43), (2.44) derived above have to be plugged into the obtained general relations. After doing that, they read

$$\sin\theta = \left(1 + \frac{\mathcal{K} + f_r + p_\varphi^2 A_r - \omega_0^2 C_r - 2\omega_0 p_\varphi P_r}{F(r,\vartheta)\left(\left(-Y_1\omega_0 + Y_2 p_\varphi\right)^2 - \omega_p^2\right)}\right)^{1/2}\Bigg|_{(r_O,\vartheta_O)}, \tag{2.47}$$

$$\sin\psi = \frac{(A_r + A_\vartheta + F(r,\vartheta)Y_2^2)p_\varphi - (P_r + P_\vartheta + F(r,\vartheta)Y_1Y_2)\omega_0}{F^{1/2}(r,\vartheta)Y_4\left[F(r,\vartheta)\left(-Y_1\omega_0 + Y_2 p_\varphi\right)^2 + \mathcal{K} - f_\vartheta + p_\varphi^2 A_r - \omega_0^2 C_r - 2\omega_0 p_\varphi P_r\right]^{1/2}}\Bigg|_{(r_O,\vartheta_O)}. \tag{2.48}$$

In order to discuss the shadow, all light rays that come from the observer position into the past have to be considered. As a boundary of the shadow, light rays asymptotically approaching the spherical light rays forming the photon region outside the horizon consisting of *unstable* spherical light rays are taken. In principle, both kinds of light rays have the same constants of motion p_φ and $\mathcal{K}$. Due to that, expressions (2.25) and (2.26) can be plugged into (2.48) to express coordinates θ and ψ as functions of the radius coordinate $r = r_p$ (p_φ and $\mathcal{K}$ depend on this radius). This allows one to derive the boundary of the shadow on the observer's sky as a parameterized curve in terms of r_p between its minimal and maximal values. These limits are given from the condition $\sin\psi = \pm 1$. The boundary values can hence be calculated from

$$(A_r + A_\vartheta + F(r,\vartheta)Y_2^2)p_\varphi - (P_r + P_\vartheta + F(r,\vartheta)Y_1Y_2)\omega_0\Big|_{(r_O,\vartheta_O)} = \tag{2.49}$$

$$\pm F(r,\vartheta)Y_4\left[F(r,\vartheta)((-Y_1\omega_0+Y_2p_\varphi)^2-\omega_p^2)+\mathcal{K}+f_r+p_\varphi^2A_r-\omega_0^2C_r-2\omega_0p_\varphi P_r\right]^{1/2}\Big|_{(r_O,\vartheta_O)}.$$

In comparison with the vacuum case, the shadow in a plasma is also a function of ω_0. As was already discussed above, in the asymptotically flat spacetime ω_0 is the light ray frequency measured by a stationary observer at infinity. The light rays considered in the current calculations are parameterized in the past-oriented direction, and ω_0 is hence negative, while the positive frequency ω_{obs} measured by the observer at (r_O,ϑ_O) reads

$$\omega_{obs}=Y_1(-\omega_0)+Y_2p_\varphi. \tag{2.50}$$

The 4-velocity of this observer is determined by the tetrad factors Y_1 and Y_2. When $Y_2=0$, the light rays of the same ω_0 return the identical ω_{obs}, but this is not true for $Y_2\neq 0$.

2.4 General Formula for the Deflection Angle

The deflection angle α is given in full generality as

$$\alpha=\Delta\varphi-\pi. \tag{2.51}$$

Recalling that motion along a straight line would be $\Delta\varphi=\pi$, the deflection angle represents the deviation from this case and hence the subtraction of π. The term $\Delta\varphi$ is given from the relation $d\varphi/dr$ and is calculated further below. However, at this stage it should be mentioned that in fact it consists of two parts which are identical but for the sign. This is important for the final form of $\Delta\varphi$ which can be thus expressed in the form

$$\Delta\varphi=-\int_\infty^R\frac{d\varphi}{dr}dr+\int_R^\infty\frac{d\varphi}{dr}dr=2\int_R^\infty\frac{d\varphi}{dr}dr. \tag{2.52}$$

For this reason, the $\pm$ sign present along with $d\varphi/dr$ in the following expressions disappears in the final formula for α.

In this section, in comparison to the previous text, the form of the Hamiltonian (1.44) will be considered. Moreover, the medium is assumed to be at rest in the chosen coordinate frame, and its individual components hence are $V^i=0$, $V^t=(-g_{tt})^{-1/2}$. Then, the Hamiltonian takes the form

$$\mathcal{H}(x^\alpha,p_\alpha)=\frac{1}{2}\left[g^{\beta\delta}p_\beta p_\delta+(n^2-1)p_t^2g_{tt}^{-1}\right]. \tag{2.53}$$

As already discussed, for a fully general dispersive medium $n=n(x^\alpha,\omega(x^\alpha))$.

Moreover, from the relation between the photon frequency $\omega(x^\alpha)$, the momentum p_α, and the medium velocity V^α (1.45) and by applying the above-mentioned assumption, one gets

$$\omega(x^\alpha)=-p_t(-g_{tt})^{-1/2}. \tag{2.54}$$

Using the form of the metric (2.1) leads to the expression

$$\omega(r,\vartheta)=-p_t\frac{1}{\sqrt{A(r,\vartheta)}}. \tag{2.55}$$

Furthermore, assuming the metric (2.1) also yields

$$\mathcal{H}(x^\alpha, p_\alpha) = \frac{1}{2}\left[\frac{p_r^2}{B(r,\vartheta)} + \frac{p_\vartheta^2}{D(r,\vartheta)} + \frac{p_\varphi^2 A(r,\vartheta)}{A(r,\vartheta)C(r,\vartheta) + P^2(r,\vartheta)}\right. \tag{2.56}$$
$$\left. - \frac{p_t^2 C(r,\vartheta)}{A(r,\vartheta)C(r,\vartheta) + P^2(r,\vartheta)} + \frac{2p_t p_\varphi P(r,\vartheta)}{A(r,\vartheta)C(r,\vartheta) + P^2(r,\vartheta)} + \frac{p_t^2(1-n^2)}{A(r,\vartheta)}\right].$$

The relation $-p_t = \omega_0$ can be again applied in the following relations, and it will be further assumed that the medium has a refractive index $n = n(r, \omega(r))$.

By applying the Hamiltonian (2.56), the equations of motion read

$$\dot{\varphi} = \frac{\partial \mathcal{H}}{\partial p_\varphi} = \frac{p_\varphi A(r,\vartheta) - P(r,\vartheta)\omega_0}{A(r,\vartheta)C(r,\vartheta) + P^2(r,\vartheta)}, \tag{2.57}$$

$$\dot{r} = \frac{\partial \mathcal{H}}{\partial p_r} = \frac{p_r}{B(r,\vartheta)}. \tag{2.58}$$

The condition $\mathcal{H}(x^\alpha, p_\alpha) = 0$ can be used for deriving an equation for component p_r. In such a defined system its form is

$$p_r = \pm\sqrt{B(r,\vartheta)}\sqrt{\frac{\omega_0^2 C(r,\vartheta) + 2\omega_0 p_\varphi P(r,\vartheta) - p_\varphi^2 A(r,\vartheta)}{A(r,\vartheta)C(r,\vartheta) + P^2(r,\vartheta)} - \frac{\omega_0^2(1-n^2)}{A(r,\vartheta)} - \frac{p_\vartheta^2}{D(r,\vartheta)}}. \tag{2.59}$$

Combination of the relations given above gives an equation of motion for the rays in the form

$$\frac{d\varphi}{dr} = \frac{\dot{\varphi}}{\dot{r}} = \frac{B(r,\vartheta)}{p_r}\frac{p_\varphi A(r,\vartheta) - P(r,\vartheta)\omega_0}{A(r,\vartheta)C(r,\vartheta) + P^2(r,\vartheta)}. \tag{2.60}$$

In the following calculations, it is assumed that the rays lie in the equatorial plane, i.e., $\vartheta = \pi/2$ and $p_\vartheta = 0$. An expression for a total deflection angle can be then derived in a fully analytical form. Moreover, studying the rays in the equatorial plane is the most intuitive case and it is also a natural choice, considering further the well-known Bardeen-Petterson effect.

Plugging the expression for p_r (2.59) into (2.60) gives

$$\frac{d\varphi}{dr} = \pm\frac{\sqrt{A(r)B(r)}\left(\frac{p_\varphi}{\omega_0} - \frac{P(r)}{A(r)}\right)}{\sqrt{A(r)C(r) + P^2(r)}} \tag{2.61}$$
$$\times\left(\frac{C(r)}{A(r)} - \frac{p_\varphi^2}{\omega_0^2} + 2\frac{p_\varphi}{\omega_0}\frac{P(r)}{A(r)} - (1-n^2)\frac{A(r)C(r) + P^2(r)}{A^2(r)}\right)^{-1/2}.$$

This equation actually describes two parts of the ray trajectory, with the r coordinate either decreasing or increasing along increasing φ. Motion in each part corresponds to a different sign in relation (2.61) – $+$ when r increases, while $-$ for r decreasing.

After some algebraic manipulations, formula (2.61) can be rearranged to take the form

$$\frac{d\varphi}{dr} = \pm\sqrt{\frac{A(r)B(r)}{A(r)C(r) + P^2(r)}}\left(\frac{n^2\left(\frac{C(r)}{A(r)} + \frac{P^2(r)}{A^2(r)}\right)}{\left(\frac{p_\varphi}{\omega_0} - \frac{P(r)}{A(r)}\right)^2} - 1\right)^{-1/2}. \tag{2.62}$$

Following the notation introduced in previous works [e.g., Perlick et al., 2015], the function $h^2(r)$ can be defined, and in this case it reads

$$h^2(r) = n^2 \left(\frac{C(r)}{A(r)} + \frac{P^2(r)}{A^2(r)} \right). \tag{2.63}$$

For photons moving in the vicinity of the Schwarzschild black hole (when $P(r) = 0$ and the remaining metric coefficients have corresponding forms) in vacuum (when $n = 1$), the function $h^2(r)$ has the physical meaning of *the photon effective potential* [Misner et al., 1973].

Moreover, in the cold plasma approximation, the refractive index n can be rewritten as

$$n^2 = 1 - \frac{\omega_p^2(r)}{\omega^2(r)} = 1 - \frac{\omega_p^2(r)}{\omega_0^2} A(r), \tag{2.64}$$

where relation (2.55) for the photon frequency $\omega(r)$ modified for the case of the equatorial plane was used. Note that the form of the plasma frequency $\omega_p(r)$ has to be specified from the properties of the medium surrounding the compact source and it enters the equation as an additional parameter. Furthermore, note that equation (2.64) characterizes only an *unmagnetized* cold plasma, while when considering magnetic field, the corresponding dispersion relation would be more complicated, with a non-isotropic tensor needed to describe the medium. In a cold plasma the function $h^2(r)$ thus is

$$h^2(r) = \frac{A(r)C(r) + P^2(r)}{A^2(r)} \left(1 - \frac{\omega_p^2(r)}{\omega_0^2} A(r) \right). \tag{2.65}$$

When going back to the more general case, the deflection angle formula in an axially symmetric stationary spacetime with a refractive medium characterized by refractive index n finally takes the form

$$\alpha = 2 \int_R^\infty \sqrt{\frac{A(r)B(r)}{A(r)C(r) + P^2(r)}} \left(\frac{h^2(r)}{\left(\frac{p_\varphi}{\omega_0} - \frac{P(r)}{A(r)} \right)^2} - 1 \right)^{-1/2} dr - \pi. \tag{2.66}$$

Parameter R denotes the minimal value of the r coordinate which a ray can reach, i.e., it is the turning point of the ray. Thus, this point is defined by the relation

$$\left. \frac{dr}{d\varphi} \right|_{r=R} = 0. \tag{2.67}$$

Considering the form of the equation of motion (2.62), the condition for R is analogous to a situation when

$$h^2(R) = \left(\frac{p_\varphi}{\omega_0} - \frac{P(R)}{A(R)} \right)^2. \tag{2.68}$$

The fraction $\frac{p_\varphi}{\omega_0}$ has the well-known physical meaning of the ray impact parameter b, and expression (2.68) hence actually describes a relation between R (in terms of the function $h^2(R)$) and b. This relation is very useful, because while R is a coordinate-dependent variable, b is a frame-independent dimensionless quantity

which is commonly used for the description of light deflection. In the case of a general axially symmetric spacetime and plasma, the impact parameter can be expressed as a function of R as

$$b = \frac{p_\varphi}{\omega_0} = \frac{P(R)}{A(R)} \pm h(R) = \frac{P(R)}{A(R)} \pm n\sqrt{\frac{C(R)}{A(R)} + \frac{P^2(R)}{A^2(R)}}. \tag{2.69}$$

When using definition (2.68), the deflection angle can be expressed in the compact form

$$\alpha = 2\int_R^\infty \sqrt{\frac{A(r)B(r)}{A(r)C(r)+P^2(r)}} \left(\frac{h^2(r)}{\left(\frac{P(R)}{A(R)} - \frac{P(r)}{A(r)} \pm h(R)\right)^2} - 1 \right)^{-1/2} dr - \pi. \tag{2.70}$$

With the help of equation (2.69), the deflection angle can be further expressed as a function of b. However, there are more elegant ways how to obtain the dependence of the deflection angle on b, and at this stage, it was sufficient just to briefly outline how it can be performed in the chosen approach.

3. Applications of the General Formulae

The general expressions obtained in Chapter 2 will be applied here to demonstrate their relevance for particular cases. Separability of different spacetimes with the usage of the conditions derived in Section 2.1 is discussed in Section 3.1, and various applications of the deflection angle formula obtained in Section 2.4 are presented in Sections 3.2, 3.3, and 3.4.

3.1 Separability of Chosen Spacetimes

As was already outlined in Section 2.1, the derived formulae can hold in principle for an arbitrary frame system and it is hence necessary to carefully choose the suitable coordinates. Moreover, the derived conditions can be used to directly decide whether in the given spacetime the equations for the rays are separable. This is shown for several examples in the following section. Moreover, if the separability can be performed, in particular cases the Carter constant is found.

3.1.1 The hairy Kerr metric

First, let me use the general expressions for the case of the hairy Kerr metric. As it is a straightforward generalization of the Kerr metric, which was already studied by Perlick and Tsupko [2017], the derived results can be easily compared with their previously found relations. A generalized form of the Kerr metric in Boyer-Lindquist coordinates is [e.g., Islam and Ghosh, 2021]

$$\begin{aligned} ds^2 = &-\left(1-\frac{2rM(r)}{\rho^2}\right)dt^2+\frac{\rho^2}{\Delta}dr^2+\rho^2 d\vartheta^2-\frac{4arM(r)}{\rho^2}\sin^2\vartheta dt d\varphi \\ &+\left(r^2+a^2+\frac{2a^2rM(r)}{\rho^2}\sin^2\vartheta\right)\sin^2\vartheta d\varphi^2, \end{aligned} \tag{3.1}$$

where $\Delta = r^2 + a^2 - 2M(r)r$, $\rho^2 = r^2 + a^2\cos^2\vartheta$. The expressions are formally the same as defined for the Kerr metric, which can be derived as a special case when $M(r) = m = const$.

The terms introduced in Section 2.1 in this case are

$$B(r,\vartheta) = \frac{\rho^2}{\Delta}, \quad D(r,\vartheta) = \rho^2, \tag{3.2}$$

$$F(r,\vartheta) = \rho^2, \quad \mathcal{F}(r) = \Delta, \quad \mathcal{G}(\vartheta) = 1, \tag{3.3}$$

$$A_r = -\frac{a^2}{\Delta}, \qquad A_\vartheta = \sin^{-2}\vartheta, \tag{3.4}$$

$$C_r = \frac{(r^2+a^2)^2}{\Delta}, \qquad C_\vartheta = -a^2\sin^2\vartheta, \tag{3.5}$$

$$P_r = -\frac{a(r^2+a^2)}{\Delta}, \qquad P_\vartheta = a. \tag{3.6}$$

The relations are formally identical with the equations found for the Kerr metric, but Δ now contains a general function $M(r)$.

When the form of $\omega_p^2(r,\vartheta)$ is taken as it was defined with (2.11) and the above-defined expressions are considered, the two equations defining $\mathcal{K}$ take the form

$$\mathcal{F}(r)\left(\frac{dS_r}{dr}\right)^2+f_r+p_\varphi^2 A_r-\omega_0^2 C_r-2\omega_0 p_\varphi P_r=\Delta\left(\frac{dS_r}{dr}\right)^2+f_r-\frac{1}{\Delta}(ap_\varphi+(r^2+a^2)\omega_0)^2 \tag{3.7}$$

and

$$\mathcal{G}(\vartheta)\left(\frac{dS_\vartheta}{d\vartheta}\right)^2+f_\vartheta+p_\varphi^2 A_\vartheta-\omega_0^2 C_\vartheta-2\omega_0 p_\varphi P_\vartheta=\left(\frac{dS_\vartheta}{d\vartheta}\right)^2+f_\vartheta+\left(\frac{p_\varphi}{\sin\vartheta}+a\sin\vartheta\omega_0\right)^2. \tag{3.8}$$

The derived formulae are formally identical with relation (27) presented in Perlick and Tsupko [2017].

A significant disagreement between the case of the Kerr metric and the hairy Kerr metric arises in the expression for the photon region. Indeed, applying the general expression (2.30) derived in the previous chapter to the hairy Kerr metric gives

$$\left[\frac{r^2\Delta}{(r-M-rM')^2}\left(1\pm\sqrt{1-\frac{f_r'(r-M-rM')}{2r^2\omega_0^2}}\right)^2-\frac{f_r+f_\vartheta}{\omega_0^2}\right]a^2\sin^2\vartheta\geq \tag{3.9}$$

$$\left[\frac{1}{r-M-rM'}\left(M(a^2-r^2)+rM'(r^2+a^2)\pm r\Delta\sqrt{1-\frac{f_r'(r-M-rM')}{2r^2\omega_0^2}}\right)+a^2\sin^2\vartheta\right]^2.$$

When one wants to reproduce the result for the Kerr case as it was obtained by Perlick and Tsupko [2017], it is necessary to set $M'=0$.

The last remaining formula to calculate is the expression for the hairy Kerr black hole shadow. However, this relation is exactly the same as for the Kerr metric derived by Perlick and Tsupko [2017], except that the definition of Δ would be as defined above and hence more general. From this point of view, stating this expression explicitly here would bring nothing new, and it is hence omitted.

It should be also mentioned that the physical systems defined by the two metrics (Kerr, hairy Kerr) differ substantially, although their formal appearance is very similar. A physically legitimate definition of the function $M(r)$ is that it proportionally decreases with increasing r, while the matter stress tensor emerges along with the presence of a non-constant $M(r)$ by maintaining energy conditions.

3.1.2 The Hartle-Thorne metric

The Hartle-Thorne (HT) metric describes both the interior and the exterior parts of a neutron star. Its form for the external gravitational field of a rotating star accurate to the second order in the angular velocity can be found in the Appendix

of Hartle and Thorne [1968]. This metric reads

$$
\begin{aligned}
ds^2 = &-\left(1-\frac{2M}{r}+\frac{2J^2}{r^4}\right)\left\{1+2P_2(\cos\vartheta)\left[\frac{J^2}{Mr^3}\left(1+\frac{M}{r}\right)\right.\right. \\
&\left.\left.+\frac{5}{8}\frac{Q-J^2/M}{M^3}Q_2^2\left(\frac{r}{M}-1\right)\right]\right\}dt^2 \\
&+\left(1-\frac{2M}{r}+\frac{2J^2}{r^4}\right)^{-1}\left\{1-2P_2(\cos\vartheta)\left[\frac{J^2}{Mr^3}\left(1-\frac{5M}{r}\right)\right.\right. \\
&\left.\left.+\frac{5}{8}\frac{Q-J^2/M}{M^3}Q_2^2\left(\frac{r}{M}-1\right)\right]\right\}dr^2 \\
&+r^2\left\{1+2P_2(\cos\vartheta)\left[-\frac{J^2}{Mr^3}\left(1+\frac{2M}{r}\right)+\frac{5}{8}\frac{Q-J^2/M}{M^3}\right.\right. \\
&\left.\left.\left\langle\frac{2M}{\sqrt{r(r-2M)}}Q_2^1\left(\frac{r}{M}-1\right)-Q_2^2\left(\frac{r}{M}-1\right)\right\rangle\right]\right\}\times\left\{d\vartheta^2+\sin^2\vartheta\left(d\varphi-\frac{2J}{r^3}dt\right)^2\right\}.
\end{aligned}
\tag{3.10}
$$

The constant factors M, J, and Q denote the mass, the total angular momentum, and the quadrupole moment of the star, respectively. The function $P_2(\cos\vartheta)$ is the Legendre polynomial of order 2 with the argument $\cos\vartheta$, while the associated Legendre functions of the second kind with the argument $\frac{r}{M}-1$ are denoted by $Q_n^m\left(\frac{r}{M}-1\right)$.

Glampedakis and Babak [2006] showed that the Hartle-Thorne metric in the given coordinate frame separates the Hamilton-Jacobi equation for geodesics only when $J=0$ and $Q=0$, i.e., in the Schwarzschild metric. Otherwise, even for the specific choice $Q=J^2/M\neq 0$ which corresponds to the Kerr metric, separability cannot be achieved.

Because the derived statement holds for *lightlike* geodesics, it is obviously still true for light rays in given coordinates in a plasma, regardless of the definition of the plasma density. In the following calculations these findings will be recovered with usage of the general conditions presented above.

To simplify the long expressions in the HT metric, let us introduce a compact notation in the form

$$
\begin{aligned}
A_1 &= 1-\frac{2M}{r}+\frac{2J^2}{r^4}, & j &= \frac{J^2}{Mr^3}, \\
K &= \frac{5}{8}\frac{Q-J^2/M}{M^3}, & j_1 &= \frac{2J}{r^3}.
\end{aligned}
\tag{3.11}
$$

Moreover, Q_n^m will be used below rather than $Q_n^m\left(\frac{r}{M}-1\right)$.

Let us further introduce

$$
\mathcal{M}_A = 1+2P_2(\cos\vartheta)\left[j\left(1+\frac{M}{r}\right)+KQ_2^2\right], \tag{3.12}
$$

$$
\mathcal{M}_B = 1-2P_2(\cos\vartheta)\left[j\left(1-\frac{5M}{r}\right)+KQ_2^2\right], \tag{3.13}
$$

$$
\mathcal{M}_\varphi = 1+2P_2(\cos\vartheta)\left[-j\left(1+\frac{2M}{r}\right)+K\left(\frac{2M}{\sqrt{r(r-2M)}}Q_2^1-Q_2^2\right)\right]. \tag{3.14}
$$

The particular metric coefficients presented in (2.1) then read

$$\begin{aligned} A(r,\vartheta) &= A_1\mathcal{M}_A - j_1^2 r^2 \sin^2\vartheta\mathcal{M}_\varphi, & B(r,\vartheta) &= A_1^{-1}\mathcal{M}_B, \\ C(r,\vartheta) &= r^2\sin^2\vartheta\mathcal{M}_\varphi, & D(r,\vartheta) &= r^2\mathcal{M}_\varphi, \\ P(r,\vartheta) &= -j_1 r^2\sin^2\vartheta\mathcal{M}_\varphi. \end{aligned} \tag{3.15}$$

From the derived expressions it can be clearly seen that the ratio of terms $B(r,\vartheta)$ and $D(r,\vartheta)$ equals

$$\frac{B(r,\vartheta)}{D(r,\vartheta)} = \frac{\mathcal{M}_B}{A_1 r^2\mathcal{M}_\varphi}. \tag{3.16}$$

However, from the separability conditions it follows that this ratio has to be a function of ϑ alone – $\mathcal{G}(\vartheta)$ – divided by a separate function of r – $\mathcal{F}(r)$. The definitions of $\mathcal{M}_B$ and $\mathcal{M}_\varphi$ clearly demonstrate that their dependence on r and ϑ requires that the separability can be performed only if $J = 0$ and $Q = 0$, i.e., for the Schwarzschild metric. In the case when $Q = J^2/M(\neq 0)$ (Kerr metric) the suitable frame transformation to Boyer-Lindquist coordinates can be applied. It is well known that in this coordinate system separability can be achieved. An explicit form of the desired coordinate transformation can be found, e.g., in Glampedakis and Babak [2006] and it is discussed in more detail further (see Section 3.2.1).

3.1.3 The Melvin universe

The Melvin universe is a specific solution of the Einstein-Maxwell equations with a uniform magnetic field. It was originally derived by Bonnor [1954] and 10 years later rediscovered by Melvin [1964]. A detailed analysis of the geodesics in the Melvin spacetime can be found in Melvin and Wallingford [1966].

The Melvin universe can be described by a metric of the form

$$ds^2 = \tilde{a}^2\left[(1+\rho^2)^2(-dt^2+d\rho^2+dz^2) + \rho^2(1+\rho^2)^{-2}d\varphi^2\right], \tag{3.17}$$

where $\tilde{a}$ is a positive constant taking the role of an overall scaling factor, t denotes the time coordinate, and ρ, z, and φ are the cylindrical polar coordinates. For the purpose of further calculations, let me introduce $\Lambda(\rho) \equiv 1+\rho^2$.

Separation in spherical coordinates

As was already discussed in Chapter 2, metric terms have to obey several conditions in order to find the individual separated terms and the Carter constant. Although the coordinate system can be arbitrary and the obtained expressions can be then written in the system of choice, the most natural frame is provided by the spherical coordinates $(t, r, \vartheta, \varphi)$. However, metric (3.17) is expressed in the cylindrical coordinates (t, ρ, z, φ). Hence, let me use a coordinate transformation

$$t = t, \tag{3.18}$$
$$\rho = r\sin\vartheta, \tag{3.19}$$
$$z = r\cos\vartheta, \tag{3.20}$$
$$\varphi = \varphi, \tag{3.21}$$

which allows one to express the Melvin universe in the spherical coordinates. It then transforms to

$$ds^2 = \tilde{a}^2 \left[\Lambda^2(r,\vartheta)(-dt^2 + dr^2 + r^2 d\vartheta^2) + r^2 \sin^2\vartheta \Lambda^{-2}(r,\vartheta) d\varphi^2\right], \tag{3.22}$$

where $\Lambda(r,\vartheta) = 1 + r^2\sin^2\vartheta$. In the case when $\Lambda(r,\vartheta) = 1$, metric (3.22) would correspond to the Minkowski spacetime.

Applying the notation from Section 2.1, individual metric terms yield

$$\begin{aligned} &A(r,\vartheta) = \tilde{a}^2\Lambda^2(r,\vartheta), && B(r,\vartheta) = \tilde{a}^2\Lambda^2(r,\vartheta), \\ &C(r,\vartheta) = \tilde{a}^2 r^2 \sin^2\vartheta\Lambda^{-2}(r,\vartheta), && D(r,\vartheta) = \tilde{a}^2 r^2 \Lambda^2(r,\vartheta), \\ &P(r,\vartheta) = 0. \end{aligned} \tag{3.23}$$

These terms return the functions

$$\frac{B(r,\vartheta)}{D(r,\vartheta)} = r^{-2} \quad \Rightarrow \quad F(r,\vartheta) = \tilde{a}^2 r^2 \Lambda^2(r,\vartheta), \quad \mathcal{F}(r) = r^2, \quad \mathcal{G}(\vartheta) = 1, \tag{3.24}$$

and

$$A(r,\vartheta)C(r,\vartheta) + P^2(r,\vartheta) = \tilde{a}^4 r^2 \sin^2\vartheta. \tag{3.25}$$

However, plugging these expressions into (2.12) when searching for separated parts of $A(r,\vartheta)$ returns

$$\frac{F(r,\vartheta)A(r,\vartheta)}{A(r,\vartheta)C(r,\vartheta) + P^2(r,\vartheta)} = \Lambda^4(r,\vartheta)\sin^{-2}\vartheta = \sin^6\vartheta(r^2 + \sin^{-2}\vartheta)^4 \neq A_r + A_\vartheta, \tag{3.26}$$

which obviously cannot be separated, while the remaining terms are

$$\frac{F(r,\vartheta)}{A(r,\vartheta)C(r,\vartheta) + P^2(r,\vartheta)} C(r,\vartheta) = r^2 = C_r, \tag{3.27}$$

$$\frac{F(r,\vartheta)}{A(r,\vartheta)C(r,\vartheta) + P^2(r,\vartheta)} P(r,\vartheta) = 0. \tag{3.28}$$

Hence, it is evident that due to the lack of feasible separation of the term $A(r,\vartheta)$, it is impossible to determine the Carter constant in this coordinate frame.

Separation in cylindrical coordinates

However, when different, more suitable, coordinates are used instead of the spherical ones, the separation can still be derived. For this reason, let me do the same procedure in the cylindrical coordinates ρ, z in which the Melvin metric was originally introduced, see (3.17). Using the original notation of Section 2.1, the discussed metric terms are

$$\begin{aligned} &A(\rho,z) = \tilde{a}^2\Lambda^2(\rho), && B(\rho,z) = \tilde{a}^2\Lambda^2(\rho), \\ &C(\rho,z) = \tilde{a}^2\rho^2\Lambda^{-2}(\rho), && D(\rho,z) = \tilde{a}^2\Lambda^2(\rho), \\ &P(\rho,z) = 0. \end{aligned} \tag{3.29}$$

Notice that these terms are only functions of ρ. For this reason, it is simple to find

$$\frac{B(\rho,z)}{D(\rho,z)} = 1 \quad \Rightarrow \quad F(\rho,z) = \tilde{a}^2\Lambda^2(\rho), \quad \mathcal{F}(\rho) = 1, \quad \mathcal{G}(z) = 1, \tag{3.30}$$

and moreover

$$A(\rho,z)C(\rho,z)+P^2(\rho,z)=\tilde{a}^4\rho^2, \tag{3.31}$$

which further yields

$$A_\rho=\rho^{-2}\Lambda^4(\rho), \qquad A_z=0, \tag{3.32}$$
$$C_\rho=1, \qquad C_z=0, \tag{3.33}$$
$$P_\rho=0, \qquad P_z=0. \tag{3.34}$$

Naturally, the derived results are not unique, as an equal constant can always be added to X_ρ and subtracted from X_z, where X denotes A, C, or P.

In order to find the Carter constant, substituting the individual parts of A, C, and P into (2.13) returns the Hamilton-Jacobi equation in the form

$$\left(\frac{dS_\rho}{d\rho}\right)^2+f_\rho(\rho)+p_\varphi^2\rho^{-2}\Lambda^4(\rho)-\omega_0^2=-\left(\frac{dS_z}{dz}\right)^2-f_z(z)\equiv-\mathcal{K}, \tag{3.35}$$

which corresponds to the results obtained in Melvin and Wallingford [1966].

Then, the photon region can be described by the expression

$$\frac{\rho\Lambda(\rho)f'_\rho(\rho)}{2(3\rho^2-1)}+\omega_0^2-f_\rho(\rho)-f_z(z)\geq 0. \tag{3.36}$$

In vacuum the entire spacetime basically represents the photon region. Since the separation in the Melvin universe was finally performed in cylindrical coordinates rather than in spherical coordinates, the photon region is filled with "cylindrical light rays" rather than with spherical light rays. Moreover, these cylindrical light rays are not restricted to a spatially limited compact region, and there is hence no meaningful definition for a "shadow" in the Melvin spacetime.

Let me briefly mention that one can assume in principle a more general case when analysing an exact solution of the Einstein-Maxwell equations describing either a Schwarzschild or a Kerr black hole embedded in a Melvin universe. For the Schwarzschild case see Ernst [1976] and see Ernst and Wild [1976] for the Kerr case. Moreover, a shadow of either of these black holes was recently discussed in Lima Jr. et al. [2021], Wang et al. [2021], respectively. Unfortunately, the light ray equations are not separable in these cases.

3.1.4 The Teo wormhole metric

One more example demonstrating how to apply the derived general formulae when searching for the generalized Carter constant is a stationary and axisymmetric metric describing a rotating traversable wormhole obtained by Teo [1998]. The necessary and sufficient conditions for separability of the Hamilton-Jacobi equation for light rays in a plasma in such a spacetime can be found from the general results. Moreover, it is possible to analytically determine the photon region and the shadow in this case. Note that in vacuum and for a specific subclass of the Teo metrics, the shadow was already obtained by Nedkova et al. [2013].

The metric describing the object takes the form

$$ds^2=-N^2dt^2+\left(1-\frac{b}{r}\right)^{-1}dr^2+r^2K^2d\vartheta^2+r^2K^2\sin^2\vartheta\left(d\varphi-\tilde{\omega}dt\right)^2, \tag{3.37}$$

where N, K, b, and $\tilde{\omega}$ are functions of r and ϑ. It is assumed that the metric is asymptotically flat. To satisfy this requirement, at $r \to \infty$ the functions present in the metric must behave as follows:

$$N = 1 - \frac{M}{r} + \mathcal{O}\left(\frac{1}{r^2}\right), \quad K = 1 + \mathcal{O}\left(\frac{1}{r}\right), \tag{3.38}$$
$$\frac{b}{r} = \mathcal{O}\left(\frac{1}{r}\right), \quad \tilde{\omega} = \frac{2J}{r^3} + \mathcal{O}\left(\frac{1}{r^4}\right).$$

The coordinates for the spacetime are chosen so that they cover the region between the "neck" of the wormhole, which is characterized by the equation $b(r, \vartheta) = r$, and infinity. Moreover, the functions N, b, and K have to be strictly positive in this range. Furthermore, it is required that $\partial b(r, \vartheta)/\partial \vartheta \to 0$ and $b(r, \vartheta) > r\partial b(r, \vartheta)/\partial r$ at the point of the neck. To get a wormhole that connects two asymptotically flat copies of a spacetime, they have to be glued together at the neck.

From the notation introduced in (2.1) one can be directly deduce that

$$\begin{aligned} &A(r, \vartheta) = N^2 - r^2 K^2 \tilde{\omega}^2 \sin^2 \vartheta, && B(r, \vartheta) = \left(1 - \frac{b}{r}\right)^{-1}, \\ &C(r, \vartheta) = r^2 K^2 \sin^2 \vartheta, && D(r, \vartheta) = r^2 K^2, \\ &P(r, \vartheta) = -\tilde{\omega} r^2 K^2 \sin^2 \vartheta. \end{aligned} \tag{3.39}$$

Application of (2.8), (2.12) implies

$$F(r, \vartheta) = r^2 K^2, \quad \mathcal{F}(r) = r^2 K^2 \left(1 - \frac{b}{r}\right), \quad \mathcal{G}(\vartheta) = 1, \tag{3.40}$$

$$A(r, \vartheta) C(r, \vartheta) + P^2(r, \vartheta) = N^2 r^2 K^2 \sin^2 \vartheta, \tag{3.41}$$

and, finally,

$$A_r = -\frac{r^2 K^2}{N^2} \tilde{\omega}^2, \qquad A_\vartheta = \sin^{-2} \vartheta, \tag{3.42}$$
$$C_r = \frac{r^2 K^2}{N^2}, \qquad C_\vartheta = 0, \tag{3.43}$$
$$P_r = -\frac{r^2 K^2}{N^2} \tilde{\omega}, \qquad P_\vartheta = 0. \tag{3.44}$$

In order to find the photon region, it is necessary to determine the following functions

$$A_r' = -2\frac{r K^2}{N^2} \tilde{\omega}^2 - r^2 \tilde{\omega}^2 \left(\frac{K^2}{N^2}\right)' - \frac{r^2 K^2}{N^2} (\tilde{\omega}^2)', \tag{3.45}$$
$$C_r' = 2\frac{r K^2}{N^2} + r^2 \left(\frac{K^2}{N^2}\right)', \tag{3.46}$$
$$P_r' = -2\frac{r K^2}{N^2} \tilde{\omega} - r^2 \tilde{\omega} \left(\frac{K^2}{N^2}\right)' - \frac{r^2 K^2}{N^2} \tilde{\omega}'. \tag{3.47}$$

It is obvious from these relations that to perform the separability of variables, each of the functions

$$\frac{K}{N}, \quad K^2\left(1-\frac{b}{r}\right), \quad \tilde{\omega}$$

have to be solely a function of r.

When this assumption holds, a new radial coordinate ℓ can be introduced, satisfying

$$d\ell = \pm\left(K\sqrt{1-\frac{b}{r}}\right)^{-1} dr. \tag{3.48}$$

This variable is useful because it depicts the radial length in a new metric obtained by the conformal transformation $g_{\mu\nu} \mapsto K^{-2}g_{\mu\nu}$. As $\ell \in (-\infty, \infty)$, the new coordinate system $(\ell, \vartheta, \varphi, t)$ captures the whole spacetime from one asymptotic end to the other, while the original Teo coordinates $(r, \vartheta, \varphi, t)$ describe only one half of the spacetime (from infinity up to the neck). To find the discussed light ray functions, it is more useful to use the original Teo coordinates.

The separated parts of A, C, and P can be substituted into (2.13), which gives the relation for the Carter constant

$$\begin{aligned} r^2K^2\left(1-\frac{b}{r}\right)\left(\frac{dS_r}{dr}\right)^2 + f_r(r) - p_\varphi^2\frac{r^2K^2}{N^2}\tilde{\omega}^2 - \omega_0^2\frac{r^2K^2}{N^2} + 2\omega_0 p_\varphi\frac{r^2K^2}{N^2}\tilde{\omega} \\ = -\left(\frac{dS_\vartheta}{d\vartheta}\right)^2 - f_\vartheta(\vartheta) - p_\varphi^2\sin^{-2}\vartheta \equiv -\mathcal{K}. \end{aligned} \tag{3.49}$$

Moreover, the equations for the derivatives of the functions S_r and S_ϑ can be expressed with the help of $\mathcal{K}$, namely

$$N^2\left(1-\frac{b}{r}\right)\left(\frac{dS_r}{dr}\right)^2 = (\omega_0 - \tilde{\omega}p_\varphi)^2 - \frac{N^2}{r^2K^2}(\mathcal{K} + f_r(r)), \tag{3.50}$$

$$\left(\frac{dS_\vartheta}{d\vartheta}\right)^2 = \mathcal{K} - f_\vartheta(\vartheta) - p_\varphi^2\sin^{-2}\vartheta. \tag{3.51}$$

Note that the special case when the plasma density is zero (i.e., in vacuum) and the metric functions N, b, K, and $\tilde{\omega}$ separately depend solely on r was already studied by Nedkova et al. [2013], and the corresponding equations were already derived there.

In the next step, relations for $\mathcal{K}$ and p_φ have to be found. From the general expressions (2.25) and (2.26) one gets

$$\tilde{\omega}p_\varphi = \frac{\omega_0\left(\mathcal{Q}' + \mathcal{Q}\frac{\tilde{\omega}'}{\tilde{\omega}}\right) \pm \omega_0\sqrt{\mathcal{Q}^2\left(\frac{\tilde{\omega}'}{\tilde{\omega}}\right)^2 + \frac{f_r'}{\omega_0^2}\left(\mathcal{Q}' + 2\mathcal{Q}\frac{\tilde{\omega}'}{\tilde{\omega}}\right)}}{\mathcal{Q}' + 2\mathcal{Q}\frac{\tilde{\omega}'}{\tilde{\omega}}}, \tag{3.52}$$

$$\mathcal{K} = \frac{\omega_0^2\mathcal{Q}\left(\mathcal{Q}\frac{\tilde{\omega}'}{\tilde{\omega}} \mp \sqrt{\mathcal{Q}^2\left(\frac{\tilde{\omega}'}{\tilde{\omega}}\right)^2 + \frac{f_r'}{\omega_0^2}\left(\mathcal{Q}' + 2\mathcal{Q}\frac{\tilde{\omega}'}{\tilde{\omega}}\right)}\right)^2}{\left(\mathcal{Q}' + 2\mathcal{Q}\frac{\tilde{\omega}'}{\tilde{\omega}}\right)^2} - f_r, \tag{3.53}$$

where

$$\mathcal{Q} \equiv \frac{r^2 K^2}{N^2}.$$

Note that the function $\mathcal{Q}$ depends on r only and, similarly to the previous cases, $'$ denotes the derivative with respect to r.

Using the derived equations for p_φ and $\mathcal{K}$ in (3.51) yields

$$\mathcal{Q}\left(\mathcal{Q}\frac{\tilde{\omega}'}{\tilde{\omega}} \mp \sqrt{\mathcal{Q}^2\left(\frac{\tilde{\omega}'}{\tilde{\omega}}\right)^2 + \frac{f_r'}{\omega_0^2}\left(\mathcal{Q}' + 2\mathcal{Q}\frac{\tilde{\omega}'}{\tilde{\omega}}\right)}\right)^2 - \frac{f_r + f_\vartheta}{\omega_0^2}\left(\mathcal{Q}' + 2\mathcal{Q}\frac{\tilde{\omega}'}{\tilde{\omega}}\right)^2 \geq$$
$$\sin^{-2}\vartheta\tilde{\omega}^{-2}\left(\mathcal{Q}' + \mathcal{Q}\frac{\tilde{\omega}'}{\tilde{\omega}} \pm \sqrt{\mathcal{Q}^2\left(\frac{\tilde{\omega}'}{\tilde{\omega}}\right)^2 + \frac{f_r'}{\omega_0^2}\left(\mathcal{Q}' + 2\mathcal{Q}\frac{\tilde{\omega}'}{\tilde{\omega}}\right)}\right)^2, \tag{3.54}$$

which is the condition for the existence of a spherical light ray around the Teo wormhole. This expression is naturally obtained also when the general formula (2.30) is used.

When assuming that the equations for p_φ and K given by (3.52) and (3.53), respectively, are functions of the radius coordinate $r = r_p$, the boundary curve of the shadow parameterized by r_p can be obtained from the equations (2.47) and (2.48) which return

$$\sin\theta = \left(\frac{\mathcal{K} - f_\vartheta}{\mathcal{Q}(\tilde{\omega}p_\varphi - \omega_0)^2 - (f_r + f_\vartheta)}\right)^{1/2}\Bigg|_{(r_O,\vartheta_O)}, \tag{3.55}$$

$$\sin\psi = \frac{p_\varphi}{\sin\vartheta\sqrt{\mathcal{K} - f_\vartheta}}\Bigg|_{(r_O,\vartheta_O)}. \tag{3.56}$$

To derive the expressions for the wormhole shadow, it is necessary to introduce an orthonormal tetrad, in this case chosen in the form

$$e_0 = \frac{1}{N}\left(\partial_t + \tilde{\omega}\partial_\varphi\right)\Big|_{(r_O,\vartheta_O)}, \tag{3.57}$$

$$e_1 = \frac{1}{rK}\partial_\vartheta\Big|_{(r_O,\vartheta_O)}, \tag{3.58}$$

$$e_2 = \frac{1}{rK\sin\vartheta}\partial_\varphi\Big|_{(r_O,\vartheta_O)}, \tag{3.59}$$

$$e_3 = -\left(1 - \frac{b}{r}\right)^{1/2}\partial_r\Bigg|_{(r_O,\vartheta_O)}. \tag{3.60}$$

Until now, the Teo wormhole was studied only generally for arbitrary forms of N, K, b, and $\tilde{\omega}$. In the following calculations, a specific example of the Teo wormhole is assumed, taking the form

$$ds^2 = \Omega(r,\vartheta)\left(-dt^2 + \frac{dr^2}{1 - \frac{r_0^2}{r^2}} + r^2 d\vartheta^2 + r^2\sin^2\vartheta\Big(d\varphi - \frac{2\,a}{r^3}dt\Big)^2\right) \tag{3.61}$$

with

$$\Omega(r,\vartheta) = 1 + \frac{(4\,a\cos\vartheta)^2}{r_0^3\,r}. \tag{3.62}$$

The parameter r_0 is a positive constant factor of the dimension of length and a is a constant with the dimension of length squared. The radius coordinate is defined between r_0 and infinity. The neck is set at point r_0, where it holds that $\Big(r/\Omega(r,\vartheta)\Big)\Big(1-r_0^2/r^2\Big)=0$.

Individual metric terms of this object are

$$A(r,\vartheta)=\Omega(r,\vartheta)\left(1-\frac{4a^2}{r^4}\sin^2\vartheta\right), \qquad B(r,\vartheta)=\Omega(r,\vartheta)\left(1-\frac{r_0^2}{r^2}\right)^{-1}, \tag{3.63}$$
$$C(r,\vartheta)=\Omega(r,\vartheta)r^2\sin^2\vartheta, \qquad D(r,\vartheta)=\Omega(r\vartheta)r^2,$$
$$P(r,\vartheta)=-\frac{2a}{r}\Omega(r,\vartheta)\sin^2\vartheta\,.$$

The functions relevant for the separation in this case read

$$F(r,\vartheta)=\Omega(r,\vartheta)r^2, \quad \mathcal{F}(r)=r^2\left(1-\frac{r_0^2}{r^2}\right), \quad \mathcal{G}(\vartheta)=1, \tag{3.64}$$
$$A(r,\vartheta)C(r,\vartheta)+P^2(r,\vartheta)=\Omega^2(r,\vartheta)r^2\sin^2\vartheta, \tag{3.65}$$

and the separated metric terms are

$$A_r=-\frac{4a^2}{r^4}, \qquad A_\vartheta=\sin^{-2}\vartheta, \tag{3.66}$$
$$C_r=r^2, \qquad C_\vartheta=0, \tag{3.67}$$
$$P_r=-\frac{2a}{r}, \qquad P_\vartheta=0. \tag{3.68}$$

To find the generalized Carter constant for such a spacetime, the plasma density has to be of the form

$$\omega_{\rm pl}(r,\vartheta)^2=\frac{f_r(r)+f_\vartheta(\vartheta)}{\Omega(r,\vartheta)r^2}\,. \tag{3.69}$$

The equations of motion generally defined by (2.21), (2.22), (2.27), and (2.28) now yield

$$\Omega^2(r,\vartheta)r^4\,\dot r^2=\Big(r^2-r_0^2\Big)\left(-\mathcal{K}+\left(\frac{2a}{r^2}\,p_\varphi-\omega_0 r\right)^2-f_r(r)\right), \tag{3.70}$$
$$\Omega^2(r,\vartheta)r^4\,\dot\vartheta^2=\mathcal{K}-\frac{p_\varphi^2}{\sin^2\vartheta}-f_\vartheta\,, \tag{3.71}$$
$$\dot\varphi=\frac{p_\varphi\Big(r^4-4a^2\sin^2\vartheta\Big)+2\,a\,\omega_0\,r^5\sin^2\vartheta}{\Omega(r,\vartheta)\,r^6\sin^2\vartheta}\,, \tag{3.72}$$
$$\dot t=\frac{\omega_0\,r^3-2\,a\,p_\varphi}{\Omega(r,\vartheta)\,r^3}\,. \tag{3.73}$$

The right-hand side of (3.70) and its derivative are equal to zero for the case of spherical light rays. It can be easily found that this is true at $r=r_0$, i.e., at the neck. Moreover, the Carter constant for the light rays satisfying this condition is a function of p_φ and hence

$$\mathcal{K}(p_\varphi)=\left(\frac{2a}{r^2}\,p_\varphi-\omega_0 r\right)^2-f_r(r)\,. \tag{3.74}$$

These spherical light rays at the neck are unstable in vacuum, but in plasma their stability depends on the function $f_r(r)$. Assuming $r \neq r_0$, calculating the right-hand side of (3.70) and its derivative when they equal zero leads to the two equations for p_φ and $\mathcal{K}$. These constants of motion for a light ray on a sphere of radius r_p read

$$p_\varphi(r_p) = \frac{\omega_0 r_p^2}{8a}\left(r_p \mp \sqrt{9r_p^2 - 4r_p\frac{f_r'(r_p)}{\omega_0^2}}\right), \tag{3.75}$$

$$\mathcal{K}(r_p) = \frac{\omega_0^2}{16}\left(3r_p \pm \sqrt{9r_p^2 - 4r_p\frac{f_r'(r_p)}{\omega_0^2}}\right)^2 - f_r(r_p)\,. \tag{3.76}$$

As a result, at the neck there is not only the photon sphere, but in general there is also a photon region universally defined by (2.30) and evaluated for the studied case as

$$\left(3r \pm \sqrt{9r^2 - 4r\frac{f_r'(r)}{\omega_0^2}}\right)^2 - 16\frac{f_r(r) + f_\vartheta(\vartheta)}{\omega_0^2} \geq \frac{r^4}{4a^2\sin^2\vartheta}\left(r \mp \sqrt{9r^2 - 4r\frac{f_r'(r)}{\omega_0^2}}\right)^2. \tag{3.77}$$

Equation (3.70) also returns the condition when the spherical light orbits in the photon region are unstable, which yields

$$0 < R''(r) = -f_r''(r) + 2\left(\frac{40a^2}{r^6}p_\varphi^2 + \omega_0^2 - \frac{4a}{r^3}\omega_0 p_\varphi\right). \tag{3.78}$$

There are several restrictions for (3.77) in vacuum. First, only the upper signs are allowed, and second, for $a < r_0^2/6$ the photon region does not exist at all, i.e., the only unstable photon orbits which can serve as limit curves for light rays defining the boundary of the shadow are those at the neck. On the contrary, the photon region exists when $a > r_0^2/6$. Such a photon region is formed by two symmetric parts which are connected in the photon sphere at the neck. The shadow boundary line results from light rays of two kinds – those which spiral towards the photon sphere and those which spiral towards unstable spherical orbits in the photon region where $r_p \neq r_0$. A new interesting effect occurring in a plasma is that the photon region may become separated from the neck, while the spherical orbits at the neck are stable. In this case, the shadow boundary is hence completely defined by light rays that spiral towards spherical orbits in the part of the photon region that lies on the same side of the neck as the observer.

The photon orbits for a wormhole defined by (3.61) with the specific choice $a = r_0^2/3$ and $a = 0.8r_0^2$, are shown in the two panels of Fig. 3.1. The plasma profile determined by the functions $f_r = 4\omega_0^2 r_0^2(r_0/r)^{1/2}$ and $f_\vartheta = 0$ was chosen. Note that in a thus defined plasma, the photon region of the Teo wormhole with $a = r_0^2/3$ does not exist.

When determining the wormhole shadow, the same tetrad as in (3.57)–(3.60)

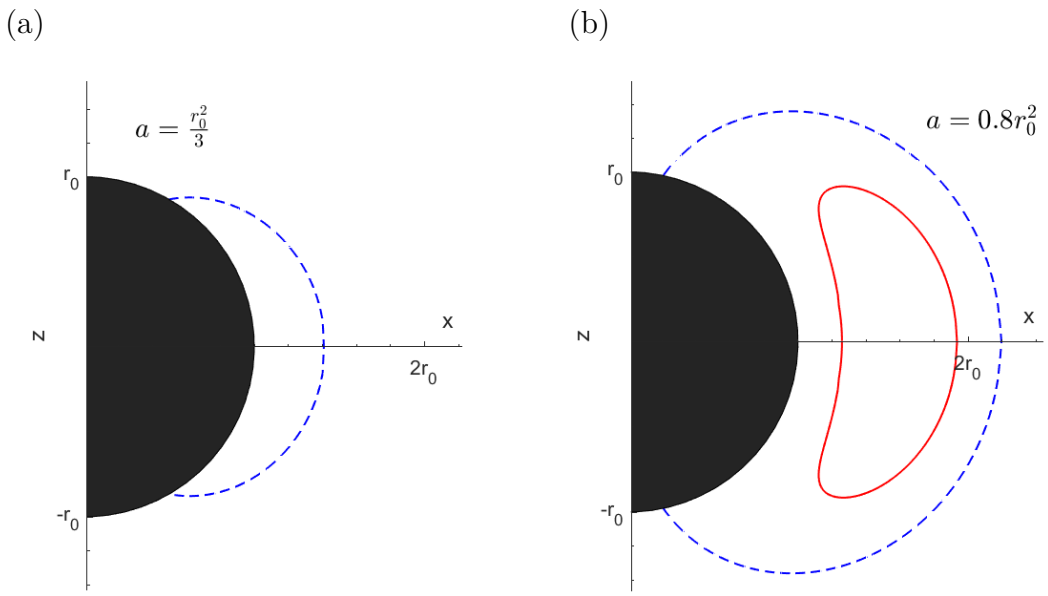

Figure 3.1: Teo wormhole photon regions with (a) $a = r_0^2/3$ and (b) $a = 0.8r_0^2$. The dashed blue curves show the boundary of the photon region in vacuum and the red solid curve corresponds to the plasma case when $f_r = 4\omega_0^2 r_0^2 (r_0/r)^{1/2}$ and $f_\vartheta = 0$. For such a plasma profile the photon region does not exist if $a = r_0^2/3$.

is used, but with the corresponding form of the given functions, i.e.,

$$e_0 = \frac{1}{\sqrt{\Omega(r,\vartheta)}}\left(\partial_t + \frac{2a}{r^3}\partial_\varphi\right)\Big|_{(r_O,\vartheta_O)}, \tag{3.79}$$

$$e_1 = \frac{1}{\sqrt{\Omega(r,\vartheta)}\,r}\partial_\vartheta\Big|_{(r_O,\vartheta_O)}, \tag{3.80}$$

$$e_2 = \frac{1}{\sqrt{\Omega(r,\vartheta)}\,r\sin\vartheta}\partial_\varphi\Big|_{(r_O,\vartheta_O)}, \tag{3.81}$$

$$e_3 = -\frac{1}{\sqrt{\Omega(r,\vartheta)}}\left(1-\frac{r_0^2}{r^2}\right)^{1/2}\partial_r\Big|_{(r_O,\vartheta_O)}. \tag{3.82}$$

Note that the observer position r_O is not the same as the neck radius r_0. The corresponding coefficients at ∂_t and ∂_φ determined from (2.40) in comparison with those in (2.41) allow one to get

$$\tilde{\alpha} = \frac{2ap_\varphi - \omega_0 r_{\rm O}^3}{\sqrt{\Omega(r_{\rm O},\vartheta_{\rm O})}\,r_{\rm O}^3}, \tag{3.83}$$

$$\tilde{\beta} = \frac{p_\varphi}{\sqrt{\Omega(r_{\rm O},\vartheta_{\rm O})}\,r_{\rm O}\sin\vartheta_{\rm O}\sin\psi\sin\theta}. \tag{3.84}$$

In order to derive the specific forms of $\tilde{\alpha}$ and $\tilde{\beta}$, relations (3.72) and (3.73) were used. The coefficients at ∂_r and ∂_ϑ can be treated in a similar manner. After doing

so, the obtained formulae for $\dot{r}$ and $\dot{\vartheta}$ have to be used in (3.70) and (3.71), along with applying the expression (3.84) for $\tilde{\beta}$. Evaluation of the celestial coordinates ψ and θ then yields

$$\tan^2\theta = \frac{\mathcal{K} - f_\vartheta(\vartheta_\mathrm{O})}{\left(\frac{2a}{r_\mathrm{O}^2}p_\varphi - \omega_0 r_\mathrm{O}\right)^2 - \mathcal{K} - f_r(r_\mathrm{O})}, \tag{3.85}$$

$$\sin^2\psi = \frac{p_\varphi^2}{\Big(\mathcal{K} - f_\vartheta(\vartheta_\mathrm{O})\Big)\sin^2\vartheta_\mathrm{O}}\,. \tag{3.86}$$

Furthermore, when assuming that $p_\varphi = p_\varphi(r_p)$ and $\mathcal{K} = \mathcal{K}(r_p)$ as known from (3.75), a part of the shadow boundary determined by light rays that spiral towards spherical light rays in the photon region can be found. This curve is parameterized by r_p. The part of the shadow boundary defined by light rays that spiral towards the photon sphere at the neck is parameterized by p_φ and can be found when applying $K = K(p_\varphi)$ from (3.74).

The shadow of the Teo metric seen by an observer set at position $r_O = 5r_0/2$ and $\vartheta_O = \pi/2$ both in vacuum and in a plasma is shown in Fig. 3.2. To depict the shape of the shadow, dimensionless Cartesian coordinates previously used in Perlick and Tsupko [2017] were adopted. They are of the form

$$X(r) = -2\tan\left(\frac{\theta(r)}{2}\right)\sin(\psi(r)), \tag{3.87}$$

$$Y(r) = -2\tan\left(\frac{\theta(r)}{2}\right)\cos(\psi(r)). \tag{3.88}$$

The coordinates are defined in the tangent plane to the celestial sphere at the pole where $\theta = 0$ and the stereographic projection onto it is performed.

3.2 Deflection in the Weak Field Approximation vs Complete Solution

A comparison of the derived general analytical formula for the deflection angle (2.70) and an approximate solution when weak field is assumed, i.e., when $M/R \ll 1$ will be performed in this section. It is an instructive way how to demonstrate the relevance of a complete solution and at what distance from the black hole it is necessary to consider it. This calculation is performed for both the Kerr metric and the HT metric and it is thus also possible to express the effect of the quadrupole moment that is generically present in the latter case. The expansion is derived up to the third order in M/R while maintaining terms up to the second order in angular velocity when the approximation of the HT metric as an external gravitational field of a rotating star is still valid. Moreover, as it will become clear further, the effect of the quadrupole moment can be observed first at this order. Because the main goal of this section is to compare directly the deflection angles for both the HT and Kerr metrics in the weak field, it is useful to compute the formula for the HT metric, although it was already discussed as an approximation of the external field of nonrelativistic stars by Hartle and Thorne [1968].

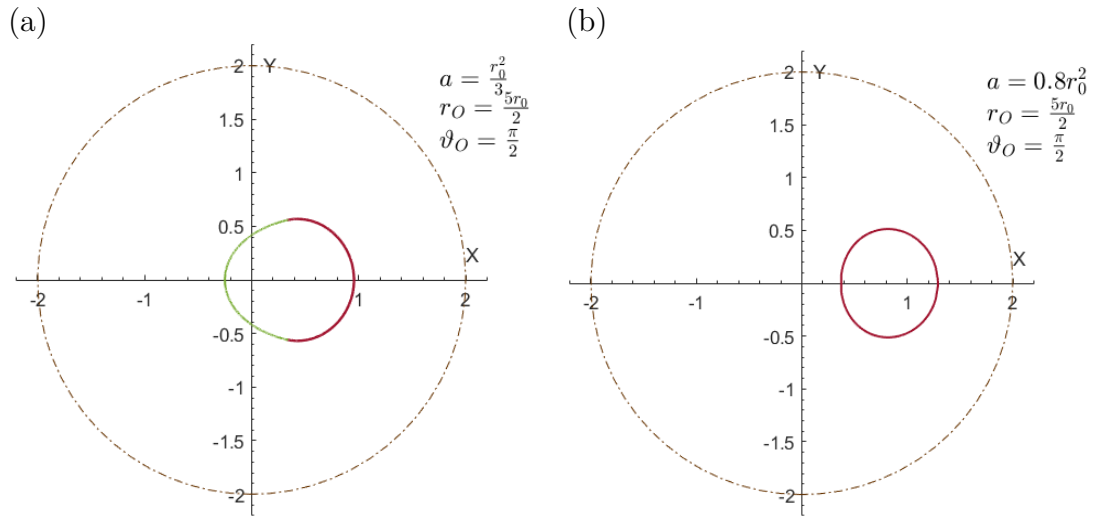

Figure 3.2: Shadow of the Teo wormhole seen by an observer at $r_O = 5r_0/2$ and $\vartheta_O = \pi/2$ when (a) $a = r_0^2/3$, $f_r = 0$, $f_\vartheta = 0$ and (b) $a = 0.8r_0^2$, $f_r = 4\omega_0^2 r_0^2 (r_0/r)^{1/2}$, $f_\vartheta = 0$. The shadow boundary determined by light rays spiraling towards spherical light rays in the photon region is marked by the thick purple curves, while boundary parts defined by light rays that spiral towards the photon sphere at the neck, i.e., when $r = r_0$, are marked by the thin green curve. The dash-dotted circles show the position of the celestial equator.

3.2.1 The Kerr metric

The expression for the deflection angle of light in a cold plasma propagating around an object described by the Kerr metric in Boyer-Lindquist coordinates in the equatorial plane was already derived and discussed, e.g., in Perlick [2000]. This formula takes the form

$$\alpha = 2\int_R^\infty \frac{\sqrt{r(r-2M)}}{r^2 - 2Mr + a^2}\left(\frac{(R-2M)^2 h^2(r)}{\left(2Ma(R-r) \pm (r-2M)h(R)\right)^2} - 1\right)^{-1/2} dr - \pi, \tag{3.89}$$

where

$$h^2(r) = r^2(r^2 - 2Mr + a^2)\left(1 - \frac{\omega_p^2(r)}{\omega_0^2}\left(1 - \frac{2M}{r}\right)\right). \tag{3.90}$$

The introduced relation can be also obtained from the derived general formula (2.70) assuming that

$$\begin{aligned} A(r) &= 1 - \frac{2M}{r}, & B(r) &= \frac{r^2}{r^2 - 2Mr + a^2}, \\ C(r) &= r^2 + a^2 + \frac{2Ma^2}{r}, & P(r) &= -\frac{2Ma}{r}. \end{aligned} \tag{3.91}$$

These terms are taken in the equatorial plane and thus they do not resemble the usual Kerr metric coefficients.

In order to make the manipulation with the equations more convenient, let me introduce a general form of the deflection angle formula in the Kerr metric in

the equatorial plane as

$$\alpha = 2\int_R^\infty f_{Kerr}(r)dr - \pi, \tag{3.92}$$

where

$$f_{Kerr}(r) = \frac{\sqrt{r(r-2M)}}{r^2-2Mr+a^2}\left(\frac{(R-2M)^2h^2(r)}{\left(2Ma(R-r)\pm(r-2M)h(R)\right)^2}-1\right)^{-1/2}. \tag{3.93}$$

Although an analytical calculation of the integral (3.92) is quite complicated in general, it is significantly simpler in the weak-field approximation. In this approximation, terms up to the third order will be derived below. The reason for the choice of this order will be clarified. Assuming a vacuum case ($\omega_p = 0$) and under the conditions of the weak field, the function $f_{Kerr}(r)$ can be treated as

$$\begin{aligned} f_{Kerr}(r) \approx \frac{R}{r\sqrt{r^2-R^2}}\Bigg(1 &+ \frac{M(R^2+rR+r^2)}{rR(r+R)} + \frac{3M^2(R^2+rR+r^2)^2}{2r^2R^2(r+R)^2} \\ &+ \frac{a^2(r^2-2R^2)}{2r^2R^2} \mp \frac{2Mar}{R^2(r+R)}\left(1+\frac{M(5R^2+4rR+2r^2)}{rR(r+R)}\right) \\ &+ \frac{3Ma^2(r^4+R(R+r)(r^2-2R^2))}{2r^3R^3(r+R)} + \frac{5M^3(R^2+rR+r^2)^3}{2r^3R^3(r+R)^3}\Bigg). \end{aligned} \tag{3.94}$$

The individual terms are then integrated as follows

$$\int_R^\infty \frac{Rdr}{r\sqrt{r^2-R^2}} = \frac{\pi}{2}, \tag{3.95}$$

$$\int_R^\infty \frac{M(R^2+rR+r^2)dr}{r^2(r+R)\sqrt{r^2-R^2}} = \frac{2M}{R}, \tag{3.96}$$

$$\int_R^\infty \frac{3M^2(R^2+rR+r^2)^2dr}{2r^3R(r+R)^2\sqrt{r^2-R^2}} = \frac{M^2}{8R^2}(15\pi-16), \tag{3.97}$$

$$\int_R^\infty \frac{2Madr}{R(r+R)\sqrt{r^2-R^2}} = \frac{2Ma}{R^2}, \tag{3.98}$$

$$\int_R^\infty \frac{a^2(r^2-2R^2)dr}{2r^3R\sqrt{r^2-R^2}} = 0, \tag{3.99}$$

$$\int_R^\infty \frac{2M^2a(5R^2+4rR+2r^2)dr}{rR^2(r+R)^2\sqrt{r^2-R^2}} = \frac{M^2a}{R^3}(5\pi-8), \tag{3.100}$$

$$\int_R^\infty \frac{3Ma^2(r^4+R(R+r)(r^2-2R^2))dr}{2r^4R^2(r+R)\sqrt{r^2-R^2}} = \frac{Ma^2}{R^3}, \tag{3.101}$$

$$\int_R^\infty \frac{5M^3(R^2+rR+r^2)^3dr}{2r^4R^2(r+R)^3\sqrt{r^2-R^2}} = \frac{M^3}{R^3}\left(\frac{61}{3}-\frac{15\pi}{4}\right). \tag{3.102}$$

Note that no term $\propto \frac{a^3}{R^3}$ is present in (3.94) by definition.

Hence, the deflection angle in the Kerr metric in Boyer-Lindquist coordinates in the weak field approximation in vacuum reads

$$\begin{aligned} \alpha_{BL} = &\frac{4M}{R} + \frac{M^2}{R^2}\left(\frac{15\pi}{4}-4\right) \mp \frac{4Ma}{R^2} \mp \frac{M^2a}{R^3}(10\pi-16) + \frac{2Ma^2}{R^3} \\ &+ \frac{M^3}{R^3}\left(\frac{122}{3}-\frac{15\pi}{2}\right). \end{aligned} \tag{3.103}$$

Terms up to the second order were previously calculated, e.g., in Perlick and Tsupko [2024]. Notice that the deflection angle formula in the weak-field approximation for the Schwarzschild metric can be obtained directly from (3.103) by assuming $a = 0$. Moreover, the first term of (3.103) is the so-called Einstein deflection angle [see Schneider et al., 1992, Bisnovatyi-Kogan and Tsupko, 2009]. Additionally, analogous formulae for the deflection angle in the Kerr metric can be derived by different techniques. This was performed in several earlier works, e.g., Iyer and Hansen [2009], Aazami et al. [2011], Crisnejo et al. [2019]. Notice that in these studies the deflection angle was expressed as a function of mass M, angular momentum per unit mass a, and impact parameter b.

However, as the ultimate goal of this part is *to compare the deflection angles in the Kerr and HT metrics*, one has to derive the deflection angles in the same coordinate system (unless they are expressed in terms of the impact parameter b). For this reason, it is desirable to apply the coordinate transformation originally introduced by Hartle and Thorne [1968], namely

$$r \to r\left[1 - \frac{a^2}{2r^2}\left(\left(1+\frac{2M}{r}\right)\left(1-\frac{M}{r}\right) - \cos^2\vartheta\left(1-\frac{2M}{r}\right)\left(1+\frac{3M}{r}\right)\right)\right], \tag{3.104}$$

$$\vartheta \to \vartheta - \frac{a^2}{2r^2}\sin\vartheta\cos\vartheta\left(1+\frac{2M}{r}\right),$$

which in the equatorial plane up to the order relevant for the present study reads

$$r \to r\left[1 - \frac{a^2}{2r^2}\left(1+\frac{M}{r}\right)\right], \quad \vartheta \to \vartheta. \tag{3.105}$$

When applying the introduced transformation through the individual terms of expansion (3.94), it turns out that the only change occurs in the term $\propto \frac{Ma^2}{R^3}$. It now changes to[1]

$$\int_R^\infty \frac{3Ma^2(r^4 + R(R+r)(r^2-R^2))dr}{2r^4R^2(r+R)\sqrt{r^2-R^2}} = \frac{2Ma^2}{R^3}. \tag{3.106}$$

Finally, the deflection angle formula for the Kerr metric with assumption $M/R \ll 1$ up to the third order in the new coordinate system yields

$$\begin{aligned}\alpha_{transf} =& \frac{4M}{R} + \frac{M^2}{R^2}\left(\frac{15\pi}{4} - 4\right) \mp \frac{4Ma}{R^2} \mp \frac{M^2a}{R^3}(10\pi - 16) + \frac{4Ma^2}{R^3} \\ &+ \frac{M^3}{R^3}\left(\frac{122}{3} - \frac{15\pi}{2}\right).\end{aligned} \tag{3.107}$$

[1]Relevant transformation factors actually occur in

$$\begin{aligned}&\frac{\sqrt{r(r-2M)}}{r^2-2Mr+a^2} \approx \frac{1}{r}\left(1 + \frac{M}{r} - \frac{a^2}{r^2} + \frac{3M^2}{2r^2} + \frac{5M^3}{2r^3} - \frac{3Ma^2}{r^3}\right) \\ \to\quad &\frac{1}{r}\left[1 + \frac{a^2}{2r^2}\left(1+\frac{M}{r}\right)\right]\left[1 + \frac{M}{r}\left(1-\frac{a^2}{2r^2}\right) - \frac{a^2}{r^2} + \frac{3M^2}{2r^2} + \frac{5M^3}{2r^3} - \frac{3Ma^2}{r^3}\right],\end{aligned}$$

and the remaining factors arising from this transformation in the other terms vanish up to the given order.

When comparing the deflection angles (3.103) and (3.107), one can see that the coordinate transformation terminates with an additional factor of 2 in (3.107) in front of the term $\frac{Ma^2}{R^3}$. This is given by the order of the expansion used in this section. Other relevant factors stemming from the coordinate transformation would occur in higher-order terms which are not considered in the present calculation.

3.2.2 The Hartle-Thorne metric

To demonstrate the difference from the Kerr metric, light deflection is studied in the equatorial plane (formula (2.70) was obtained under this condition anyway) and at the first approximation, the situation without a quadrupole moment when $K = 0$ (cf. (3.11)) is considered. Under these assumptions, the relevant HT metric terms present in the deflection angle formula take the form

$$A(r) = 1 - \frac{2M}{r} - j \equiv A_0, \tag{3.108}$$

$$A(r)B(r) = 1 \equiv AB_0, \tag{3.109}$$

$$A(r)C(r) + P^2(r) = r^2\left(1 - \frac{2M}{r}\right) \equiv ACP_0, \tag{3.110}$$

$$1 - \frac{\omega_p^2(r)}{\omega_0^2}A(r) = 1 - \frac{\omega_p^2(r)}{\omega_0^2}\left(1 - \frac{2M}{r} - j\right) \equiv 1 - \frac{\omega_p^2(r)}{\omega_0^2}A_0, \tag{3.111}$$

$$\frac{P(r)}{A(r)} = -\frac{2J}{r}\left(1 + \frac{2M}{r}\right) \equiv PA_0, \tag{3.112}$$

$$h^2(r) = \frac{r^2\left(1 - \frac{2M}{r}\right)}{\left(1 - \frac{2M}{r} - j\right)^2}\left(1 - \frac{\omega_p^2(r)}{\omega_0^2}\left(1 - \frac{2M}{r} - j\right)\right). \tag{3.113}$$

The simplified form of the deflection angle for the HT metric in this case is

$$\alpha_{HT0} = 2\int_R^\infty f_{HT0}(r)dr - \pi, \tag{3.114}$$

where

$$f_{HT0}(r) = \frac{1}{\sqrt{ACP_0}}\left(\frac{ACP_0\left(1 - \frac{\omega_p^2(r)}{\omega_0^2}A_0\right)}{A_0^2\left(\frac{P(R)}{A(R)} - \frac{P(r)}{A(r)} \pm h(R)\right)^2} - 1\right)^{-1/2}.$$

Moreover, when vacuum is considered, i.e., $\omega_p(r) = 0$, one gets

$$f_{HT0}(r) = \frac{1}{\sqrt{r^2\left(1 - \frac{2M}{r}\right)}}\left(\frac{\frac{r^2\left(1-\frac{2M}{r}\right)}{\left(1-\frac{2M}{r}-\frac{J^2}{Mr^3}\right)^2}}{\left(PA_0(R) - PA_0(r) \pm h(R)\right)^2} - 1\right)^{-1/2}.$$

In the weak-field approximation, i.e., when $M/r \ll 1$, we expand the result

to obtain

$$f_{HT0}(r) \approx \frac{R}{r\sqrt{r^2-R^2}}\left[1+\frac{M(R^2+rR+r^2)}{rR(r+R)}+\frac{3M^2(R^2+rR+r^2)^2}{2r^2R^2(r+R)^2}\right. \tag{3.115}$$
$$\mp\frac{2Jr}{R^2(r+R)}\left(1+\frac{M(5R^2+4rR+2r^2)}{rR(r+R)}\right)+\frac{J^2(R^2+Rr+r^2)}{MrR^3(r+R)}$$
$$\left.+\frac{5M^3(R^2+rR+r^2)^3}{2r^3R^3(r+R)^3}\right].$$

In order to get the full analytical form of the deflection angle, individual terms obtained in the expansion have to be integrated. The result is

$$\int_R^\infty \frac{Rdr}{r\sqrt{r^2-R^2}}=\frac{\pi}{2}, \tag{3.116}$$
$$\int_R^\infty \frac{M(R^2+rR+r^2)dr}{r^2(r+R)\sqrt{r^2-R^2}}=\frac{2M}{R}, \tag{3.117}$$
$$\int_R^\infty \frac{3M^2(R^2+rR+r^2)^2dr}{2r^3R(r+R)^2\sqrt{r^2-R^2}}=\frac{M^2}{8R^2}(15\pi-16), \tag{3.118}$$
$$\int_R^\infty \frac{2Jdr}{R(r+R)\sqrt{r^2-R^2}}=\frac{2J}{R^2}, \tag{3.119}$$
$$\int_R^\infty \frac{2MJ(5R^2+4rR+2r^2)dr}{rR^2(r+R)^2\sqrt{r^2-R^2}}=\frac{MJ}{R^3}(5\pi-8), \tag{3.120}$$
$$\int_R^\infty \frac{J^2(R^2+rR+r^2)dr}{Mr^2R^2(r+R)\sqrt{r^2-R^2}}=\frac{2J^2}{MR^3}, \tag{3.121}$$
$$\int_R^\infty \frac{5M^3(R^2+rR+r^2)^3dr}{2r^4R^2(r+R)^3\sqrt{r^2-R^2}}=\frac{M^3}{R^3}\left(\frac{61}{3}-\frac{15\pi}{4}\right). \tag{3.122}$$

In comparison with the Kerr metric, most of the terms present for the HT metric are identical, except for the term proportional to $\frac{a^2}{R^2}$ (equivalently to $\frac{J^2}{M^2R^2}$ in the HT metric). Such a term is not present in the expansion of the HT metric, while it drops out during the integration in the Kerr metric.

Finally, the corresponding part of the deflection angle in the HT metric in the weak-field approximation in vacuum yields

$$\alpha_{HT0} =\frac{4M}{R}+\frac{M^2}{R^2}\left(\frac{15\pi}{4}-4\right)\mp\frac{4J}{R^2}\mp\frac{MJ}{R^3}(10\pi-16)+\frac{4J^2}{MR^3} \tag{3.123}$$
$$+\frac{M^3}{R^3}\left(\frac{122}{3}-\frac{15\pi}{2}\right).$$

The derived expression is the same as the deflection angle formula (3.107) obtained for the Kerr metric after the coordinate transformation (3.105) when setting $J=-Ma$.

Furthermore, it is desirable to add the effect of the quadrupole moment in its lowest order. When terms proportional to both $\frac{J}{MR}$ and $\frac{Q}{R^3}$, i.e., $\propto \frac{JQ}{MR^4}$ are

neglected, one gets additional factors in the given terms in the form

$$A(r) = A_0 - KQ_2^2, \tag{3.124}$$

$$A(r)B(r) = AB_0, \tag{3.125}$$

$$A(r)C(r) + P^2(r) = ACP_0 - K\frac{2Mr^2}{\sqrt{r(r-2M)}}Q_2^1, \tag{3.126}$$

$$1 - \frac{\omega_p^2(r)}{\omega_0^2}A(r) = 1 - \frac{\omega_p^2(r)}{\omega_0^2}\left(A_0 - KQ_2^2\right), \tag{3.127}$$

$$\frac{P(r)}{A(r)} = PA_0, \tag{3.128}$$

$$h^2(r) = \frac{ACP_0 - K\frac{2Mr^2}{\sqrt{r(r-2M)}}Q_2^1}{\left(A_0 - KQ_2^2\right)^2}\left(1 - \frac{\omega_p^2(r)}{\omega_0^2}\left(A_0 - KQ_2^2\right)\right). \tag{3.129}$$

The deflection angle for the HT metric is then modified to

$$\alpha_{HT} = 2\int_R^\infty f_{HT}(r)dr - \pi, \tag{3.130}$$

where

$$f_{HT}(r) = \sqrt{\frac{AB_0}{ACP_0 - K\frac{2Mr^2}{\sqrt{r(r-2M)}}Q_2^1}} \tag{3.131}$$
$$\times\left(\frac{\left(ACP_0 - K\frac{2Mr^2}{\sqrt{r(r-2M)}}Q_2^1\right)\left(1 - \frac{\omega_p^2(r)}{\omega_0^2}\left(A_0 - KQ_2^2\right)\right)}{\left(A_0 - KQ_2^2\right)^2\left(PA_0(R) - PA_0(r) \pm h(R)\right)^2} - 1\right)^{-1/2}.$$

Notice that the functions Q_2^1 and Q_2^2 explicitly present in the expression for $f_{HT}(r)$ are functions of r, whereas the function $h(R)$ also includes the functions Q_2^1 and Q_2^2, but as functions of R. These are also present in the lowest term including the quadrupole moment in $f_{HT}(r)$, namely

$$f_K(r) = K\frac{M}{\sqrt{r(r-2M)}}Q_2^1(r) + K\frac{r^2}{r^2 - R^2} \tag{3.132}$$
$$\times\left(\frac{M}{\sqrt{r(r-2M)}}Q_2^1(r) - \frac{M}{\sqrt{R(R-2M)}}Q_2^1(R) + Q_2^2(R) - Q_2^2(r)\right)$$
$$\approx \frac{2}{5}K\left[\frac{M^4(R^4 - r^2R^2 - r^4)}{r^4R^4} + \frac{4M^3(r^3 - R^3)}{rR^3(r^2 - R^2)}\right].$$

Additionally, let me present here also a mixed term combining both the plasma ($\sim \omega_p$) and quadrupole ($\sim K$) parts. It has the form

$$f_{pl}(r) = \frac{r^2}{r^2 - R^2}\left[\frac{\omega_p^2(r)}{2\omega_0^2}\left(1 - KQ_2^2(r)\right) - \frac{\omega_p^2(R)}{2\omega_0^2}\left(1 - KQ_2^2(R)\right)\right] \tag{3.133}$$
$$\approx \frac{r^2(\omega_p^2(r) - \omega_p^2(R))}{2\omega_0^2(r^2 - R^2)} - \frac{4KM^3\left(R^3\omega_p^2(r) - r^3\omega_p^2(R)\right)}{5\omega_0^2 rR^3(r^2 - R^2)} = f_{pKerr}(r) - f_{pHT}(r).$$

The introduced relations were derived by applying the simplifications which hold for the following expressions

$$\frac{2M}{\sqrt{r(r-2M)}}Q_2^1 - Q_2^2 = \frac{3(2M^2-r^2)}{2M^2}\ln\left(\frac{r}{r-2M}\right) - \frac{2M^2-3rM-3r^2}{rM}, \tag{3.134}$$

$$\frac{2M}{\sqrt{r(r-2M)}}Q_2^1 = \frac{3(M-r)}{M}\ln\left(\frac{r}{r-2M}\right) + \frac{2M^2-12rM+6r^2}{r(r-2M)}, \tag{3.135}$$

$$Q_2^2 = \frac{3r(r-2M)}{2M^2}\ln\left(\frac{r}{r-2M}\right) + \frac{(r-M)(2M^2+6rM-3r^2)}{rM(r-2M)}. \tag{3.136}$$

In the weak-field approximation ($M/r \ll 1$) these formulae take the form in the leading order

$$\frac{2M}{\sqrt{r(r-2M)}}Q_2^1 \approx \frac{4}{5}\frac{M^4}{r^4}, \quad Q_2^2 \approx \frac{8}{5}\frac{M^3}{r^3}. \tag{3.137}$$

When the simplified deflection angle formula for the HT metric (3.123) obtained in the weak-field approximation is considered, it can be extended by the additional quadrupole and plasma terms as

$$\begin{aligned}\alpha_{HT} &= 2\int_R^\infty f_{HT}(r)dr - \pi \\ &= 2\int_R^\infty \left[f_{HT0}(r) + \frac{R}{r\sqrt{r^2-R^2}}\left(f_K(r)+f_{pl}(r)\right)\right]dr - \pi,\end{aligned} \tag{3.138}$$

where the partial terms were already derived and take the form given by (3.115), (3.132), and (3.133).

Integration of the additional terms in comparison to the vacuum and the $K=0$ case returns

$$\begin{aligned}&\int_R^\infty \frac{R}{r\sqrt{r^2-R^2}}f_K(r)dr = \frac{2}{5}K\int_R^\infty\left[\frac{M^4(R^4-r^2R^2-r^4)}{r^5R^3\sqrt{r^2-R^2}} + \frac{4M^3(r^3-R^3)}{r^2R^2(r^2-R^2)^{3/2}}\right]dr \\ &= \frac{2}{5}K\left(-\frac{9\pi M^4}{16R^4} + \frac{8M^3}{R^3}\right),\end{aligned} \tag{3.139}$$

$$\begin{aligned}&\int_R^\infty \frac{R}{r\sqrt{r^2-R^2}}f_{pKerr}(r)dr = \frac{R}{2\omega_0^2}\int_R^\infty \frac{r(\omega_p^2(r)-\omega_p^2(R))dr}{(r^2-R^2)^{3/2}} = \frac{1}{2}\alpha_{refr}(R), \\ &\int_R^\infty \frac{R}{r\sqrt{r^2-R^2}}f_{pHT}(r)dr = \frac{4KM^3}{5\omega_0^2}\int_R^\infty \frac{\left(R^3\omega_p^2(r)-r^3\omega_p^2(R)\right)dr}{r^2R^2(r^2-R^2)^{3/2}} = \frac{1}{2}\alpha_{refrHT}(R).\end{aligned} \tag{3.140}$$

In the case of a homogeneous plasma when $\omega_p(r)=\omega_p(R)$, angle α_{refr} vanishes.

Combining all the above calculated terms gives the complete form of the deflection angle in the HT metric in the weak-field approximation in the form

$$\alpha = \alpha_{HT0} + \frac{32}{5}\frac{KM^3}{R^3} - \frac{9\pi}{20}\frac{KM^4}{R^4} + \alpha_{refr}(R) - \alpha_{refrHT}(R). \tag{3.141}$$

To provide a specific example of a plasma profile, let me define the plasma frequency as $\omega_p^2(r) = \mathcal{C}r^{-k}$, where $\mathcal{C}$ and k are constants. Then, the last two terms of (3.141) can be written as

$$\alpha_{refr}(R) = -\frac{R\mathcal{C}k}{\omega_0^2}\int_R^\infty \frac{r^{-k-1}dr}{(r^2-R^2)^{1/2}} = \frac{\mathcal{C}k}{\omega_0^2 R^k}\int_0^1 \frac{u^k du}{(1-u^2)^{1/2}} \tag{3.142}$$
$$= \frac{\mathcal{C}\sqrt{\pi}}{\omega_0^2 R^k}\frac{\Gamma\left(\frac{k}{2}+\frac{1}{2}\right)}{\Gamma\left(\frac{k}{2}\right)},$$

$$\alpha_{refrHT}(R) = -\frac{8KM^3R\mathcal{C}(k+3)}{5\omega_0^2}\int_R^\infty \frac{r^{-k-4}dr}{(r^2-R^2)^{1/2}} \tag{3.143}$$
$$= \frac{8KM^3\mathcal{C}(k+3)}{5\omega_0^2 R^{k+3}}\int_1^0 \frac{u^{k+3}du}{(1-u^2)^{1/2}} = \frac{8KM^3\mathcal{C}\sqrt{\pi}}{5\omega_0^2 R^{k+3}}\frac{\Gamma\left(\frac{k}{2}+2\right)}{\Gamma\left(\frac{k}{2}+\frac{3}{2}\right)},$$

where

$$\Gamma(z) = \int_0^\infty t^{z-1}e^{-t}dt. \tag{3.144}$$

Formula (3.142) was already derived in Bisnovatyi-Kogan and Tsupko [2010]. However, in the present approximation the deflection angle depends also linearly on the quadrupole moment Q, as seen in (3.143) when recalling that $K \sim Q$.

3.2.3 Visual comparison

Having obtained analytical forms of the deflection angles in the Kerr and HT metrics in the weak-field approximation, it would be further instructive to demonstrate visually the difference between the exact and approximate solutions. Such comparison is performed in vacuum, i.e., no terms $\propto \omega_p$ are considered in the present section. This assumption is still valid because, as it is shown further, cold plasma presence basically causes only a decrease of the deflection angles when compared with vacuum, and this case hence provides an upper estimate of possible light deflection. This approach thus serves as a good estimate when using an exact formula is necessary. Note that in the case of very large radial distances (when $r \gg M$), terms proportional to all parameters but M become negligible and the solution takes the form of deflection in the Schwarzschild metric for an arbitrary spacetime.

Fig. 3.3 shows the dependence of the exact and approximate deflection angles in vacuum as functions of the closest radial distance R around an object described by the Kerr metric (panel a) and by the HT metric (panel b). The exact solutions for the deflection angles, obtained by using equation (2.70) with corresponding definitions of A, B, C, and P, are drawn by the solid curves, while the approximate relation calculated from either (3.107) or (3.141) where $\omega_p = 0$ is shown by the dashed curves. It is nicely seen that at sufficiently large radial distances in both cases, an approximate formula for the deflection angle can replace the exact solution with satisfactory accuracy. Moreover, it is clearly seen that whereas the exact solution at small radial distances asymptotically reaches the photon sphere radii, the approximate solution deviates and yields finite deflections even at smaller R. Because of the presence of the angular momentum, the Kerr and

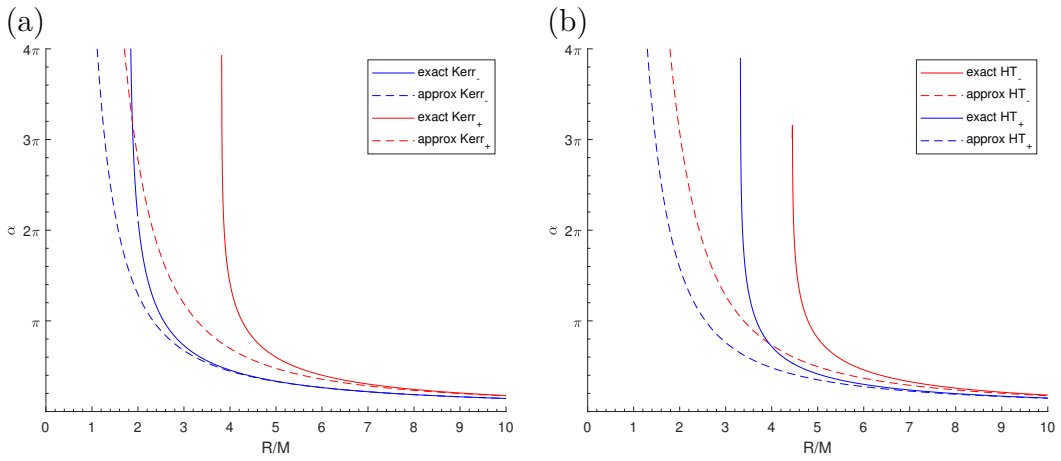

Figure 3.3: Exact and approximate deflection angles for the (a) Kerr metric with $J = 0.8$ and (b) HT metric with $J = 0.8$, $Q = 2.5$ as a function of minimal radial distance R. The deflection angles derived by using the exact general formula (2.70) are drawn by solid curves, and the approximate solutions calculated in the weak-field approximation are shown by the dashed curves.

HT metrics exhibit two branches of solutions, corresponding to the co-rotating (+)/counter-rotating (-) rays, respectively.

In Fig. 3.3a it can be seen that in the Kerr metric, sufficient correspondence (the difference is less than 10%) between the exact and approximate solutions occurs already around $4M$ in the branch with a negative sign of a, which is significantly closer to the photon sphere radius than the positive branch. On the contrary, the solution with a negative sign gives worse accuracy of the approximate solution in the HT metric (see Fig. 3.3b). This is caused by the different sign in the definition of J in the Kerr and HT metrics (for the correspondence between the Kerr and HT metric one has to set $J = -Ma$, cf. Hartle and Thorne [1968]). Hence, the branches are transposed. The angular momentum values were set to be equal to $J = 0.8$ in both cases to directly expose the effect of the quadrupole moment. The quadrupole moment in Fig. 3.3b was chosen to be $Q = 2.5$. In comparison with the Kerr metric, due to the presence of the quadrupole moment the position of the photon sphere radius is further in radial distances for both branches in the HT metric case. In the Kerr metric the correspondence between the approximate and exact solutions occurs already around $4M$ in the negative branch and around $7M$ in the positive branch. On the contrary, in the HT metric the coincidence of both solutions in the negative branch is at around $8M$ and in the positive branch it is at around $6M$.

3.3 Plasma Effect on Light Trajectories

Having studied the relevance of the weak-field approximation, it is desirable to include plasma in the model. In the remaining parts, the exact formula (2.70) is applied because the plasma effect can thus be solved completely, rather than concentrating only on its highest contribution part. It is expected that the presence of plasma will change the light deflection in the vicinity of a gravitating object and that this modification will depend on the plasma properties. According to Per-

lick and Tsupko [2024], the plasma frequency was defined as $\omega_p(r)^2 = 10\omega_0^2 \left(\frac{M}{r}\right)^k$, where $k = 3/2, 5/2, 7/2$, respectively. This is a useful definition of a plasma because it has a natural profile at large radial distances, it is expressed as a function of the ratio M/r which was previously discussed in connection with the weak-field approximation, and it is a function of the constant of motion ω_0 which can be further set equal to 1. The deflection angles around an object described by the Schwarzschild and Kerr metrics surrounded by a plasma with the above defined profile were previously studied in Perlick and Tsupko [2024]. Note that the parameter M occurring in the definition of $\omega_p(r)$ is characterized as the mass of a given gravitating object, and it has hence the same interpretation as in the expansion terms in the weak-field approximation.

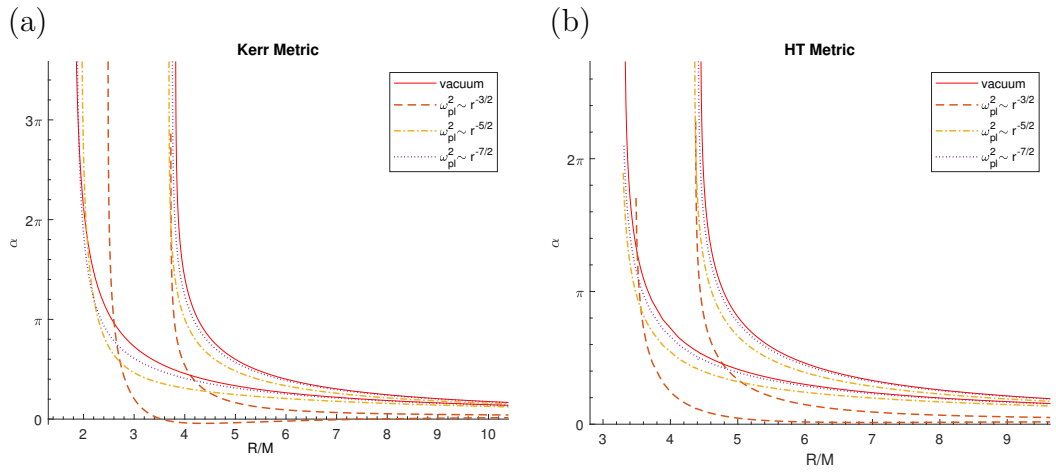

Figure 3.4: Comparison of the deflection angles in vacuum (solid red curves) and various plasma cases (dashed, dot-dashed, and dotted curves) for the (a) Kerr metric with $J = 0.8$ and (b) HT metric with $J = 0.8$, $Q = 2.5$. In panel (a), the branch closer to $R/M = 0$ corresponds to the rays with negative angular momentum, the other to rays with positive angular momentum. In panel (b), the rays with negative angular momentum occur in the branch further from the origin.

Exact solutions for the deflection angle α as a function of R in vacuum and in a plasma with different profiles defined by the specific choice of k are shown in Fig. 3.4. Results obtained for the Kerr metric are shown in panel (a), while for the HT metric they are plotted in panel (b). Red solid curves show the deflection angles obtained in vacuum, and the dashed curves demonstrate the deflection-angle behaviour in plasma. The obtained results clearly demonstrate a statement already mentioned that the light rays in the presence of plasma are less bent than in vacuum. Although this finding might seem to be counterintuitive, it is absolutely logical when one recalls that the refractive index in a plasma is < 1, while in common non-vacuum media with $n > 1$ the rays would be bent more. Moreover, from the definition of the plasma frequency (or more precisely the plasma density[2]) one can also see that the plasma effects become substantially

[2]When taking $\omega_p^2(r) = \mathcal{C}_e N(r)$, where $\mathcal{C}_e$ is a constant factor and $N(r)$ usually stands for electron density, it can be easily seen that the radial dependence of plasma frequency is actually given by the definition of plasma density.

weak with a larger radial distance and the plasma effect is hence more attenuated than for a gradual decrease in vacuum. The chosen profile of plasma frequency functions thus results in the fact that the plasma frequency significantly decreases at larger r and the light deflection in plasma is then close to deflection angles in vacuum. The deflection angles at small radial distances are generally limited by the photon sphere radius.

Notice the peculiar profile of the deflection angle in plasma with $k = 3/2$ (brown dashed curves), where is the plasma effect substantially stronger than in the other cases. The deflection angle is in this case steeply decreased already at low R, much closer to the photon sphere radius, and it remains significantly lower than in the vacuum or other plasma cases even at large radial distances. This represents a nice manifestation that plasma presence can indeed substantially change the deflection angles not only sufficiently close to the gravitating object, but this effect can also remain at larger radial distances. However, for such a significant behaviour the definition of plasma frequency must be chosen appropriately. Still, one can detect a system where the rays are potentially less influenced by gravity (their closest radial distance is large), but they are continually influenced by the plasma.

Furthermore, the deflection angles for the Kerr metric with negative angular momentum in plasma where $k = 3/2$ are slightly negative at small R. This feature can be observed at radial distances between around $3.5M$ and $6M$. Such values can be understood as a situation when light ray in fact bends to the opposite side and plasma presence thus causes a completely different trajectory than in vacuum. Although for the chosen toy plasma profiles the revealed negative deflection angles are small, in some other types of plasmas this effect could be more apparent.

The substantial difference between the HT metric and the Kerr metric is the choice of the quadrupole moment. It would be expected that the quadrupole moment present in the HT metric would lead to a quantitative change of the deflection angles (they are in general larger than in the Kerr metric), but no significant qualitative change is observed. The most significant effect of plasma on the deflection angles occurs in the range from the photon sphere radius to few closest radial distances, with specific values varying in both solution branches. The solution with the negative angular momentum in the Kerr metric (corresponding to positive angular momentum in the HT metric) has the most obvious plasma influence at radial distances up to around $6M$, while in the branch with the positive angular momentum in the Kerr metric (negative branch in the HT metric) this effect extends slightly further, approximately between $7M$ and $8M$.

3.4 Ray Tracing in Axisymmetric Spacetimes

To make the derived results even more instructive, they are presented in the following paragraph as individual rays propagating around given gravitating objects. The plasma definition introduced in the previous section is used, with the same choices of the coefficient k, except $k = 3/2$ omitted because the obtained ray trajectories are rather disorganized with all these choices.

For deriving the individual ray trajectories the equations of motion (2.57), (2.58) and the corresponding relations for p_φ and p_r were applied. The plots were computed for all rays starting at the same initial point, but having different

impact parameters (defined by Eq. (2.69)), $2, 5, 8, 10$ specifically. Note that there is a connection between the impact parameter b and the closest radial distance R applied in the previous sections which was studied in detail in Appendix D of Bezděková and Bičák [2023].

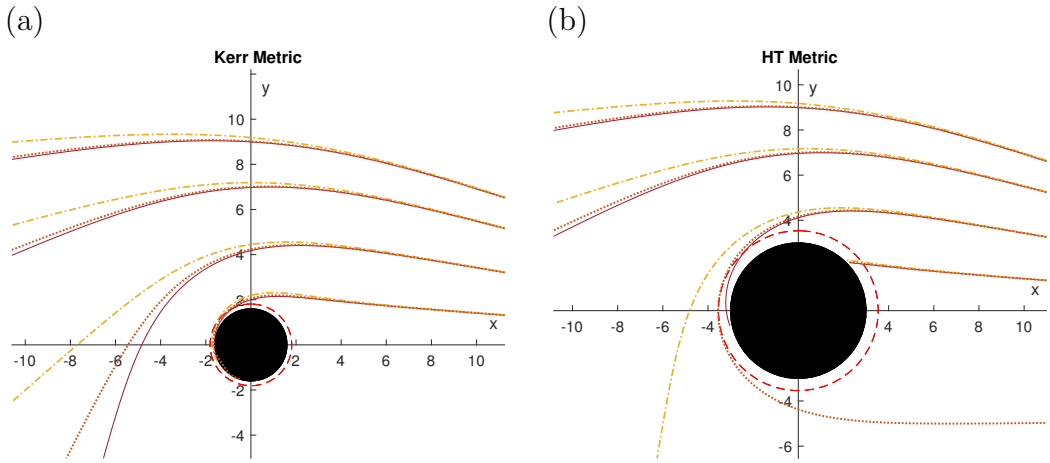

Figure 3.5: Comparison of ray trajectories characterized by impact parameters with values $2, 5, 8, 10$ in vacuum (solid lines) and plasma cases (dash-dotted and dotted lines) when $k = 5/2$ (yellow) and $k = 7/2$ (orange). The dashed circle shows the circular photon orbit. The compact gravitating object corresponds to (a) the Kerr metric with $J = 0.8$ and (b) the HT metric with $J = 0.8$, $Q = 2.5$.

The ray behaviour around an object described by the Kerr and HT metrics is shown in panels (a) and (b) of Fig. 3.5, respectively. Trajectories of rays propagating in vacuum are plotted by solid purple curves and those propagating in a plasma are shown by the dash-dotted and dotted curves. Rays in a plasma with $k = 5/2$ are marked yellow, while rays in a plasma with $k = 7/2$ are marked orange. The obtained ray trajectories clearly show that the rays in a plasma are generally less bent than in vacuum as $n < 1$. Additionally, the higher value of k causes the rays to be less bent.

The position of the circular photon orbits is drawn by red dashed circles. However, objects described by the Kerr and HT metrics have actually two circular photon orbits, one for co-rotating, the other for counter-rotating rays. Not to make the figure too crowded, only orbits with a positive angular momentum as defined in the HT metric are considered in the presented plots. Radii of black circles representing the size of the chosen gravitating object are defined as their event horizons.

The obtained ray profiles clearly demonstrate that the rays of one impact parameter can be captured by the black hole or not, but this strongly depends on the chosen plasma profile. This is particularly obvious for the HT metric in Fig. 3.5b. However, when the impact parameters are too small, even an arbitrary plasma profile cannot secure the rays from being captured by the black hole.

The plots also show how significantly different the ray trajectories generally can be and it is also clear that the plasma enters the overall results as a significant participant. Additionally, it is evident that the effect of the plasma decreases for rays with larger impact parameters, which is a consequence of the gradual decrease of the plasma density so that the light trajectories are then less affected

by its presence. Moreover, the gravitation of the central object is also weaker at distances corresponding to larger impact parameters.

Fig. 3.5 also illustrates the effect of the quadrupole moment. Comparing the objects characterized by the Kerr and HT metrics with the same angular momentum, it is apparent that the one defined by the HT metric has a significantly larger event horizon than in the case of the Kerr metric and it thus influences the ray trajectories with larger impact parameters. It is obvious that a larger quadrupole moment causes larger effects at sufficiently further radial distances and it hence leads to strong changes of light trajectories with high impact parameters.

4. Light Deflection in a Moving Medium

Calculations performed in this chapter are carried out in settings different from those assumed in the previous sections. While an axially symmetric stationary spacetime was assumed for deriving the results in Chapter 2, one step backwards is now taken and a black hole described by a spherically symmetric metric is considered. The reason for this lies in various definitions of the medium surrounding the object which is here more complicated. An overwhelming majority of previous studies employing Synge's approach focuses on systems where just non-moving cold plasma occurs. Even though this approximation has many useful properties, as discussed in detail in the following section, it is not sufficient and it is hence desirable to study other media. Possible solutions how this can be performed in the suggested formalism are presented below. The results described in this chapter were originally presented in Bezděková et al. [2024].

4.1 Uniqueness of Cold Plasma Approximation and Going Beyond

As indicated in previous chapters, the cold plasma approximation is very frequently used in systems describing light propagation in the vicinity of a compact gravitating object surrounded by a refractive and dispersive medium. Indeed, the Hamiltonian for light in a cold plasma in relativistic applications is very specific with several important properties.

To derive the Hamiltonian (1.48), one has to define the medium equation for the cold plasma first. This approximation is applied in systems in which it is assumed that the thermal velocity of the medium is much lower than the wave phase speed, i.e.,

$$\frac{\omega}{k} \gg v_{th}. \tag{4.1}$$

In the most extreme case the thermal velocity is set to zero. The refractive index in this case can be expressed from the equation

$$n^2 = 1 - \frac{\omega_p^2(x^\alpha)}{\omega^2(x^\alpha)}. \tag{4.2}$$

The plasma frequency $\omega_p(x^\alpha)$ is defined by expression (1.49), while the wave frequency $\omega(x^\alpha)$ can be derived from relation (1.45).

Applying the definition of the refractive index (4.2) in the medium equation (1.46) yields

$$\omega_p^2(x^\alpha) = -p^\beta p_\beta, \tag{4.3}$$

which represents the relativistic form of the dispersion relation in a cold plasma between the plasma frequency ω_p and the frequency 4-vector p_β. Moreover, plugging (4.2) in the general formula (1.44) leads to the Hamiltonian in the form given by (1.48). For convenience, it is copied here again in view of the following

discussion, i.e.,

$$\mathcal{H}(x^\alpha, p_\alpha) = \frac{1}{2}\left[g^{\beta\delta}p_\beta p_\delta + \omega_p^2(x^\alpha)\right].$$

The Hamiltonian given above is independent of the medium velocity V^α due to the specific form of refractive index given by (4.2).

However, it is still necessary to characterize the photon frequency ω which *is* a function of the medium velocity. The reason for this originates from the fact that the refractive index n has to be real in regions where the rays can occur, at least in principle. This is satisfied when $\omega \geq \omega_p$. This condition would have to be studied independently for any rays described solely by Hamilton's equations. Fortunately, the theory involves one supplemental restriction set on the Hamiltonian itself which guarantees its conservation, i.e., $\mathcal{H}(x^\alpha, p_\alpha) = 0$. This directly leads to the conclusion that for the light rays one gets $\omega = \sqrt{k^2 + \omega_p^2}$, and the condition $\omega \geq \omega_p$ thus holds automatically.

The fact that the Hamiltonian above is independent of the plasma velocity has several consequences for light propagation. Due to it, light rays moving in a cold plasma are not directly affected by the motion of the medium and their trajectories thus remain the same for both static and moving cold plasma, while their constants of motion do not change. This means that two rays with identical photon frequency at infinity and identical impact parameters follow the same paths even though one travels in a static cold plasma and the other in a moving cold plasma.

Note that the photon Hamiltonian above is formally identical to the Hamiltonian of a particle with mass m moving in the gravitational field in vacuum, which has the form [Misner et al., 1973]

$$\mathcal{H}(x^\alpha, p_\alpha) = \frac{1}{2}\left[g^{\beta\delta}p_\beta p_\delta + m^2\right]. \tag{4.4}$$

If the cold plasma is homogeneous and hence $\omega_p(x^\alpha) = const.$, this correspondence can be used for an alternative interpretation of the discussed Hamiltonian: it describes a particle (*photon*) with an effective mass ω_p moving in the gravitational field in vacuum. However, this equivalence is still useful even in a non-homogenous plasma, i.e., when $\omega_p(x^\alpha) \neq const.$ Although the intuition is not so straightforward in this case, the Hamiltonian (1.48) can be viewed as one describing the motion of a massive particle in vacuum with a dissipating/fluctuating effective mass (depending on the exact definition of ω_p). This also demonstrates the known fact that photons in a plasma generally do not follow geodesics, which is a consequence of the refractive nature of the plasma. Nevertheless, note that the *physical* momentum and mass of a particular photon differ from p and ω_p discussed here, as they formally read $\hbar p$ and $\hbar\omega_p$, respectively. For a detailed discussion about this feature of the cold plasma approximation, see Kulsrud and Loeb [1992].

Besides its useful algebraic properties which significantly simplify the calculations of specific problems, the cold plasma approximation is also relevant in many astrophysical applications, at least up to the first order in relevant parameters. Cold plasma is believed to occur in the interstellar medium or in the ionospheres of planets (in the vicinity of the Earth it has been studied for decades). However, it is evident that it is not always reasonable to assume just the cold plasma

approximation. Hot plasma forms stars, black hole accretion discs, or astrophysical jets. When one wants to proceed one step further and see how different velocity definitions impact the light trajectories, it is necessary to abandon the cold plasma approximation. Moreover, a non-static medium has to be assumed. In principle, there are several physically relevant ways how to define the medium velocity satisfying the given conditions. These are discussed in following sections.

4.2 Radially Falling Medium

Contrary to the previous chapters, propagation of light rays in this section is assumed around a gravitating object described by a general spherically symmetric metric and the medium surrounding the object is moving in the radial direction. This assumption can be applied to describe radially falling matter onto a black hole. A general form of the deflection angle in this case is discussed first, where it is also indicated which difficulties occur in this general approach. Application of the general formalism to three particular forms of the refractive index is performed afterwards.

4.2.1 Deflection angle in general

The metric describing a spherically symmetric and static object can be generally written as

$$ds^2 = -A(r)dt^2 + B(r)dr^2 + C(r)(d\vartheta^2 + \sin^2\vartheta\, d\varphi^2), \tag{4.5}$$

where $A(r)$, $B(r)$, and $C(r)$ are positive functions. Moreover, note that because the spacetime is regarded to be spherically symmetric, they are solely functions of radial coordinate. This assumption is also true for the considered dispersive medium, as its refractive index takes on the general form $n(r, \omega(r))$, i.e., it is spherically symmetric as well.

As it was already discussed above, the medium surrounding the compact object is not static (this was assumed in Section 2.4 where $V^i = 0$); instead, it is falling towards a black hole. Hence, the individual 4-velocity components of the medium are defined as

$$V^\alpha = (V^0, V^r, 0, 0). \tag{4.6}$$

Moreover, it is required that the V^r component is only a function of radial coordinate, i.e.,

$$V^r = f(r). \tag{4.7}$$

Because the medium is expected to fall radially on the compact object, it is assumed $f(r) < 0$.

It is now easy to find V^0 from the normalization condition

$$V^\alpha V_\alpha = -1, \tag{4.8}$$

which in this case leads to the expression

$$V^0(r) = \sqrt{\frac{1 + B(r)f^2(r)}{A(r)}}. \tag{4.9}$$

To make the desired formulae more compact, it will be further written just $V^0(r)$, keeping in mind its actual form given by (4.9) which can be substituted anywhere as needed.

The photon frequency generally given by (1.45) now has to be derived from the relation

$$\omega(r) = -p_t V^0(r) - p_r V^r = -p_t V^0(r) - p_r f(r). \tag{4.10}$$

Although the photon frequency is obtained from a more complicated relation than for the static medium, it still is only a function of r, independent of time, and p_t is hence again a constant of motion. This conclusion can be also derived from the equation of motion for $\dot{p}_t$.

The introduced spacetime is assumed to be asymptotically flat, i.e., it satisfies $A(r) \to 1$, $B(r) \to 1$ at $r = \infty$. Moreover, $f(r) \to 0$ at $r = \infty$ and also, to define the deflection angle properly, $C(r)/r^2 \to 1$ for $r = \infty$. Due to that, the expression (4.10) at infinity gives the relation between ω_0 (the photon frequency at infinity) and the constant of motion p_t in the same form as in the previous chapters, i.e.,

$$p_t = -\omega_0. \tag{4.11}$$

For further applications, it is more convenient to rewrite equation (4.10) as a function of ω_0 in the form

$$\omega(r) = \omega_0 V^0(r) - p_r f(r). \tag{4.12}$$

In comparison to the axially symmetric spacetime, the equatorial plane, where $\vartheta = \pi/2$ and $p_\vartheta = 0$, can be considered without a loss of generality. Applying the metric in the form (4.5) and the photon frequency given by (4.10) in the Hamiltonian (1.44) leads to

$$\mathcal{H}(x^\alpha, p_\alpha) = \frac{1}{2}\left[\frac{p_r^2}{B(r)} + \frac{p_\varphi^2}{C(r)} - \frac{\omega_0^2}{A(r)} + w(r, \omega(r))\right], \tag{4.13}$$

where

$$w(r, \omega(r)) = -(n^2 - 1)\omega^2(r), \quad n = n(r, \omega(r)). \tag{4.14}$$

The function $w(r, \omega(r))$ will be exploited further when it will be necessary to capture the main properties of light propagation in a medium in the gravitational field for which it is more useful than the refractive index $n(r, \omega(r))$ alone. Note that in a cold plasma $w = \omega_p^2(r)$.

The equations of motion for p_t and p_φ are

$$\dot{p}_t = -\frac{\partial \mathcal{H}}{\partial t} = 0, \tag{4.15}$$

$$\dot{p}_\varphi = -\frac{\partial \mathcal{H}}{\partial \varphi} = 0, \tag{4.16}$$

and it can be explicitly seen that both p_t and p_φ are indeed constants of motion.

The equation of motion for coordinate r yields

$$\dot{r} = \frac{\partial \mathcal{H}}{\partial p_r} = \frac{p_r}{B(r)} + \frac{1}{2}\frac{\partial w}{\partial \omega}\frac{\partial \omega(r)}{\partial p_r}, \tag{4.17}$$

and it can be further rewritten with the usage of relation (4.10). Moreover, introducing the variable $w_\omega(r;\omega_0) \equiv \partial w/\partial\omega$ (defined solely for a concise formulation of the expressions) leads to the form

$$\dot{r} = \frac{p_r}{B(r)} - \frac{1}{2} w_\omega(r;\omega_0) f(r). \tag{4.18}$$

The equation of motion for φ is

$$\dot{\varphi} = \frac{\partial \mathcal{H}}{\partial p_\varphi} = \frac{p_\varphi}{C(r)}. \tag{4.19}$$

To obtain a fully analytic form of the deflection angle, it is desirable to find an expression for p_r which could be applied in further calculations. This is typically performed by applying the condition $\mathcal{H}(x^\alpha, p_\alpha) = 0$, where the form of $\mathcal{H}(x^\alpha, p_\alpha)$ would be taken in this general case from (4.13). The obtained relation for p_r would be then plugged into (4.18) and this would be further used along with (4.19) to derive the corresponding equation for $d\varphi/dr$. However, generally it is not guaranteed that this procedure allows one to find an analytic formula for p_r. Nevertheless, searching for a form of p_r can be always performed numerically at least.

In the further step, let me assume that an analytic expression for $p_r(r; p_\varphi, \omega_0)$ exists. Then, applying (4.18) and (4.19) leads to a general relation

$$\frac{d\varphi}{dr} = \frac{p_\varphi}{C(r)} \left(\frac{p_r(r; p_\varphi, \omega_0)}{B(r)} - \frac{1}{2} w_\omega(r;\omega_0) f(r) \right)^{-1}. \tag{4.20}$$

The deflection angle can be derived by integrating the obtained relation from the closest radial distance R reached by the ray to infinity. It is now desirable to obtain the final formula as a function of R and ω_0 only, as it is assumed that these two quantities can be in principle evaluated (ω_0 is measurable), while the value of p_φ is more problematic. To exclude p_φ from the formula, one has to find $p_\varphi(R;\omega_0)$ which can be derived from the expression

$$\frac{p_r(R; p_\varphi, \omega_0)}{B(R)} - \frac{1}{2} w_\omega(R;\omega_0) f(R) = 0. \tag{4.21}$$

This equation was obtained from the constraint at $r = R$ where $dr/d\varphi = 0$. Note that this condition actually defines the position of the closest radial distance R.

4.2.2 Deflection angle for three particular examples

As it was outlined in the previous section, an analytic formula for the deflection angle ($d\varphi/dr$) can be written if and only if the exact analytic expression for p_r can be derived, which is typically found from the condition $\mathcal{H}(x^\alpha, p_\alpha) = 0$. This evidently cannot be performed in a general case without knowing the specific form of the function $w(r, \omega(r))$, which is generically defined by (4.14) and it might depend on the photon frequency $\omega(r)$ in a complicated way. Note that the dependence of $w(r, \omega(r))$ on $\omega(r)$ is crucial, as the photon frequency is a function of p_r, which can be seen in (4.12).

When the form of the refractive index and its dependence on the photon frequency are known, it is possible to find an analytic solution for the deflection angle in the integral form, even if the refractive index is not specified for a particular physical situation. For instance, when one assumes a rather general form of the refractive index, such as

$$n^2(r,\omega(r,p_r)) = a_0(r) + \frac{a_1(r)}{\omega(r,p_r)} + \frac{a_2(r)}{\omega^2(r,p_r)}, \tag{4.22}$$

where coefficients $a_0(r)$, $a_1(r)$ and $a_2(r)$ are some functions of r, the deflection angle formula can be derived. The functions $a_0(r)$, $a_1(r)$, and $a_2(r)$ can attain any values, positive, zero, or negative, requiring only that the overall expression for n^2 is non-negative and the corresponding group velocity in such a medium is less than c.

Taking the refractive index in the form (4.22) and the Hamiltonian (4.13) gives

$$\begin{aligned}\mathcal{H}(x^\alpha,p_\alpha) = \frac{1}{2}\Bigg[&\frac{p_r^2}{B(r)} + \frac{p_\varphi^2}{C(r)} - \frac{\omega_0^2}{A(r)} - a_0(r)\omega^2(r,p_r) - a_1(r)\omega(r,p_r) \\ &-a_2(r) + \omega^2(r,p_r)\Bigg],\end{aligned} \tag{4.23}$$

where the expression for $\omega(r,p_r)$ is known from (4.12).

After applying the definition of $\omega(r,p_r)$, the Hamiltonian (4.23) becomes a quadratic polynomial of p_r, which is quite convenient for finding a solution for p_r. This leads to a compact analytic form of the deflection angle. In order to find the solution, it is suitable to rewrite the Hamiltonian (4.23) as

$$\mathcal{H}(x^\alpha,p_\alpha) = \frac{1}{2}\left[\mathcal{A}_r(r)p_r^2 + 2\mathcal{B}_r(r)p_r + \mathcal{C}_r(r,p_\varphi)\right]. \tag{4.24}$$

The functions $\mathcal{A}_r(r)$, $\mathcal{B}_r(r)$, $\mathcal{C}_r(r,p_\varphi)$ depend on r, possibly on p_φ, and they should not be replaced by the metric coefficients introduced in (4.5). Furthermore, they can also contain ω_0 as a parameter. When the velocity of the medium is given by (4.6), without loss of generality the function $\mathcal{C}_r(r,p_\varphi)$ can be defined as follows

$$\mathcal{C}_r(r,p_\varphi) = \frac{p_\varphi^2}{C(r)} - \frac{\omega_0^2}{A(r)} + \mathcal{C}_{r1}(r). \tag{4.25}$$

The functions introduced in the Hamiltonian (4.24) can be expressed as functions of the metric coefficients and variables in the refractive index (4.22), namely

$$\mathcal{A}_r(r) = \frac{1}{B(r)} + (1-a_0(r))f^2(r), \tag{4.26}$$

$$\mathcal{B}_r(r) = \left[(a_0(r)-1)\,\omega_0 V^0(r) + \frac{1}{2}a_1(r)\right] f(r), \tag{4.27}$$

$$\mathcal{C}_r(r,p_\varphi) = \frac{p_\varphi^2}{C(r)} - \frac{\omega_0^2}{A(r)} - a_2(r) + \omega_0 V^0(r)\left[(1-a_0(r))\omega_0 V^0(r) - a_1(r)\right], \tag{4.28}$$

$$\mathcal{C}_{r1}(r) = -a_2(r) + \omega_0 V^0(r)\left[(1-a_0(r))\omega_0 V^0(r) - a_1(r)\right]. \tag{4.29}$$

To see some remarkable features of the Hamiltonian in the form (4.24), the deflection angle will be now calculated from it. First, one has to write down the equations of motion. They now take on a quite simple form,

$$\dot{r} = \mathcal{A}_r(r)p_r + \mathcal{B}_r(r), \tag{4.30}$$

and

$$\dot{\varphi} = \frac{p_\varphi}{C(r)}. \tag{4.31}$$

Then, p_r can be easily found from the condition $\mathcal{H}(x^\alpha, p_\alpha) = 0$ in a general form as

$$p_r = \frac{-\mathcal{B}_r(r) \pm \sqrt{\mathcal{B}_r^2(r) - \mathcal{A}_r(r)\mathcal{C}_r(r, p_\varphi)}}{\mathcal{A}_r(r)}, \tag{4.32}$$

or

$$\mathcal{A}_r(r)p_r + \mathcal{B}_r(r) = \pm\sqrt{\mathcal{B}_r^2(r) - \mathcal{A}_r(r)\mathcal{C}_r(r, p_\varphi)}. \tag{4.33}$$

Such an expression for p_r turns out to be very useful because after using it in the equation for $\dot{r}$ (4.30), one simply gets

$$\dot{r} = \pm\sqrt{\mathcal{B}_r^2(r) - \mathcal{A}_r(r)\mathcal{C}_r(r, p_\varphi)}. \tag{4.34}$$

This is quite a noteworthy observation – if the Hamiltonian can be written as (4.24), the condition $\mathcal{H}(x^\alpha, p_\alpha) = 0$ then straightforwardly leads to the algebraic equation for $\dot{r}$ in form (4.34). This simplifies the calculations significantly and the expression for deflection angle is just

$$\frac{d\varphi}{dr} = \pm\frac{p_\varphi}{C(r)}\left[\mathcal{B}_r^2(r) - \mathcal{A}_r(r)\mathcal{C}_r(r, p_\varphi)\right]^{-1/2}. \tag{4.35}$$

In order to make the obtained formula more compact and similar to the deflection angle relations presented in the previous studies [e.g., Tsupko, 2021, Bezděková and Bičák, 2023], it is further rewritten as

$$\frac{d\varphi}{dr} = \pm\frac{1}{\sqrt{\mathcal{A}_r(r)C(r)}}\left(\frac{\omega_0^2}{p_\varphi^2}h^2(r) - 1\right)^{-1/2}, \tag{4.36}$$

where the function

$$h^2(r) = \frac{C(r)}{A(r)}\left[1 + \frac{A(r)}{\omega_0^2}\left(\frac{\mathcal{B}_r^2(r)}{\mathcal{A}_r(r)} - \mathcal{C}_{r1}(r)\right)\right] \tag{4.37}$$

is a generalization of the function (2.63) originally introduced for the axially symmetric metric, but when setting $P(r) = 0$ it can be applied to the spherically symmetric case. Considering that $dr/d\varphi = 0$ at $r = R$ (at the closest radial distance), it can be stated that

$$\frac{p_\varphi^2}{\omega_0^2} = h^2(R), \tag{4.38}$$

and thus

$$\frac{d\varphi}{dr} = \pm\frac{1}{\sqrt{\mathcal{A}_r(r)C(r)}}\left(\frac{h^2(r)}{h^2(R)} - 1\right)^{-1/2}. \tag{4.39}$$

Note that the condition $dr/d\varphi = 0$ at $r = R$ can be achieved also when either $\mathcal{A}_r(R) = 0$ or $C(R) = 0$, but these cases are not relevant in the present discussion.

Finally, one can define the deflection angle α for light rays propagating from infinity to the black hole, reaching their closest radial distance, R, and heading back to infinity, in the form

$$\alpha = 2 \int_R^\infty \frac{1}{\sqrt{\mathcal{A}_r(r) C(r)}} \left(\frac{h^2(r)}{h^2(R)} - 1 \right)^{-1/2} dr \, - \, \pi \, . \tag{4.40}$$

As it was carefully analyzed above, the expression is independent of the constant p_φ and the formula (4.40) thus depends solely on the closest approach R and the photon frequency at infinity ω_0. Note that an analogous expression for the deflection angle in vacuum would depend only on R.

Let me emphasize that the relation (4.40), eventually (4.39), was obtained considering a quite general refractive index (4.22) and the Hamiltonian in the specific form (4.24), where functions $\mathcal{A}_r(r)$, $\mathcal{B}_r(r)$, and $\mathcal{C}_r(r, p_\varphi)$ are arbitrary. With a such-defined Hamiltonian it is possible to identify the dependence on p_r easily. When the functions $\mathcal{A}_r(r)$, $\mathcal{B}_r(r)$, and $\mathcal{C}_r(r, p_\varphi)$ are defined for a chosen refractive index function, the deflection angle formula can be found by substituting the corresponding values in (4.40). The specific form of the deflection angle hence depends on the chosen plasma profile.

In principle, there are at least three examples with different definitions of the refractive index which can be solved analytically. All of them are described by the Hamiltonian (4.24) with prescribed forms of the functions $\mathcal{A}_r(r)$, $\mathcal{B}_r(r)$, and $\mathcal{C}_r(r, p_\varphi)$. Below, these are identified for the discussed examples and the final expressions for the corresponding functions $h^2(r)$ are presented as well.

Example 1. – cold plasma

This well-known plasma definition is characterized by a refractive index generally given by (4.2). However, in this particular case let me assume a simpler definition, namely

$$n^2 = 1 - \frac{\omega_p^2(r)}{\omega^2(r)}. \tag{4.41}$$

Then, the function $w(r, \omega(r))$ introduced by (4.14) is independent of $\omega(r)$, and it reduces to

$$w(r, \omega(r)) = \omega_p^2(r). \tag{4.42}$$

Furthermore, both expressions (1.48) and (4.13) can be applied in this case to derive the Hamiltonian in the form

$$\mathcal{H}(x^\alpha, p_\alpha) = \frac{1}{2} \left[\frac{p_r^2}{B(r)} + \frac{p_\varphi^2}{C(r)} - \frac{\omega_0^2}{A(r)} + \omega_p^2(r) \right]. \tag{4.43}$$

Knowing all the relations defined above, it is easy to find the functions $\mathcal{A}_r(r)$, $\mathcal{B}_r(r)$, and $\mathcal{C}_{r1}(r)$. These are now

$$\mathcal{A}_r(r) = \frac{1}{B(r)}, \tag{4.44}$$

$$\mathcal{B}_r(r) = 0, \tag{4.45}$$

$$\mathcal{C}_{r1}(r) = \omega_p^2(r). \tag{4.46}$$

The deflection angle formula (4.40) is simplified to

$$\alpha = 2\int_R^\infty \sqrt{\frac{B(r)}{C(r)}}\left(\frac{h^2(r)}{h^2(R)}-1\right)^{-1/2} dr - \pi, \tag{4.47}$$

and the function $h(r)$ here is given by

$$h^2(r) = \frac{C(r)}{A(r)}\left(1 - A(r)\frac{\omega_p^2(r)}{\omega_0^2}\right). \tag{4.48}$$

This is a more general approach how to calculate already known results, but from a broader perspective. Note that expressions (4.47) and (4.48) were previously obtained in Perlick et al. [2015]; see their Eqs.(20) and (17), respectively.

Example 2. – non-dispersive medium

In this medium the refractive index is solely a function of r, i.e., it is independent of the photon frequency $\omega(r)$ and hence

$$n = n(r). \tag{4.49}$$

The Hamiltonian in the equatorial plane for such a medium formally still takes the form of (4.13), namely

$$\mathcal{H}(x^\alpha, p_\alpha) = \frac{1}{2}\left[\frac{p_r^2}{B(r)} + \frac{p_\varphi^2}{C(r)} - \frac{\omega_0^2}{A(r)} + w(r,\omega(r))\right], \tag{4.50}$$

but n present in $w(r,\omega(r))$ is now only a function of r and the dependence on $\omega(r)$ is thus explicitly stated there.

From the known Hamiltonian the functions $\mathcal{A}_r(r)$, $\mathcal{B}_r(r)$, and $\mathcal{C}_{r1}(r)$ can be defined as

$$\mathcal{A}_r(r) = \frac{1}{B(r)} - (n^2(r)-1)f^2(r), \tag{4.51}$$

$$\mathcal{B}_r(r) = (n^2(r)-1)\omega_0 V^0(r) f(r), \tag{4.52}$$

$$\mathcal{C}_{r1}(r) = -(n^2(r)-1)(\omega_0 V^0(r))^2. \tag{4.53}$$

This yields the function $h(r)$ as

$$h^2(r) = \frac{C(r)}{A(r)}\left(1 + A(r)\frac{(n^2(r)-1)(V^0(r))^2}{1-(n^2(r)-1)B(r)f^2(r)}\right). \tag{4.54}$$

After applying this form of $h(r)$, it can be seen that the deflection angle is a function of $f(r)$ which is directly related to the motion of the medium. Hence, there is a clear difference in light deflection between a static and a moving medium.

Example 3. – general non-cold plasma medium

Let me assume a medium which is dispersive, but not a cold plasma, and which can be generally described by the refractive index

$$n^2 = 1 + \frac{a(r)}{\omega(r)}. \tag{4.55}$$

The Hamiltonian in the equatorial plane for light rays propagating in such a medium then is

$$\mathcal{H}(x^\alpha, p_\alpha) = \frac{1}{2}\left[\frac{p_r^2}{B(r)} + \frac{p_\varphi^2}{C(r)} - \frac{\omega_0^2}{A(r)} - a(r)\omega(r)\right]. \tag{4.56}$$

Note the different power of $\omega(r)$ in the Hamiltonian in this example in comparison with the non-dispersive case. The coefficients $\mathcal{A}_r(r)$, $\mathcal{B}_r(r)$, and $\mathcal{C}_{r1}(r)$ identified from the Hamiltonian (4.56) are

$$\mathcal{A}_r(r) = \frac{1}{B(r)}, \tag{4.57}$$

$$\mathcal{B}_r(r) = \frac{1}{2}a(r)f(r), \tag{4.58}$$

$$\mathcal{C}_{r1}(r) = -a(r)\omega_0 V^0(r). \tag{4.59}$$

Finally, the function $h(r)$ has the form

$$h^2(r) = \frac{C(r)}{A(r)}\left[1 + A(r)\frac{a^2(r)}{\omega_0^2}\left(\frac{1}{4}B(r)f^2(r) + \frac{\omega_0 V^0(r)}{a(r)}\right)\right]. \tag{4.60}$$

4.3 Rotating Medium

One more example of a moving medium is discussed below, namely a medium rotating in the equatorial plane of a spherically symmetric black hole, where it creates a geometrically thin accretion disc. The light propagation is considered to happen in this plane, but due to the symmetry of the system, the described configuration can be assumed without any loss of generality as the same setting including the medium would work in an arbitrary plane. The metric of the gravitating object is still given by (4.5).

Note that some relations already defined in the previous section are stated here again, since while they formally remain the same as for the radially falling medium, their implicit dependence on the discussed variables might be different.

As it was already described, the medium is now assumed to be rotating, which defines its 4-velocity components as

$$V^\alpha = (V^0, 0, 0, V^\varphi). \tag{4.61}$$

Again, V^φ can be introduced as a known function of r, i.e.,

$$V^\varphi = f(r). \tag{4.62}$$

Moreover, the velocity of the medium is independent of t, and so the component p_t is a constant of motion.

It is easy to obtain the form of V^0 from the 4-velocity normalization, which is very similar to the previous case (cf. (4.9)), leading to

$$V^0 = \sqrt{\frac{1 + C(r)f^2(r)}{A(r)}}. \tag{4.63}$$

As demonstrated in the previous section, it is more convenient to use only $V^0(r)$ in further calculations rather than the full expression, but it is suitable to have (4.63) at hand to be substituted as necessary.

The general form of the photon frequency (1.45) in this medium reduces to

$$\omega(r) = -p_t V^0(r) - p_\varphi V^\varphi = -p_t V^0(r) - p_\varphi f(r). \tag{4.64}$$

The spacetime metric is still defined the same as in the previous section, and it is still required that $f(r) \to 0$ at $r = \infty$. For this reason, one can see that $p_t = -\omega_0$. Hence, $\omega(r)$ given by the expression (4.64) can be rewritten to

$$\omega(r) = \omega_0 V^0(r) - p_\varphi f(r). \tag{4.65}$$

As stated above, it is assumed that both the motions of the photon and of the medium occur in the equatorial plane. As a result, $\vartheta = \pi/2$ and $p_\vartheta = 0$, and the Hamiltonian now is

$$\mathcal{H}(x^\alpha, p_\alpha) = \frac{1}{2}\left[\frac{p_r^2}{B(r)} + \frac{p_\varphi^2}{C(r)} - \frac{\omega_0^2}{A(r)} + w(r, \omega(r))\right], \tag{4.66}$$

which is formally identical with (4.13), except for the function

$$w(r, \omega(r)) = -(n^2 - 1)\omega^2(r), \quad n = n(r, \omega(r)) \tag{4.67}$$

expressed with the usage of (4.65) rather than (4.12).

Because $\omega(r)$ is now defined in a different way than in the previous section, also the Hamiltonian (4.66) and its dependence on p_r and p_φ vary in comparison with the Hamiltonian (4.13) discussed in the case of a radially falling medium. This difference will hence manifest itself also in a different approach to the calculation of the deflection angle. There are two terms proportional to p_r^2 in the Hamiltonian (4.13) (one stemming from $g^{\beta\delta}p_\beta p_\delta$, the other occurring in $w(r, \omega(r))$) and only one term proportional to p_φ^2. While the constant p_φ can be easily expressed from the restriction $\mathcal{H}(x^\alpha, p_\alpha) = 0$, the component p_r cannot, and it is hence necessary to search for possible simplifications how to solve this problem. In the Hamiltonian (4.66) the situation is quite the opposite. There is only one term including p_r and the component p_φ is present in one separate term and also inside the function $w(r, \omega(r))$. Thus, it is straightforward to find a relation for p_r from $\mathcal{H}(x^\alpha, p_\alpha) = 0$ in this case, but it does not hold for p_φ. For this reason, special attention has to be paid to how to express the dependence on p_φ.

The equations of motion for the Hamiltonian (4.66) are

$$\dot{r} = \frac{\partial \mathcal{H}}{\partial p_r} = \frac{p_r}{B(r)}, \tag{4.68}$$

$$\dot{\varphi} = \frac{\partial \mathcal{H}}{\partial p_\varphi} = \frac{p_\varphi}{C(r)} + \frac{1}{2}\frac{\partial w}{\partial \omega}\frac{\partial \omega(r)}{\partial p_\varphi}. \tag{4.69}$$

The equations of motion for p_t and p_φ remain completely identical to those obtained in the previous case in the form (4.15) and (4.16), respectively. Consequently, both are the constants of motion. It is further useful to express the derivative $\partial\omega(r)/\partial p_\varphi$ explicitly, which yields

$$\dot{\varphi} = \frac{p_\varphi}{C(r)} - \frac{1}{2} w_\omega(r; \omega_0) f(r). \tag{4.70}$$

The differentiation term $w_\omega(r;\omega_0)$ formally corresponds to the one present in (4.18), but $\omega(r)$ inside is now defined with (4.65).

Unlike for the radially falling medium, here one can easily derive an equation for p_r from the condition $\mathcal{H}(x^\alpha, p_\alpha) = 0$. It takes the form

$$p_r = \pm\sqrt{B(r)}\sqrt{\frac{\omega_0^2}{A(r)} - \frac{p_\varphi^2}{C(r)} - w(r,\omega(r))}. \tag{4.71}$$

When the desired expression for p_r is applied in (4.68), the equation for the ray trajectory can be written as

$$\frac{d\varphi}{dr} = \pm\sqrt{\frac{B(r)}{C(r)}}\left\{\frac{\frac{C(r)}{p_\varphi^2}\left[\frac{\omega_0^2}{A(r)} - w(r,\omega(r))\right] - 1}{\left[1 - \frac{C(r)}{2p_\varphi}w_\omega(r;\omega_0)f(r)\right]^2}\right\}^{-1/2}. \tag{4.72}$$

It is further useful to get rid of p_φ in the trajectory equation and express the deflection angle again solely as a function of R and ω_0. This can be performed when applying $dr/d\varphi = 0$ at the closest radial distance R and hence deriving $p_\varphi(R;\omega_0)$. When looking carefully at the equation of motion (4.68), one finds out that this can be found from the relation

$$p_r(R; p_\varphi, \omega_0) = 0. \tag{4.73}$$

Furthermore, calculations along the similar lines as at the beginning of Section 4.2.2 can be performed, but here the governing momentum component is p_φ rather than p_r. This means that the refractive index still takes the general form (4.22), i.e.,

$$n^2(r,\omega(r,p_\vartheta)) = a_0(r) + \frac{a_1(r)}{\omega(r,p_\vartheta)} + \frac{a_2(r)}{\omega^2(r,p_\vartheta)}, \tag{4.74}$$

repeated to emphasize that in this formulation $\omega(r)$ is defined as (4.65) and it hence differs from expression (4.22). The same holds also for the Hamiltonian (4.66) which can now be expressed as

$$\begin{aligned}\mathcal{H}(x^\alpha, p_\alpha) = \frac{1}{2}\Bigg[&\frac{p_r^2}{B(r)} + \frac{p_\varphi^2}{C(r)} - \frac{\omega_0^2}{A(r)} - a_0(r)\omega^2(r,p_\varphi) - a_1(r)\omega(r,p_\varphi) \\ &-a_2(r) + \omega^2(r,p_\varphi)\Bigg].\end{aligned} \tag{4.75}$$

Although the structure of the Hamiltonian corresponds to (4.23), it is in fact a completely different equation because of the definition of $\omega(r)$, given here by (4.65).

To make the different character of the Hamiltonian (4.75) more apparent, it is now expressed as

$$\mathcal{H}(x^\alpha, p_\alpha) = \frac{1}{2}\left[\mathcal{A}_\varphi(r)p_\varphi^2 + 2\mathcal{B}_\varphi(r)p_\varphi + \mathcal{C}_\varphi(r,p_r)\right], \tag{4.76}$$

where $\mathcal{A}_\varphi(r)$, $\mathcal{B}_\varphi(r)$, $\mathcal{C}_\varphi(r,p_r)$ are additional functions of r and p_r, which generally differ from the functions $\mathcal{A}_r(r)$, $\mathcal{B}_r(r)$, $\mathcal{C}_r(r,p_\varphi)$ introduced in the Hamiltonian

(4.24), but they also contain ω_0 as a parameter. It is useful to set explicitly the dependence on p_r in the discussed relations, which for the assumed medium velocity is present only as

$$\mathcal{C}_\varphi(r,p_r)=\frac{p_r^2}{B(r)}+\mathcal{C}_{\varphi 1}(r). \tag{4.77}$$

With the known Hamiltonian and the defined form of the refractive index (4.74) it is then possible to find the functions $\mathcal{A}_\varphi(r)$, $\mathcal{B}_\varphi(r)$, $\mathcal{C}_\varphi(r,p_r)$, obtaining

$$\mathcal{A}_\varphi(r)=\frac{1}{C(r)}+(1-a_0(r))f^2(r), \tag{4.78}$$

$$\mathcal{B}_\varphi(r)=\left[(a_0(r)-1)\omega_0 V^0(r)+\frac{1}{2}a_1(r)\right]f(r), \tag{4.79}$$

$$\mathcal{C}_\varphi(r,p_r)=\frac{p_r^2}{B(r)}-\frac{\omega_0^2}{A(r)}-a_2(r)+\omega_0 V^0(r)\left[(1-a_0(r))\omega_0 V^0(r)-a_1(r)\right]. \tag{4.80}$$

After finding their forms for a given refractive index, it can be seen that the function $\mathcal{B}_\varphi(r)$ is exactly the same as the function $\mathcal{B}_r(r)$, while the functions $\mathcal{A}_\varphi(r)$, $\mathcal{C}_\varphi(r,p_r)$ differ from the functions $\mathcal{A}_r(r)$, $\mathcal{C}_r(r,p_\varphi)$.

The equations of motion for the Hamiltonian in the form (4.76) are

$$\dot{r}=\frac{p_r}{B(r)}, \tag{4.81}$$

$$\dot{\varphi}=\mathcal{A}_\varphi(r)p_\varphi+\mathcal{B}_\varphi(r). \tag{4.82}$$

Then, the condition $\mathcal{H}(x^\alpha,p_\alpha)=0$ is easily applied to express p_r as

$$p_r=\pm\sqrt{B(r)\left[-\mathcal{A}_\varphi(r)p_\varphi^2-2\mathcal{B}_\varphi(r)p_\varphi-\mathcal{C}_{\varphi 1}(r)\right]}, \tag{4.83}$$

which one may substitute in the relation for $\dot{r}$ to get

$$\dot{r}=\pm\sqrt{\frac{-\mathcal{A}_\varphi(r)p_\varphi^2-2\mathcal{B}_\varphi(r)p_\varphi-\mathcal{C}_{\varphi 1}(r)}{B(r)}}. \tag{4.84}$$

The derived formulae can now be used in the equation for the deflection angle, the final form of which is

$$\frac{d\varphi}{dr}=\pm\sqrt{B(r)\mathcal{A}_\varphi(r)}\left\{\frac{\mathcal{B}_\varphi^2(r)-\mathcal{A}_\varphi(r)\mathcal{C}_{\varphi 1}(r)}{(\mathcal{A}_\varphi(r)p_\varphi+\mathcal{B}_\varphi(r))^2}-1\right\}^{-1/2}. \tag{4.85}$$

To make the deflection angle formula more compact, it is useful to define the function $h(r)$ similarly to (4.37) as it was introduced in the previous sections, but in this case it is more general, namely

$$h^2(r)=\frac{1}{\mathcal{A}_\varphi^2(r)}\left(\mathcal{B}_\varphi^2(r)-\mathcal{A}_\varphi(r)\mathcal{C}_{\varphi 1}(r)\right). \tag{4.86}$$

As usual, it is desirable to find an expression describing the dependence of p_φ on the closest radial distance R and on the photon frequency at infinity ω_0. In this case, it leads to a quadratic equation with solutions

$$p_\varphi=\frac{-\mathcal{B}_\varphi(R)\pm\sqrt{\mathcal{B}_\varphi^2(R)-\mathcal{A}_\varphi(R)\mathcal{C}_{\varphi 1}(R)}}{\mathcal{A}_\varphi(R)}=-\frac{\mathcal{B}_\varphi(R)}{\mathcal{A}_\varphi(R)}\pm h(R). \tag{4.87}$$

This formulation is particularly convenient for the given definitions of the Hamiltonian and the refractive index and it can be applied in the deflection angle formula. It can be finally expressed as

$$\frac{d\varphi}{dr} = \pm\sqrt{B(r)\mathcal{A}_\varphi(r)}\left[\frac{h^2(r)}{\left(\frac{\mathcal{B}_\varphi(r)}{\mathcal{A}_\varphi(r)} - \frac{\mathcal{B}_\varphi(R)}{\mathcal{A}_\varphi(R)} \pm h(R)\right)^2} - 1\right]^{-1/2}, \tag{4.88}$$

and the total deflection angle formula hence reads

$$\alpha = 2\int_R^\infty \sqrt{B(r)\mathcal{A}_\varphi(r)}\left[\frac{h^2(r)}{\left(\frac{\mathcal{B}_\varphi(r)}{\mathcal{A}_\varphi(r)} - \frac{\mathcal{B}_\varphi(R)}{\mathcal{A}_\varphi(R)} \pm h(R)\right)^2} - 1\right]^{-1/2} dr - \pi. \tag{4.89}$$

Notice a formal agreement between the obtained relation and the formula (2.70) which indicates that there are two solutions depending on the relative motion of light and medium. Thus, the light deflection will behave similarly in the case when either a medium or a black hole rotates.

Note that in comparison with the radially falling medium, the function $h(r)$ was defined more generally, and the same holds for the coefficient $\mathcal{C}_{\varphi 1}(r)$. This is due to the fact that in this case one cannot obtain a direct relation between $\frac{p_\varphi}{\omega_0}$, i.e., the impact parameter, and $h(r)$. In fact, this was the main purpose for defining $h(r)$. It cannot be derived for the rotating medium, and it is hence more instructive to derive a relation between $h(r)$ and p_φ alone, as performed in the present section.

4.4 Perturbative Approach

When dealing with light propagation around a relativistic object in a medium, a completely different procedure how to solve this problem can be applied. This approach is taken in the present section, where the corresponding equations are derived with the assumption that the effect of the medium can be described as a small perturbation. There are different ways how to calculate them, and two specific perturbation methods are discussed below. In the first part I define the medium as a linear perturbation of vacuum, while in the second part perturbation of a cold plasma is considered. This might be useful in order to compare different aspects which occur in the presence of a medium and how they arise in different perturbation schemes.

4.4.1 Perturbation of vacuum

In the case of a perturbative description, as performed by Läänemets et al. [2022], one can assume that the presence of a medium is actually a small perturbation with respect to the vacuum case (the medium is thin), i.e.,

$$n^2(x^\alpha) = 1 + \epsilon n_1^2(x^\alpha), \tag{4.90}$$

and after substituting this relation in (1.44), the Hamiltonian takes the form

$$\mathcal{H}(x^\alpha, p_\alpha) = \frac{1}{2}\left[g^{\beta\delta}p_\beta p_\delta - \epsilon n_1^2(x^\alpha)(p_\gamma V^\gamma)^2\right] \equiv \mathcal{H}_0 + \epsilon\mathcal{H}_1, \tag{4.91}$$

with the corresponding right-hand sides of the equations of motion taking the form

$$\frac{\partial \mathcal{H}}{\partial p_r} = \frac{p_r}{B(r)} + \epsilon \partial_{p_r} \mathcal{H}_1, \tag{4.92}$$

$$\frac{\partial \mathcal{H}}{\partial p_\varphi} = \frac{p_\varphi}{C(r)} + \epsilon \partial_{p_\varphi} \mathcal{H}_1. \tag{4.93}$$

From the condition $\dot{r} = 0$ at $r = R$, it can be derived that

$$p_r = -\epsilon B(R) \partial_{p_r} \mathcal{H}_1|_{r=R}\,, \tag{4.94}$$

i.e., at this point there is only a contribution of the first order, and from the condition $\mathcal{H}(x^\alpha, p_\alpha) = 0$ at $r = R$ it further follows that

$$p_\varphi^2 = C(R) \left(\frac{\omega_0^2}{A(R)} - 2\epsilon \mathcal{H}_1|_{r=R} \right). \tag{4.95}$$

The term $\propto p_r^2$ was omitted because it is a higher-order term at this point.

Applying the condition $\mathcal{H}(x^\alpha, p_\alpha) = 0$ at an arbitrary position while assuming the previous relations one gets

$$p_r = p_{r0} + \epsilon \frac{B(r)}{p_{r0}} \left(\frac{C(R)}{C(r)} \mathcal{H}_1|_{r=R} - \mathcal{H}_1 \right), \tag{4.96}$$

where

$$p_{r0} = \pm \omega_0 \sqrt{\frac{B(r)}{A(r)}} \left(1 - \frac{C(R)A(r)}{C(r)A(R)} \right)^{1/2}. \tag{4.97}$$

The deflection angle formula can then be derived from the relation

$$\frac{d\varphi}{dr} = \frac{\frac{p_\varphi}{C(r)} + \epsilon \partial_{p_\varphi} \mathcal{H}_1}{\frac{p_r}{B(r)} + \epsilon \partial_{p_r} \mathcal{H}_1}, \tag{4.98}$$

which leads to the expression

$$\begin{aligned} \frac{d\varphi}{dr} = {} & \frac{\omega_0 B(r) \sqrt{C(R)}}{p_{r0} C(r) \sqrt{A(R)}} + \epsilon \frac{B(r)}{p_{r0}} \left[\partial_{p_\varphi} \mathcal{H}_1 - \frac{\sqrt{C(R)A(R)}}{\omega_0 C(r)} \mathcal{H}_1|_{r=R} \right. \\ & \left. - \frac{B(r)}{p_{r0}} \frac{\omega_0 \sqrt{C(R)}}{C(r)\sqrt{A(R)}} \partial_{p_r} \mathcal{H}_1 + \frac{B(r)}{p_{r0}^2} \frac{\omega_0 \sqrt{C(R)}}{C(r)\sqrt{A(R)}} \left(\mathcal{H}_1 - \frac{C(R)}{C(r)} \mathcal{H}_1|_{r=R} \right) \right]. \end{aligned} \tag{4.99}$$

The first term (zeroth-order term) in (4.99) corresponds to formula (24) in Tsupko [2021] when setting $n = 1$. The obtained equation thus shows the effect of the presence of the medium seen as a perturbation characterized by the order of the parameter ϵ. Note that in this description an *arbitrary* medium is seen as a perturbation.

4.4.2 Perturbation of a cold plasma

However, for the purpose of the present study, it is more useful to explore the case when a small perturbation from the cold plasma case rather than from vacuum is assumed, and thus

$$n(x^\alpha) = n_0(x^\alpha) + \epsilon n_1(x^\alpha). \tag{4.100}$$

The individual parts of $n(x^\alpha)$ are defined in such a way that

$$w = -(n_0^2 - 1)\omega^2(r) - 2\epsilon n_0 n_1 \omega^2(r) = w_0 + 2\epsilon w_1, \tag{4.101}$$

where

$$w_0 = \omega_p^2(r)\,, \quad w_1 = -n_0 n_1 \omega^2(r)\,. \tag{4.102}$$

The introduced notation is further applied in the corresponding Hamiltonian, yielding

$$\mathcal{H}(x^\alpha, p_\alpha) = \frac{1}{2}\left[\frac{p_r^2}{B(r)} + \frac{p_\varphi^2}{C(r)} - \frac{\omega_0^2}{A(r)} + \omega_p^2(r)\right] + \epsilon w_1 \equiv \mathcal{H}_0 + \epsilon\mathcal{H}_1\,. \tag{4.103}$$

It is now nicely seen that the unperturbed part indeed describes the cold plasma case.

Next, the equations of motion for the system have to be found. The momentum derivatives of the Hamiltonian are obtained, i.e.,

$$\frac{\partial\mathcal{H}}{\partial p_r} = \frac{p_r}{B(r)} + \epsilon\partial_{p_r} w_1, \tag{4.104}$$

$$\frac{\partial\mathcal{H}}{\partial p_\varphi} = \frac{p_\varphi}{C(r)} + \epsilon\partial_{p_\varphi} w_1. \tag{4.105}$$

They are formally the same as when the perturbation of vacuum is assumed, but the definition of w_1 differs from $\mathcal{H}_1$ in the vacuum case. Again, the condition $\dot{r} = 0$ at $r = R$ can be used to find a possible expression for p_r. It takes the form

$$p_r = -\,\epsilon B(R)\partial_{p_r} w_1|_{r=R}\,, \tag{4.106}$$

i.e., individual perturbation terms can be found order by order. Then, the equation $\mathcal{H}(x^\alpha, p_\alpha) = 0$ at $r = R$ in this case can be used to express the momentum

$$p_\varphi = \sqrt{C(R)\left(\frac{\omega_0^2}{A(R)} - \omega_p^2(R)\right)} - \epsilon\sqrt{C(R)}\frac{w_1|_{r=R}}{\sqrt{\frac{\omega_0^2}{A(R)} - \omega_p^2(R)}} \equiv p_{\varphi 0} + \epsilon p_{\varphi 1}. \tag{4.107}$$

Similarly to the previous calculations, only terms up to $\mathcal{O}(\epsilon)$ were considered. Moreover, an analogous approach can be used also when searching for the form of ω_0 which leads to

$$\omega_0 = \sqrt{A(R)\left(\frac{p_\varphi^2}{C(R)} + \omega_p^2(R)\right)} + \epsilon\sqrt{A(R)}\frac{w_1|_{r=R}}{\sqrt{\frac{p_\varphi^2}{C(R)} + \omega_p^2(R)}} \equiv \omega_{00} + \epsilon\omega_{01}. \tag{4.108}$$

What remains to be found is the form of p_r as a perturbative series. This can be performed by using the equation $\mathcal{H}(x^\alpha, p_\alpha) = 0$ at an arbitrary value of r, yielding

$$p_r = p_{r0} + \epsilon\frac{B(r)}{p_{r0}}\left(\frac{\omega_{00}\omega_{01}}{A(r)} - w_1\right), \tag{4.109}$$

where

$$p_{r0} = \pm\sqrt{B(r)\left(\frac{\omega_{00}^2}{A(r)} - \frac{p_\varphi^2}{C(r)} - \omega_p^2(r)\right)}. \tag{4.110}$$

Note that here it is assumed that w_1 is a function of ω_{00} and p_{r0} expressed by (4.110).

However, as there are now two perturbed variables, ω_0 and p_φ, there are also two possibilities how to express p_r. The second option is

$$p_r = p_{r0} - \epsilon\frac{B(r)}{p_{r0}}\left(\frac{p_{\varphi 0}p_{\varphi 1}}{C(r)} + w_1\right), \tag{4.111}$$

but now

$$p_{r0} = \pm\sqrt{B(r)\left(\frac{\omega_0^2}{A(r)} - \frac{p_{\varphi 0}^2}{C(r)} - \omega_p^2(r)\right)}. \tag{4.112}$$

The variable w_1 is now a function of $p_{\varphi 0}$ and p_{r0} given by (4.112).

After deriving all the parameters in the form of perturbations, it is now possible to express also the deflection angle in the form of a perturbed function. Indeed, using the corresponding relations in

$$\frac{d\varphi}{dr} = \frac{\frac{p_\varphi}{C(r)} + \epsilon\partial_{p_\varphi}w_1}{\frac{p_r}{B(r)} + \epsilon\partial_{p_r}w_1} \tag{4.113}$$

leads to

$$\frac{d\varphi}{dr} = \left(\frac{p_{\varphi 0}}{C(r)} + \epsilon\frac{p_{\varphi 1}}{C(r)} + \epsilon\partial_{p_\varphi}w_1\right)\left(\frac{p_{r0}}{B(r)} - \epsilon\frac{1}{p_{r0}}\left(\frac{p_{\varphi 0}p_{\varphi 1}}{C(r)} + w_1\right) + \epsilon\partial_{p_r}w_1\right)^{-1} \tag{4.114}$$

$$= \frac{B(r)}{C(r)}\frac{p_{\varphi 0}}{p_{r0}} + \epsilon\frac{B(r)}{p_{r0}}\left\{\frac{p_{\varphi 1}}{C(r)} + \partial_{p_\varphi}w_1 + \frac{B(r)}{C(r)}\frac{p_{\varphi 0}}{p_{r0}}\left[\frac{1}{p_{r0}}\left(\frac{p_{\varphi 0}p_{\varphi 1}}{C(r)} + w_1\right) - \partial_{p_r}w_1\right]\right\}$$

when the series of p_φ is considered, while when applying the perturbation of ω_0 one gets

$$\frac{d\varphi}{dr} = \left(\frac{p_\varphi}{C(r)} + \epsilon\partial_{p_\varphi}w_1\right)\left(\frac{p_{r0}}{B(r)} - \epsilon\frac{1}{p_{r0}}\left(\frac{\omega_{00}\omega_{01}}{A(r)} - w_1\right) + \epsilon\partial_{p_r}w_1\right)^{-1} \tag{4.115}$$

$$= \frac{B(r)}{C(r)}\frac{p_\varphi}{p_{r0}} + \epsilon\frac{B(r)}{p_{r0}}\left\{\partial_{p_\varphi}w_1 + \frac{B(r)}{C(r)}\frac{p_\varphi}{p_{r0}}\left[\frac{1}{p_{r0}}\left(\frac{\omega_{00}\omega_{01}}{A(r)} - w_1\right) - \partial_{p_r}w_1\right]\right\}.$$

There are thus two ways how to derive the deflection angle – either as a function of (R, ω_0) or as a function of (R, p_φ). The particular choice depends on the given variables and on the specific application of the formulae.

5. Allowed Regions in the Kerr Metric in a Cold Plasma

This chapter describes an innovative approach when the light rays propagating in a medium around a compact object are characterized by their impact parameters, rather than by their deflection properties. Due to that it is possible to find regions around a compact object which the rays are forbidden to enter. The suggested approach thus provides a global description of the photon motion and various effects detectable by an observer at different positions can then be easily found. Results presented in this and the following chapters are based on calculations performed by Balek et al. [2023].

5.1 Allowed Regions in Terms of Impact Parameter

In order to derive the description in terms of impact parameters, let me now write the Hamiltonian (1.44) in a slightly different notation to emphasize some of its other properties. The dispersion relation in the rest frame of the medium in which the light propagates is $|\mathbf{p}| = n\omega$, and it can be further expressed in a Lorentz invariant form as

$$p^2 - (n^2 - 1)\omega^2 = 0, \quad \omega = -p \cdot V, \tag{5.1}$$

where p^α is the wave 4-vector and V^α is the 4-velocity of the medium already introduced in Chapter 1. Notice that this relation holds both in a flat spacetime and in a curved spacetime (with substitution $\eta_{\mu\nu} \to g_{\mu\nu}$) in the geometrical optics approximation (for more details, see Chapter 1). In the cold plasma approximation the Hamiltonian (1.48) is applied and the dispersion relation hence reads

$$p^2 + \omega_p^2 = 0. \tag{5.2}$$

The Kerr metric is assumed in further calculations. Let me recall that its form in the Boyer-Lindquist coordinates can be found from (3.1), where $M(r) = m = const.$ is chosen. A plasma medium of the same symmetries as those of the metric is considered. The rays are assumed to move in the equatorial plane where $\vartheta = \pi/2$. In a such-defined system the Kerr metric has a block-diagonal form

$$g_{\mu\nu} = \begin{pmatrix} g_{AB} & 0 \\ 0 & g_{rr} \end{pmatrix}, \tag{5.3}$$

where $A, B = t, \varphi$, and then $p^2 = g^{AB}p_A p_B + g_{rr}\dot{r}^2$. Note that the equation of motion in the form $\dot{r} = p^r$ was used in the expression for p^2. Moreover, the dispersion relation (5.2) now takes the form

$$\dot{r}^2 = -g^{rr}(g^{AB}p_A p_B + \omega_p^2). \tag{5.4}$$

As described already in previous sections, the covariant components t and φ of the momentum 4-vector are constants of motion. In accordance with the introduced

notation we denote them as $p_t = -\omega_0$ and $p_\varphi = \omega b$, where ω_0 is the wave frequency at infinity and b represents the impact parameter. Notice that both quantities (ω_0 and b) can be in principle measured by distant observers, and it is hence assumed that the rays can reach them. It is also worth emphasizing that rays of given ω_0 and b can reach radius r if and only if $\dot{r}^2 > 0$, i.e., the right-hand side of (5.4) is not negative, and in the special cases when $\dot{r}^2 = 0$ such radius corresponds to either the turning point (closest radial distance) or a circular orbit.

To furthermore simplify the calculations, the Kerr mass factor is taken as $m = 1$ and the metric then involves only one parameter, i.e., the angular momentum per unit mass a. It is also useful to introduce new functions present in the metric under given simplifications, namely

$$f = 1 - 2u, \quad \mathcal{A} = 1 + a^2u^2 + 2a^2u^3, \quad \mathcal{D} = 1 - 2u + a^2u^2, \tag{5.5}$$

where $u = r^{-1}$. These functions are related by the identity

$$f\mathcal{A} + 4a^2u^4 = \mathcal{D}. \tag{5.6}$$

Then, the Kerr metric in the equatorial plane can be written as

$$ds^2 = -fdt^2 - 4ar^{-1}dtd\varphi + \mathcal{A}r^2d\varphi^2 + \mathcal{D}^{-1}dr^2. \tag{5.7}$$

Applying this form of the metric and introducing the relations for p_t and p_φ allow one to express

$$g^{AB}p_Ap_B = -\frac{\omega_0^2}{\mathcal{D}r^2}\left(\mathcal{A}r^2 - 4ar^{-1}b - fb^2\right) \equiv -\frac{\omega_0^2}{\mathcal{D}r^2}F_{vac}. \tag{5.8}$$

The justification for introducing the function F_{vac} will become clearer after substituting (5.8) in (5.4) and applying $g^{rr} = \mathcal{D}$ which leads to

$$\dot{r}^2 = \omega_0^2 F r^{-2}, \quad \text{where } F = F_{vac} - \mathcal{D}r^2\frac{\omega_p^2}{\omega_0^2}. \tag{5.9}$$

It is evident that when $\omega_p = 0$, i.e., in vacuum, the right-hand side of the equation of motion for $\dot{r}$ is proportional to F_{vac}. With the above relation it is now straightforward to study regions in the (r, b)-plane where the light rays can occur. Moreover, it can be seen that in these regions necessarily $F \geq 0$, while at turning points (where $\dot{r} = 0$) $F = 0$. Additionally, the radii of circular light orbits are found at positions where not only $F = 0$, but also $F' = 0$ (taking prime as the differentiation with respect to r).

In the following sections it is analysed how the allowed regions for rays evolve in the (r, b)-plane when the Kerr metric is considered in the equatorial plane and it is surrounded by a cold plasma. In order to perform the calculations fully, it is necessary to choose a suitable plasma profile. For this purpose the approximation of a nonsingular isothermal sphere [see, e.g., Bisnovatyi-Kogan and Tsupko, 2010, Liu et al., 2017] is assumed, for which $N_e(r) \propto (r^2 + r_c^2)^{-1}$. To avoid problems with the singularity at $r = 0$, the plasma is assumed to have a core of radius r_c.

Two specific situations are analyzed in detail. First, light rays of a fixed frequency ω_0 at infinity are considered. Second, light rays are assumed to have a fixed "telescope frequency" ω_{obs} measured by an observer with a given 4-velocity

u^μ_{obs} at the established radius r_{obs}. The latter case is well justified when considering that at an arbitrary position (outside the black hole horizon) the observer in principle encounters light of a broad spectrum of frequencies ω, coming both from distant sources (stars) and from sources close to the horizon, and out of them they can always detect the one which is ω_{obs}.

The observer with a fixed "telescope frequency" can be defined in various ways. The most traditional one is to assume that they are at rest with respect to a given locally nonrotating frame (LNRF) or falling freely from rest at infinity. Both configurations are discussed below.

To find relations between the parameters describing the LNRF and freely falling observers, one has to recall that a particle moving in the equatorial plane is characterized by a 4-velocity of the form

$$u^\mu = \Gamma(1, v, 0, \Omega), \quad \Gamma = \frac{dt}{d\tau}, \quad v = \frac{dr}{dt}, \quad \Omega = \frac{d\varphi}{dt}, \tag{5.10}$$

where v and Ω are the radial and angular coordinate velocities, respectively. Moreover, Γ denotes the (Lorentz) conversion factor between the time of distant observers t and the proper time τ of the particle. It is now desirable to find these parameters for the two introduced sets of observers.

The LNRF observers are characterized by

$$\Gamma_{obs} = \sqrt{\frac{\mathcal{A}_{obs}}{\mathcal{D}_{obs}}}, \quad v_{obs} = 0, \quad \Omega_{obs} = \frac{2au^3_{obs}}{\mathcal{A}_{obs}}, \tag{5.11}$$

while a freely falling particle obeys

$$\hat{\Gamma}_{obs} = \frac{\mathcal{A}_{obs}}{\mathcal{D}_{obs}}, \quad \hat{v}_{obs} = -\frac{\mathcal{D}_{obs}}{\mathcal{A}_{obs}}\sqrt{\alpha_{obs}}, \quad \Omega_{obs} = \frac{2au^3_{obs}}{\mathcal{A}_{obs}}, \tag{5.12}$$

where $\alpha_{obs} = \mathcal{A}_{obs} - \mathcal{D}_{obs} = 2u_{obs}(1 + a^2u^2_{obs})$. Notice that the angular velocity Ω_{obs} remains the same for both classes of observers. For a detailed derivation of the introduced formulae from the geodesic equations, see, e.g., Bičák and Stuchlík [1976].

The frequency seen by an observer with the given 4-velocity u^μ can be found as

$$\omega_{obs} = -p \cdot u = \omega_0\Gamma(1 - v\frac{\eta_{obs}}{\mathcal{D}_{obs}} - \Omega b), \tag{5.13}$$

where η_{obs} denotes the rescaled light radial velocity detected at r_{obs}, i.e.,

$$\eta_{obs} = \frac{\dot{r}_{photon,obs}}{\omega_0} = \pm\sqrt{F_{obs}}u_{obs}. \tag{5.14}$$

To be more specific, the frequency derived for the locally nonrotating observer then reads

$$\omega_{obs} = \omega_0\Gamma_{obs}(1 - \Omega_{obs}b), \tag{5.15}$$

and for the freely falling observer it is

$$\omega_{obs} = \omega_0\hat{\Gamma}_{obs}(1 - \xi_{obs}\eta_{obs} - \Omega_{obs}b), \tag{5.16}$$

where $\xi_{obs} = \mathcal{D}^{-1}_{obs}\hat{v}_{obs} = -\mathcal{A}^{-1}_{obs}\sqrt{\alpha_{obs}}$.

5.2 Allowed Regions for Rays with Fixed ω_0

Before studying the effects of the plasma presence on the accessible regions for rays, they are briefly analyzed in vacuum. To find them, one has to solve the relation $F_{vac} = 0$ for b, which defines the boundaries between allowed and forbidden regions. This leads to a quadratic equation with two solutions which can be written in two equivalent forms, namely

$$\mathring{b}_{\pm} = \frac{1}{f}(-2ar^{-1} \pm \sqrt{\mathcal{D}}r) = \frac{\mathcal{A}r^2}{2ar^{-1} \pm \sqrt{\mathcal{D}}r}. \tag{5.17}$$

It can be seen that the two solutions $\mathring{b}_{\pm}$ meet at the horizon r_h, where $\mathcal{D} = 0$ and thus $r_h = 1+\sqrt{1-a^2}$, and at $r \gg 1$ they both approach the same asymptotes as $\mathring{b}_{\pm} \sim \pm r$. The first formulation of the solutions in (5.17) also reveals that there is a singularity at $r = 2$ (static limit) for $\mathring{b}_{-}$, as $f \to 0$, but not for $\mathring{b}_{+}$ (cf. the second formulation of the solutions in (5.17)).

As shown in Fig. 5.1, where the allowed regions for the rays in vacuum in the (r, b)-plane are depicted, there are two detached regions forbidden for rays. They are shaded and bounded by black bold curves and inside them $F_{vac} < 0$. Their boundaries are formed by either a combination of $\mathring{b}_{+}$ and $\mathring{b}_{-}$ (the "upper corner") or solely by $\mathring{b}_{-}$ (the "lower corner"). Note that in the latter case the position of the static limit naturally appears as an asymptote. There are also two areas which are accessible, at least in principle, by rays and which lie outside the forbidden regions. They are labeled in Fig. 5.1 as $\mathring{\mathcal{O}}_{\mathcal{I}}$ and $\mathring{\mathcal{O}}_{\mathcal{II}}$ and are located between the two corners or to the left of the upper corner at $r < 2$, respectively.

Note that the photon orbits are located at the minimum of the upper corner (co-rotating orbit) and at the maximal point of the lower corner (counter-rotating orbit).

One additional aspect of light observed in the allowed regions should be further discussed. When assuming an arbitrary (not necessarily LNRF) observer with $v = 0$, the observed wave frequency is $\omega_{obs} = \omega_0\Gamma(1 - \Omega b)$. Although inevitably $\omega_{obs} > 0$, this is not necessarily true for ω_0. On the contrary, its sign has to be derived at a given point of the (r, b)-plane by setting possible values of the angular velocity Ω.

The angular velocities of co- and counter-rotating circular photon orbits can be used as limiting cases. In vacuum, their impact parameters are $b = \mathring{b}_{\pm}$ and their 4-velocity satisfies

$$u^2_{photon} = -\omega_0\dot{t}_{photon} + p_\varphi\dot{\varphi}_{photon} \propto -1 + b\Omega = 0. \tag{5.18}$$

The velocity has to vanish because the rays are assumed to stay on the given orbit ($\dot{r} = 0$). From this relation it is clearly seen that the angular velocities for these rays are directly related to the light impact parameters as they are inverse to each other, i.e., $\mathring{b}_{\pm} = \Omega^{-1}_{\pm}$. Hence, the given values of Ω in the allowed regions lie between $b/\mathring{b}_{-} < \Omega b < b/\mathring{b}_{+}$ for $b > 0$ and they have to satisfy $\Omega b < b/\mathring{b}_{-}$ when $b < 0$.

This causes the light signals to have various signs of ω_0 in different accessible regions. While $\omega_0 > 0$ in $\mathring{\mathcal{O}}_{\mathcal{I}}$, in $\mathring{\mathcal{O}}_{\mathcal{II}}$ it satisfies $\omega_0 < 0$. Although rays with $\omega_0 < 0$ might seem rather suspicious, they represent only a special case of a "particle"

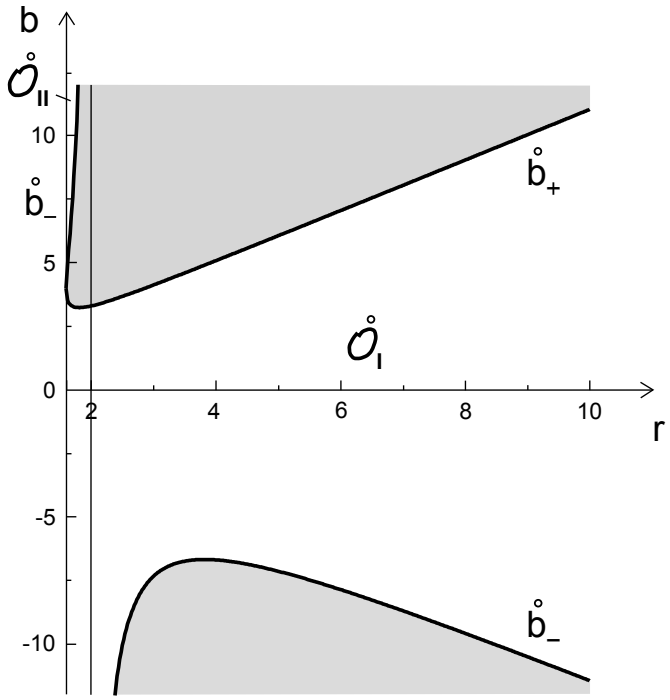

Figure 5.1: Allowed regions for rays in vacuum around an object described by the Kerr metric with $a = 0.8$. Radial distances r (abscissa) from the black hole are plotted as a function of ray impact parameters b (ordinate). The shaded areas bounded by the black lines $\mathring{b}_+$ and $\mathring{b}_-$ ("corners") are forbidden for the rays, while the white regions $\mathring{\mathcal{O}}_{\mathcal{I}}$ and $\mathring{\mathcal{O}}_{\mathcal{II}}$ are accessible for rays, at least in theory. The thin vertical line at $r = 2$ denotes the static limit and it represents the asymptote of the inner boundary of forbidden regions given by $\mathring{b}_-$. Note that the minimal radial value in the plot is the horizon radius which for the chosen a equals $r_h = 1.6$.

with negative energy, which is frequently discussed as a necessary constituent of the well known Penrose process (see, e.g., Misner et al. [1973], §33.7).

Next, let me include plasma in the system. Light rays propagating in it are assumed to have a fixed frequency ω_0 at infinity which is positive in $\mathring{\mathcal{O}}_{\mathcal{I}}$ and negative in $\mathring{\mathcal{O}}_{\mathcal{II}}$. Moreover, the boundaries of the allowed regions are given in this case by $F = 0$, where F is defined in (5.9). This condition gives again a quadratic equation with solutions

$$b_\pm = \frac{1}{f}\left(-2ar^{-1} \pm r\sqrt{(1 - f\zeta^2)\mathcal{D}}\right), \tag{5.19}$$

where $\zeta = \omega_p/\omega_0$. Note that the solutions (5.19) formally correspond to the vacuum solutions $\mathring{b}_\pm$ given by (5.17) if one replaces $\mathcal{D} \to (1 - f\zeta^2)\mathcal{D}$. From this it can be further seen that the functions $b_\pm$ approach the same asymptotes as $\mathring{b}_\pm$ at $r \gg 1$, i.e., $b_\pm \sim \pm r$. Moreover, also the behaviour of b_- is similar to $\mathring{b}_-$ around the static limit ($r = 2$), reaching a singularity there.

However, although the qualitative profile of the functions $b_\pm$ corresponds to the vacuum solutions $\mathring{b}_\pm$, their quantitative shapes depend substantially on the chosen plasma parameters. Generally, it can be stated that $b_\pm$ are closer to each other than $\mathring{b}_\pm$ and the forbidden regions for rays are hence larger. For particular choices of plasma parameters it can even happen that they merge and form a

neck, so that a ray of any impact parameter heading from the black hole cannot reach a distant observer or opposite. Formation of the neck is discussed in detail in Section 6.1.

It is a natural consequence that the larger the forbidden regions, the smaller the allowed ones. The regions $\mathcal{O}_I$ and $\mathcal{O}_{II}$ are then actually just parts of the larger vacuum regions $\mathring{\mathcal{O}}_{\mathcal{I}}$ and $\mathring{\mathcal{O}}_{\mathcal{II}}$. Due to this, $\omega_0 > 0$ in $\mathcal{O}_I$, while $\omega_0 < 0$ in $\mathcal{O}_{II}$. Moreover, if there is a neck, $\mathcal{O}_I$ is effectively split into two parts, $\mathcal{O}_{IA}$ and $\mathcal{O}_{IB}$ (see Fig. 5.2).

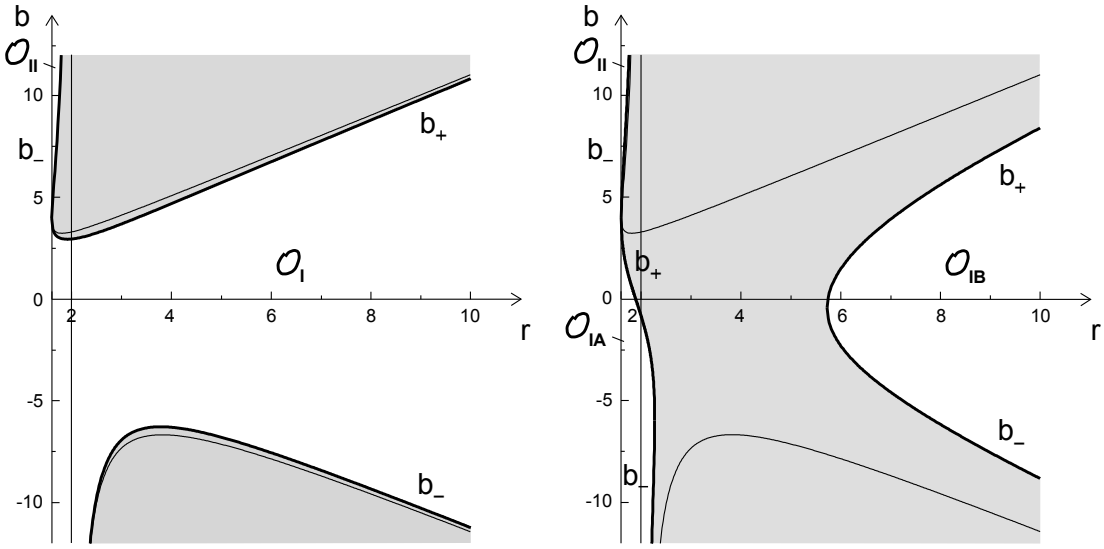

Figure 5.2: Comparison of the allowed regions for rays in a plasma with fixed frequency ω_0 at infinity and for rays in vacuum. Kerr metric with $a = 0.8$ was assumed and the plasma parameters were set as $r_c = 1$, $r_{ref} = 1.8$ (so the reference radius lies halfway between the horizon and the static limit), and $q = 1$ and 3.5 in the left and right panels, respectively. Forbidden regions for rays in a plasma are shaded, while the remaining white areas correspond to either regions $\mathcal{O}_I$ or $\mathcal{O}_{IA}$, $\mathcal{O}_{IB}$ and $\mathcal{O}_{II}$. Boundaries of the forbidden regions in vacuum are drawn by thin black curves which lie exclusively in the shaded regions. Thin vertical line shows the position of the static limit for the chosen Kerr metric ($r = 2$), which also represents an asymptote of the boundary of the allowed regions. In region $\mathcal{O}_I$, possibly in $\mathcal{O}_{IA}$ and $\mathcal{O}_{IB}$, the frequency $\omega_0 > 0$, while $\omega_0 < 0$ in $\mathcal{O}_{II}$.

In terms of practical calculations, it is necessary to define the plasma properties and incorporate them somehow into the equations. Because a specific choice of ω_p and ω_0 might lead to a broad variety of combinations, it seems more useful to work only with their ratio. To do that, a reference radial distance, r_{ref}, is randomly chosen (requiring only that it lies outside the horizon) and the corresponding plasma parameter can be slightly rearranged as follows:

$$\zeta = \frac{\omega_p(r)}{\omega_0}\frac{\omega_p(r_{ref})}{\omega_p(r_{ref})} = \pm\frac{\omega_p(r_{ref})}{|\omega_0|}\sqrt{\frac{N_e(r)}{N_e(r_{ref})}} = \pm\frac{\omega_p(r_{ref})}{|\omega_0|}\sqrt{\frac{r_{ref}^2 + r_c^2}{r^2 + r_c^2}} \equiv \pm q\sqrt{\mathcal{P}}. \tag{5.20}$$

When working with the plasma, its profile as a nonsingular isothermal sphere with $N_e(r) \propto (r^2 + r_c^2)^{-1}$ is assumed, and the definition of the plasma frequency (1.49)

is utilized. The parameter $\mathcal{P}$ thus represents the ratio of electron densities at r and r_{ref}. The signs + and − in (5.20) refer to regions $\mathcal{O}_I$ and $\mathcal{O}_{II}$, respectively.

The accessible regions for light rays with fixed ω_0 for two different choices of q are depicted in Fig. 5.2. As described above, the forbidden regions for rays in a plasma (shaded areas) are larger than those in vacuum. Moreover, the value of q used in the right panel is larger than q_{crit} (see Section 6.1) and thus a neck occurs.

5.3 Rays with Fixed ω_{obs} for LNRF Observers

In this section a LNRF observer set at $r = r_{obs}$ with a telescope receiving frequency ω_{obs} is considered. This frequency can then be calculated using equation (5.15). It was already argued that it is more practical to study the relevant expressions as a function of the ratio $\zeta = \omega_p/\omega_{obs}$ rather than of ω_{obs} itself. For this class of observers one gets

$$\zeta = \pm q\Gamma_{obs}(1 - \Omega_{obs}b)\sqrt{\mathcal{P}}, \tag{5.21}$$

where $\pm$ is the relative sign between ω_0 and ω_{obs}. In this case the reference radius corresponds to the position of the observer, and hence both q and $\mathcal{P}$ are functions of r_{obs}.

However, in the following calculations it is assumed that q is independent of r_{obs}, and hence, along with changing ω_p at different r_{obs} also the telescope frequency ω_{obs} has to vary, decreasing for larger r. It is thus possible to express the effect of plasma also on rays propagating at $r \gg 1$, although the plasma is thin there. Moreover, for locally nonrotating plasma $\omega = \omega_{obs}$ and because $n^2 \geq 0$, only rays with $q < 1$ can reach the observer. Nevertheless, the restriction for q is more general, since n has to be always real in the regions with $F \geq 0$. This can be also seen, e.g., in equation (6.25) in Section 6.4.

To find the allowed regions for rays with fixed frequency ω_{obs} as seen by LNRF observers, one has to use relation (5.21) in equation (5.9) and solve for b. It is again a quadratic equation, as in the case with fixed ω_0 where $\zeta = const.$, but the individual polynomial coefficients are shifted. This shift causes that the asymptotes of solutions $b_\pm$ for $r \gg 1$ behave as $b_\pm \sim \pm Cr$, where $C < 1$, while in the previous case $C = 1$. Moreover, the branch b_- does not have to reach a singularity at the static limit $r = 2$, but it can occur already at $r < 2$. The exact value depends on the chosen plasma parameters. In Section 6.2 it is shown how both C and the asymptote radius increase as a function of observer position r_{obs}, which can span from the horizon to infinity. Moreover, it is also shown that in this case the function diverging at the given asymptote can be b_+ rather than b_-.

In this case a neck between the forbidden regions can emerge in the (r, b)-plane. The neck exists for such values of r which cause the discriminant of $F = 0$ to be negative. It is worth noting that the neck can appear for both the observer radii close to the horizon and far away, but there is a radial interval $\rho_{obsA} < r_{obs} < \rho_{obsB}$, where it disappears. Note that for observers at ρ_{obsA} and ρ_{obsB} the neck effectively shrinks into a point at radii ρ_A and ρ_B, respectively. Their derivation and their values for specific cases are discussed in detail in Section 6.3.

When ω_{obs} is fixed, rays that actually reach the observer are not the only ones adjusted to be received by the telescope. In principle, there are also "ghost rays"

which bounce on their way back to the observer and have a suitable combination of frequency ω_0 and impact parameter b, so their frequency measured by the observer, ω_{obs}, is just the tuned value. For this type of rays the allowed regions $\mathcal{O}_I$ and $\mathcal{O}_{II}$ exist, and they are of a similar shape as those obtained for a fixed ω_0. However, sometimes the frequency ω_{obs} associated with the "ghost rays" has to be negative, according to their value of the impact parameter. To show this, one has to recall that there are limit impact parameters given by $b_{lim} = \Omega_{obs}^{-1}$. One knows from (5.15) that $\omega_{obs} \propto \omega_0(1 - b/b_{lim})$, so that when $\omega_0 > 0$ in $\mathcal{O}_I$ and $\omega_0 < 0$ in $\mathcal{O}_{II}$, in the upper part of $\mathcal{O}_I$ where $b > b_{lim}$ one has to set $\omega_{obs} < 0$, same as in the lower part of $\mathcal{O}_{II}$ where $b < b_{lim}$.

Regions accessible for rays with fixed ω_{obs} as seen by LNRF observers are depicted in Fig. 5.3. The white areas bounded by thick grey curves represent allowed regions for rays that potentially reach the observer at r_{obs}, either directly or after bouncing back. The remaining free regions around the shaded corners and the shaded strip in the right panel (where a neck emerges) define allowed regions for "ghost rays", however, they never reach the observer.

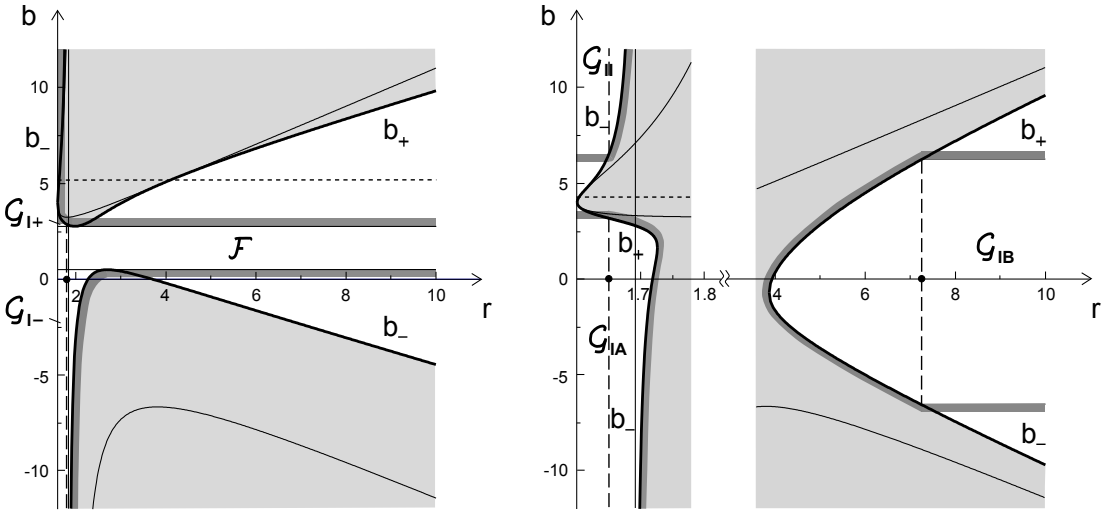

Figure 5.3: Allowed regions for rays in a plasma with fixed frequency ω_{obs} seen by a LNRF observer. Kerr and plasma parameters were chosen as $a = 0.8$ and $r_c = 1$, respectively. The frequency ratio was set to be $q = 2/3$. The observer positions are marked by a dot; in the left panel at $r_{obs} = 1.8$, while in the right panel two values are applied, namely 1.65 and 7.25 in its left and right parts, respectively. Forbidden regions for rays, including the "ghost rays", are shaded. Boundaries between the accessible and forbidden areas for rays in vacuum are drawn by thin curves. Solid vertical lines show the asymptote of the inner boundaries of forbidden regions. Dotted horizontal lines denote values of b_{lim}, which divide the regions with "ghost rays" according to the relevant sign of ω_{obs}. It has to be negative at $r > 2$ above b_{lim}, while for $r < 2$ this happens for impact parameters under b_{lim} up to b at the horizon. Dashed vertical lines depict rays at the moment of arriving at the observer. Regions bounded by the thick grey lines, labeled as $\mathcal{F}$, $\mathcal{G}_{I+}$ and $\mathcal{G}_{I-}$ in the left panel and $\mathcal{G}_{IA}$, $\mathcal{G}_{II}$ and $\mathcal{G}_{IB}$ in the right panel, are accessible for rays truly reaching the observer. Region $\mathcal{G}_{II}$ in the left panel, ranging from $b > 25.7$, as well as $b_{lim} = 276.5$ of the right part in the right panel, are not depicted because of their large b values.

The observer position r_{obs} chosen in the left panel of Fig. 5.3 belongs to the interval $(\rho_{obsA}, \rho_{obsB})$, and hence there is no neck. This allows the rays of impact parameters from the free band $\mathcal{F}$ to propagate easily between infinity and the horizon back and forth. Otherwise, the allowed regions are always bounded from one side. For r_{obs} smaller than the position where function b_+ reaches its minimum (which is the case in the left panel), the observer can detect the rays coming from regions $\mathcal{G}_{I+}$ and $\mathcal{G}_{I-}$, but not the rays from $\mathcal{G}_{II}$ (not shown in the left panel) which is separated from $\mathcal{F}$. All these regions are inaccessible for rays from infinity.

The values of r_{obs} used in the right panel of Fig. 5.3 do not belong to the interval $(\rho_{obsA}, \rho_{obsB})$ and thus a neck is formed. Depending on the exact choice of r_{obs}, rays can reach the observer either from regions $\mathcal{G}_{IA}$ and $\mathcal{G}_{II}$ (when $r_{obs} < \rho_{obsA}$), or from region $\mathcal{G}_{IB}$ (if $r_{obs} > \rho_{obsB}$). Both situations are depicted in the right panel of Fig. 5.3.

When looking at a set of LNRF observers located at various distances r_{obs}, the allowed regions for rays can be identified in the (r_{obs}, b)-plane in a similar manner as the regions $\mathcal{O}_I$ and $\mathcal{O}_{II}$ presented for fixed ω_0 in the left panel of Fig. 5.2. Their boundaries are then formed by functions $B_\pm$ which are solutions of the equation $F|_{r=r_{obs}} = 0$. These functions can be expressed as the second form of the solutions in (5.17), where r is replaced by r_{obs} and the transformation $\mathcal{D}_{obs} \to \mathcal{D}_{obs}(1-q^2)^{-1}$ is performed (cf. equation (6.25)). Strictly speaking, the correspondence between the solutions with fixed ω_0 and in the (r_{obs}, b)-plane is more complicated as there has to be a specific choice of the frequency ratio $q < q_{crit}$, where q_{crit} is introduced in Section 6.4. However, at the current stage this fact does not hinder us from describing the main properties of the allowed regions in the (r_{obs}, b)-plane.

The main difference between the rays discussed in the (r, b)-plane and (r_{obs}, b)-plane is that in the latter case the allowed regions contain two rays of the same telescope frequency at one point; one oriented towards the black hole ($\dot{r}_{photon} < 0$) and the other away from it ($\dot{r}_{photon} > 0$). According to the original orientation of the rays, it is possible to separate the allowed regions in the (r_{obs}, b)-plane into areas $\mathcal{O}_h$ and $\mathcal{O}_i$ such that at least one ray begins at the horizon or at infinity, respectively. These regions can be viewed in Fig. 5.4. Of course, in some parts of the allowed regions both kinds of rays meet. This region is further denoted as $\mathcal{O}_{h+i}$, as it effectively represents the intersection of $\mathcal{O}_h$ and $\mathcal{O}_i$. The regions labeled as $\mathcal{O}'_h$ and $\mathcal{O}'_i$ correspond to segments of $\mathcal{O}_h$ and $\mathcal{O}_i$ which are complements to $\mathcal{O}_{h+i}$.

Rays forming the region $\mathcal{O}_{h+i}$ correspond to those present in the (r, b)-plane in the free band, and it is hence equivalent to $\mathcal{F}$ introduced in the left panel of Fig. 5.3. Along the same lines, regions $\mathcal{O}'_h$ and $\mathcal{O}'_i$ consist of rays originating in allowed regions bounded from one side, similarly to regions from Fig. 5.3 – either $\mathcal{G}_{I+}$, $\mathcal{G}_{I-}$ in the left panel or $\mathcal{G}_{IA}$, $\mathcal{G}_{II}$ and $\mathcal{G}_{IB}$ in the right panel.

The boundaries of region $\mathcal{O}_{h+i}$ can be found as the minimum of b_+, which at the same time represents the maximum of $\mathcal{F}$. It is hence the upper limit of $\mathcal{O}_{h+i}$, while its bottom part is limited by the local maximum of b_- for r larger than its asymptote (minimum of $\mathcal{F}$). These two limits are denoted in Fig. 5.4 as $\mathcal{B}_+$ and $\mathcal{B}_-$, respectively. It should be emphasized that the boundaries of $\mathcal{O}_{h+i}$ are not part of this region, as rays with $b = \mathcal{B}_\pm$ have a limited access to the observers because they do not get over the peak of the corresponding forbidden

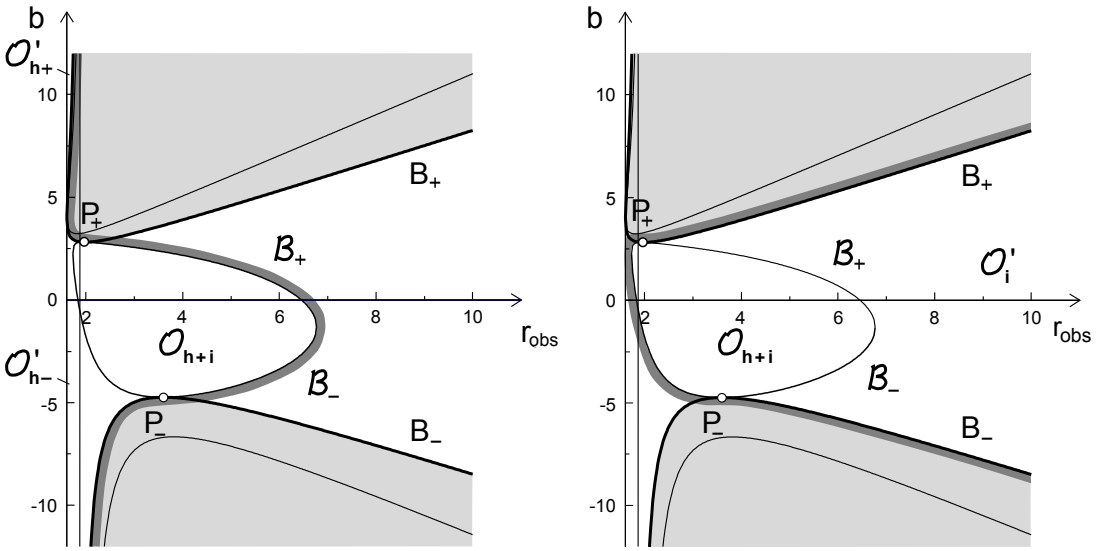

Figure 5.4: Allowed regions for rays seen by LNRF observers in the (r_{obs}, b)-plane. The values of parameters a, r_c, and q remain the same as in Fig. 5.3. Similarly as in the previous plots, the forbidden regions for rays are shaded, but here the rays can be detected by observers at various radii r_{obs}. Boundaries of the allowed regions in vacuum are drawn by thin curves. Solid vertical lines show the positions of the asymptotes of the boundary between allowed and forbidden regions. The white area bounded by thin and thick curves in the center of both panels is $\mathcal{O}_{h+i}$. In this region rays originally coming to the observer from both the black hole horizon and infinity meet. The regions $\mathcal{O}'_{h\pm}$ in the left panel are formed solely by rays reaching the observers from the horizon, while in region $\mathcal{O}'_i$ in the right panel rays detected by the observers come from infinity. Points $P_\pm$ divide the boundary of $\mathcal{O}_{h+i}$ into parts, where the relevant regions adjoin. In the left panel it is region $\mathcal{O}_h$, consisting of two parts, located between the horizon and the thick curve connecting P_+ and P_-, while in the right panel region $\mathcal{O}_i$ is limited from below only by the thick curve between points P_+ and P_-.

region standing in their way.

The positions of minimal and maximal values of b_+ and b_-, respectively, depend on the choice of r_{obs}. When it continuously increases from ρ_{obsA} to ρ_{obsB}, the functions $\mathcal{B}_\pm$ intersect with functions $B_\pm$ at two points, which are labeled in Fig. 5.4 as $P_\pm$. These points divide the boundary of $\mathcal{O}_{h+i}$ into two parts, where $\mathcal{O}'_h$ meets $\mathcal{O}_{h+i}$ from the left, while $\mathcal{O}'_i$ is adjacent from the right. A derivation of the position of points $P_\pm$ and a detailed description of the behaviour of the functions $B_\pm$ and $\mathcal{B}_\pm$ in their neighbourhood can be found in Section 6.4.

The allowed regions in the (r_{obs}, b)-plane describing rays detectable by LNRF observers located at various radii from the Kerr black hole are depicted in Fig. 5.4. In the left panel the region $\mathcal{O}_h$ is shown, composed of $\mathcal{O}_{h+i}$, the neighbouring region $\mathcal{O}'_{h-}$, and the detached part $\mathcal{O}'_{h+}$. The region $\mathcal{O}_i$ consisting of $\mathcal{O}_{h+i}$ and $\mathcal{O}'_i$ is shown in the right panel of Fig. 5.4. Point P_+ is located at r slightly lower than the static limit, and reasons for this, as well as other technical details, are clarified in Section 6.4.

Note that the boundaries between the allowed and forbidden regions in vacuum shown in Fig. 5.4 (thin curves inside the shaded areas) correspond to the

boundaries already obtained in the (r, b)-plane because in vacuum they are independent of ω_0.

5.4 Rays with Fixed ω_{obs} for Freely Falling Observers

Having (5.16) at hand, the parameter ζ corresponding to an observer freely falling from rest at infinity can be expressed as

$$\zeta = q\hat{\Gamma}_{obs}(1 - \xi_{obs}\eta_{obs} - \Omega_{obs}b)\sqrt{\mathcal{P}}. \tag{5.22}$$

Unlike in the previous case, the presented formula can be applied solely to rays that truly reach the observer, as η_{obs} defined with (5.14) is imaginary elsewhere. For this reason, ω_{obs} is exclusively positive and hence there are no "ghost rays" as for LNRF observers. Due to that, there is no $\pm$ in equation (5.22).

For this class of observers, it is necessary to find η_{obs} first. This can be performed by squaring equation (5.14) and solving the corresponding quadratic equation for η_{obs}. The allowed regions in the (r_{obs}, b)-plane can be found from the condition $F_{obs}u_{obs}^2 \geq 0$, similarly as in the previous case. However, here it is necessary to require that the quadratic equation has real solutions and its discriminant hence is not negative. In Section 6.5 it is shown that the boundaries between the accessible and forbidden regions are given by relations analogous to $B_\pm$ obtained for LNRF observers, but with the replacement $q \to \tilde{q}_{NR} = q\Gamma_{obs}/\left[1 + q^2(\Gamma_{obs}^2 - 1)\right]^{1/2}$. This set of solutions is further denoted as $\tilde{B}_\pm$. When q is defined as a function of r_{obs} to return $\tilde{q}_{NR} = const.$, the allowed regions for falling observers are of the same shape as those derived for locally nonrotating observers.

Here again, there are two rays for each r_{obs} in the allowed regions, but they differ by rescaled radial velocities $\eta_{obs}^{(\pm)}$ which represent two solutions of the corresponding quadratic equation and thus it is not only a sign by which they vary. Considering the (r_{obs}, b)-plane, $\eta_{obs}^{(-)}$ is negative in $\mathcal{O}_I$, while $\eta_{obs}^{(+)}$ is positive inside this region and zero at its boundary (corresponding to $B_\pm$). Similarly, $\eta_{obs}^{(+)}$ is positive everywhere in $\mathcal{O}_{II}$ and $\eta_{obs}^{(-)}$ is negative there except for the line B_-. In $\mathcal{O}_{II}$ also the sign of $\dot{r}_{photon,obs}$ differs from the sign of η_{obs}, as $\omega_0 < 0$ there (cf. (5.14)).

For the purpose of further description, rays of velocities $\eta_{obs}^{(+)}$ in region $\mathcal{O}_I$ and $\eta_{obs}^{(-)}$ in region $\mathcal{O}_{II}$ are characterized as "rays of class I", while the complementary rays in the given regions are "rays of class II". From the sign analysis of $\eta_{obs}^{(\pm)}$ it follows that the rays of class II are oriented towards the black hole, as is a subset of the rays of class I which lie between impact parameters $\tilde{B}_\pm$ and $B_\pm$.

The discussion related to regions $\mathcal{O}_h$ and $\mathcal{O}_i$ in the same manner as in the previous section is more complicated because there are two classes of rays which behave differently. For this reason, these classes of rays are analysed separately and the categorization of rays belonging to corresponding regions is now maximally extended in time. Then, rays are part of region $\mathcal{O}_h$ if they either begin or end on the horizon, and they belong to region $\mathcal{O}_i$ when either their beginning or end is at infinity.

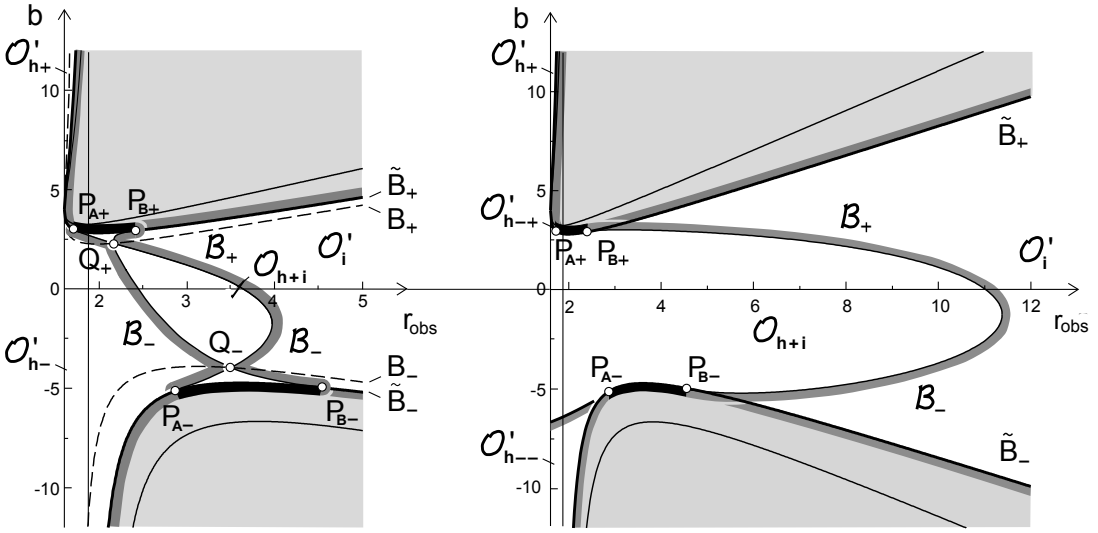

Figure 5.5: Allowed regions seen by freely falling observers in the (r_{obs}, b)-plane for rays of class I (left panel) and II (right panel). Parameters a, r_c, and q have the same values as in the previous figures. The shaded areas are forbidden for rays and the thin curves inside them show boundaries of the allowed regions in vacuum. The dashed curves in the left panel denote the boundaries $B_\pm$, where the radial velocity $\eta^{(+)}_{obs}$ changes sign. The region $\mathcal{O}_h$ in the case of rays from class I $\left(\text{with } \eta^{(+)}_{obs}\right)$ consists of $\mathcal{O}_{h+i}$ and $\mathcal{O}'_{h\pm}$, while the region $\mathcal{O}_i$ contains, in addition to $\mathcal{O}_{h+i}$, the region $\mathcal{O}'_i$. In the case of rays from class II $\left(\text{with } \eta^{(-)}_{obs}\right)$, the region $\mathcal{O}_{h+i}$ extends straight from the horizon and the region $\mathcal{O}'_{h-}$ is thus divided into two segments, $\mathcal{O}'_{h-+}$ and $\mathcal{O}'_{h--}$. Unlike in the case of LNRF observers, where it involved just a pair of points, region $\mathcal{O}_{h+i}$ meets the boundary of the forbidden regions at the arcs $P_{A+}P_{B+}$ and $P_{A-}P_{B-}$ marked by thick black segments. Moreover, the arcs connecting points P_{A+}, P_{A-} and P_{B+}, P_{B-} in the left panel create a boundary of region $\mathcal{O}_{h+i}$, intersecting the curves $B_\pm$ at points $Q_\pm$.

Fig. 5.5 shows the allowed regions for rays detected by freely falling observers at various distances from a black hole, i.e., in the (r_{obs}, b)-plane. The behaviour of rays from class I and II is depicted independently, in the left and right panel, respectively. The positions of the corresponding regions $\mathcal{O}_h$ and $\mathcal{O}_i$ are shown for both classes of rays in the figure. In Fig. 5.5 the regions $\mathcal{O}_{h+i}$, in the sense of the original definition of $\mathcal{O}_h$ and $\mathcal{O}_i$, can be related to the regions $\mathcal{O}'_i$ and $\mathcal{O}'_h$. The part of the region $\mathcal{O}_{h+i}$ in the left panel located between curves $\tilde{B}_\pm$ and $B_\pm$ and the region $\mathcal{O}_{h+i}$ in the right panel adjoin region $\mathcal{O}'_i$ and the horizon, while the remaining boundary of $\mathcal{O}_{h+i}$ in the left panel is shared only with $\mathcal{O}'_h$. In Section 6.5 it is demonstrated how the shape of the regions depicted in Fig. 5.5 can be derived without defining explicit relations for the accessible regions in the (r, b)-plane.

Rays with impact parameters $\tilde{B}_\pm$, which form the boundaries of the forbidden regions, have only one nonzero rescaled radial velocity $\tilde{\eta}_{obs}$ at each point. Their trajectories are rather peculiar because those coming from infinity return back *after* they meet the observer and rays originating near the horizon bounce back already *before* they reach the observer. This is due to their radial velocities which are given as $\dot{r}_{photon,obs} = \omega_0 \tilde{\eta}_{obs} < 0$. Furthermore, there are also rays which can

continue straight from infinity to the horizon instead of being bounced back. This kind of rays is located along the arcs $P_{A+}P_{B+}$ and $P_{A-}P_{B-}$, which are highlighted in Fig. 5.5 by thick black segments. These segments play a similar role as the points P_+ and P_- discussed in the previous section, i.e., they can be linked by curves connecting points P_{A+}, P_{A-} and P_{B+}, P_{B-} that allow one to distinguish which part of the boundary of $\mathcal{O}_{h+i}$ separates it from regions $\mathcal{O}'_h$ and $\mathcal{O}'_i$.

Notice that the rays of class I that are situated in the allowed region limited by the curves B_+ and B_- reflect back once they reach the observer. The region $\mathcal{O}_{h+i}$ is constricted to a point at the curves $B_\pm$, which are denoted by $Q_\pm$ in Fig. 5.5. Altogether, $\mathcal{O}_{h+i}$ consists of three separate parts connected at points $Q_\pm$ – two segments of triangular shape on the top and bottom and a central region between them. In addition, the central part is adjacent to the region $\mathcal{O}'_i$ at points $Q_\pm$, in a similar manner as $\mathcal{O}_{h+i}$ is adjacent to $\mathcal{O}_i$ at points $P_\pm$ in the case of LNRF observers. The region $\mathcal{O}_{h+i}$ is substantially broader for rays from class II than from class I, and it also extends down to the horizon for the former class of rays.

The shapes of the allowed regions for both kinds of rays are described in detail in Section 6.5. Formation of a smaller region $\mathcal{O}'_I$ for the rays of class I, where the rays bounce back after reaching the observer, is also discussed. It is shown that the choice $\tilde{q}_{NR} < 1/\sqrt{2}$ has to be made in order to extend $\mathcal{O}'_I$ down to the horizon. This is the case shown in Fig. 5.5.

6. Technical Aspects of Constructing Allowed Regions for Rays in a Plasma

This chapter is devoted to some more technical issues which occur when dealing with the allowed regions around a black hole in a cold plasma. While they were mostly outlined in the previous chapter, here they are discussed in detail. The presented calculations hence serve as a useful tool for better understanding the results presented in Chapter 5, although their proper analysis is not necessary for a basic overview about the allowed regions.

6.1 Neck Occurrence for Fixed ω_0

As mentioned in Section 5.2, in the case with fixed frequency ω_0 a neck connecting both forbidden regions can occur. The circumstances under which the neck forms are analyzed below.

In this case the solutions for the impact parameter, $b_\pm$, are given by (5.19). Let me rewrite this equation with the usage of (5.20) to get

$$b_\pm = \frac{1}{f}\left[-2au \pm \sqrt{(1-q^2 f\mathcal{P})\mathcal{D}u^{-2}}\right]. \tag{6.1}$$

The term $f\mathcal{P}$ present in the square root in (6.1) is important in order to describe the behaviour of the boundary functions $b_\pm$ at specific values of r (or u analogously). This term satisfies

$$f\mathcal{P} \propto \frac{(1-2u)u^2}{(1+r_c^2u^2)}, \quad \frac{d(f\mathcal{P})}{du} \propto 1-3u-r_c^2u^3. \tag{6.2}$$

These relations reveal some important properties. First, it is obvious that $f\mathcal{P}$ is positive for $0 < u < 1/2$ which corresponds to the radial distances from infinity up to the static limit, while at these boundary points (i.e., at $u = 0$ and $u = 1/2$) it vanishes. Second, its derivative decreases as u increases (and r decreases) and it reaches zero at some $u_C < 1/2$. This means that the maximum of $f\mathcal{P}$ lies somewhere outside the static limit of the black hole, which is situated at $r = 2$. For convenience we denote $q_{crit} = (f\mathcal{P})^{-1/2}|_{u=u_C}$. Then, with the choice $q = q_{crit}$ the functions b_+ and b_- intersect at r_C as the square root in (6.1) vanishes. Since their shapes lead to the formation of forbidden regions as two "corners" pointing towards each other, their peaks meet at r_C when $q = q_{crit}$.

This behaviour can be further clarified by considering that in the neighbourhood of r_C the expressions for $b_\pm$ can be written as

$$b_\pm = g_1 + g_2(r-r_C) \pm g_3|r-r_C|, \tag{6.3}$$

where the coefficients g_1, g_2, and g_3 are independent of r. This expression reveals that at $r = r_C$ there is a spike-like minimum and maximum for b_+ and b_-, respectively. Furthermore, when $q > q_{crit}$ the term in the square root of (6.1)

becomes negative in an interval (r_A, r_B), which includes r_C. This interval extends for larger q. Thus, the two originally detached forbidden regions for rays merge through a neck of a width given by r_A and r_B. The interval (r_A, r_B) is always above the static limit for arbitrary $q > q_{crit}$ because the square root in (6.1) is real for $r < 2$.

When using the black hole and plasma parameters applied in Fig. 5.2, one gets $r_C = 3.104$ and consequently $(f\mathcal{P})|_{u=u_C} = 0.1418$, $q_{crit} = 2.656$. With the value $q = 3.5$ chosen in the right panel of Fig. 5.2 the neck lies between $r_A = 2.268$ and $r_B = 5.727$.

6.2 Allowed Regions at Extreme Radial Values with Fixed ω_{obs}

When the rays are assumed to have a fixed ω_{obs} as detected by LNRF observers, their allowed regions can be determined from $F = 0$, where F originally given by (5.9) yields

$$F = \mathcal{A}r^2 - Q^2 + 2(-2ar^{-1} + Q^2\Omega_{obs})b - (f + Q^2\Omega_{obs}^2)b^2 \tag{6.4}$$

with $Q = q\Gamma_{obs}\sqrt{\mathcal{D}\mathcal{P}}r$. This leads to a set of two functions $b_\pm$ which can be expressed via the general solutions of a quadratic equation. These two functions can be then either solved numerically or expressed graphically as performed in Section 5.3. However, the limiting solutions of (6.4) are discussed analytically in this section to describe how these functions evolve.

Let me first consider the case when $r \gg 1$. Then, $\sqrt{\mathcal{D}\mathcal{P}} \simeq \sqrt{r_{obs}^2 + r_c^2}$ and

$$F \simeq r^2 + 2(q\Gamma_{obs}\sqrt{r_{obs}^2 + r_c^2})^2\Omega_{obs}b - (1 + (q\Gamma_{obs}\sqrt{r_{obs}^2 + r_c^2})^2\Omega_{obs}^2)b^2. \tag{6.5}$$

The solutions of $F = 0$ in the leading order of r are $b_\pm = \pm Cr$, where

$$C = (1 + (q\Gamma_{obs}\sqrt{r_{obs}^2 + r_c^2})^2\Omega_{obs}^2)^{-1/2}. \tag{6.6}$$

It can be seen that $C < 1$ and hence the forbidden regions expand for fixed ω_{obs} in comparison to the case when ω_0 is fixed.

It is clear that the shape of C will change with respect to r_{obs}. In order to describe this, it is useful to write

$$q\Gamma_{obs}\sqrt{r_{obs}^2 + r_c^2}\Omega_{obs} \propto \frac{\sqrt{r_{obs}^2 + r_c^2}}{r_{obs}^3\sqrt{\mathcal{A}_{obs}\mathcal{D}_{obs}}}. \tag{6.7}$$

One thus sees that this term decreases for a given r_{obs} above the static limit (from ∞ to 0), and C thus increases between the horizon and infinity, ranging from 0 to 1. For the choice of parameters applied in Fig. 5.3 one gets $C = 0.681$ in the left panel and $C = 0.9997$ for the right part of the right panel.

It was already discussed in the previous chapter that there exists an asymptote of either b_- or b_+. Its value can be found when setting the term $\propto b^2$ in (6.4) equal to 0. This yields

$$f = -Q^2\Omega_{obs}^2 = -q^2\Gamma_{obs}^2\mathcal{D}\mathcal{P}r^2\Omega_{obs}^2. \tag{6.8}$$

Since f can be negative only for $r < 2$, the asymptote can occur exclusively below the static limit. Notice that the asymptote is located precisely at $r = 2$ in the case when ω_0 is fixed while in the other case it is shifted closer to the horizon. Moreover, recall that the position of the asymptote represents not only the boundary of a forbidden region for rays, but also the innermost radius where a neck can occur (for details see Section 6.3).

The value of $-f$ decreases from positive values to 0 between the horizon and the static limit, while $\mathcal{D}r^2$ increases in this interval of radii, starting from 0 at the horizon. The exact position of the asymptote is hence given by the remaining terms and implicitly by r_{obs}. At the horizon $\Gamma_{obs} \to \infty$, while $\Omega_{obs} \to 0$ for $r \to \infty$. Then, the larger the assumed observer position, the closer to the static limit the asymptote is. This is a natural conclusion when one realizes that the fixed ω_{obs} case merges with the fixed ω_0 case for $r_{obs} \to \infty$. In Fig. 5.3 the used parameter values yield the position of the asymptotes at $r = 1.836$ in the left panel and at $r = 1.691$ in the left part of the right panel.

While in the case with fixed ω_0 one always gets similar results as in vacuum, i.e., that the asymptote lies at $r = 2$ and the diverging function is b_-, this needs not to be the case with fixed ω_{obs}. It has been shown already that the asymptote position can be closer to the horizon in the latter case, and moreover, the divergent function can be b_+ rather than b_-. The reason for this can be explained when one studies the term $\propto b$ in (6.4) more carefully. If this term is negative at the position of the asymptote, the divergent function is b_-, while it is b_+ in the opposite case. Furthermore, if the diverging function is b_+, a neck necessarily occurs and the boundary of the forbidden regions touches the asymptote from the opposite side than if the diverging function is b_-. That is, the function b_+ falls to $-\infty$ from the left side of the asymptote and aims to $+\infty$ from the right side of it.

At the asymptote position, the term $\propto b$ in (6.4) can be rewritten as

$$\left(-2ar^{-1} - \frac{f}{\Omega_{obs}}\right)\Big|_{f=-Q^2\Omega_{obs}^2} \propto \frac{\mathcal{A}_{obs} r_{obs}^3 (2-r)}{4a^2} - 1. \tag{6.9}$$

This term remains positive below some r_1 which is larger than the outer horizon radius and can be found from

$$r_1 = r_{h+} + r_{h-}\left(1 - \frac{4a^2}{\mathcal{A}_{obs} r_{obs}^3 r_{h-}}\right), \tag{6.10}$$

where $r_{h\pm}$ denote the two horizon positions (roots of $\mathcal{D} = 0$). Note that these positions satisfy the equality $2 = r_{h+} + r_{h-}$.

With the parameter values used in the left part of the right panel of Fig. 5.3 one finds that $r_1 = 1.625$, which is less than the asymptote position (1.691) and the diverging function hence has to be b_-. Additionally, to obtain b_+ as the diverging function requires $q > q_{rev} = (\Gamma_{obs}\Omega_{obs})^{-1}\sqrt{-f/(D\mathcal{P})}|_{r=r_1}$ ("rev" stands for "reversed"). In the case shown in Fig. 5.3, $q_{rev} = 1.421$ and hence $q < q_{rev}$.

6.3 Neck Occurrence for Fixed ω_{obs}

The allowed regions for rays with fixed ω_{obs} seen by LNRF observers can be determined from $F = 0$ with F defined by (6.4). This equation has a discriminant Δ

of the form

$$\Delta = (1 - q^2\Gamma_{obs}^2 f_+ \mathcal{P})\mathcal{D}r^2, \quad f_+ = f + 4ar^{-1}\Omega_{obs} - \mathcal{A}r^2\Omega_{obs}^2. \tag{6.11}$$

This relation differs from the discriminant obtained in the vacuum case, where $\Delta = \mathcal{D}r^2$, by the extra factor in the brackets. However, the bracket factor is crucial for determining the occurrence of a neck, which can connect the forbidden regions for rays in the (r, b)-plane as described in the previous chapter. The interval (r_A, r_B) describing the neck extent can be calculated by setting $\Delta = 0$, which in this case reduces to the condition $1 - q^2\Gamma_{obs}^2 f_+ \mathcal{P} = 0$. Note that the neck formation in the case with fixed ω_0 is limited to sufficiently large $q > q_{crit}$ (see Section 6.1 for details), but this is not true in the case with fixed ω_{obs}. The parameter q can now be chosen arbitrarily and the neck forms, requiring that r_{obs} does not lie in the interval $(\rho_{obsA}, \rho_{obsB})$, where the discriminant of (6.4) equals or is larger than zero. This statement can be proven when the form of (6.11) is studied in the two limiting situations in which r_{obs} is chosen close to the horizon or far from it. Let me now discuss these two cases separately.

In the vicinity of the horizon position r_h, one can expand the corresponding expressions in terms of $\epsilon_h = r - r_h$, assuming that $\epsilon_h \ll 1$. Then,

$$\mathcal{D} \simeq 2\sqrt{1 - a^2}u_h^2\epsilon_h, \quad \mathcal{A}_h = 4u_h^2. \tag{6.12}$$

Note that in the leading order it is reasonable to take the value of $\mathcal{A}$ precisely at the horizon. Furthermore, the observer is assumed to be displaced from the horizon by $\epsilon_{obs} \ll 1$. This leads to

$$\Gamma_{obs} \simeq \sqrt{\frac{\mathcal{A}_h}{\mathcal{D}_{obs}}} \simeq 2(2\sqrt{1 - a^2}\epsilon_{obs})^{-1/2}, \quad \Omega_{obs} \simeq \frac{1}{2}au_h. \tag{6.13}$$

Hence, the bracket term in (6.11) close to the horizon reduces to

$$1 - q^2\Gamma_{obs}^2 f_+ \mathcal{P} \simeq 1 - 4q^2(2\sqrt{1 - a^2}\epsilon_{obs})^{-1} f_+, \tag{6.14}$$

where

$$rf_+ = r - 2 + 4a\Omega_{obs}(1 - \frac{\mathcal{A}r^3}{4a}\Omega_{obs}) \simeq [1 - \frac{1}{4}a^2(3 + a^2u_h^2)]\epsilon_h. \tag{6.15}$$

Recall that $\mathcal{P} \simeq 1$ when both r_{obs} and r are assumed to lie close to the horizon.

Then, when $\epsilon_{obs} \ll 1$ a neck occurs in the (r, b)-plane with the inner edge oriented away from the horizon limited by some ϵ_A. Considering that (6.14) has to vanish at this point, with the usage of (6.15) one reveals that ϵ_A is given by

$$\epsilon_A = \frac{q^{-2}\epsilon_{obs}}{4}\frac{2r_h\sqrt{1 - a^2}}{1 - \frac{1}{4}a^2(3 + a^2u_h^2)} = q^{-2}\epsilon_{obs}\frac{2r_h^3\sqrt{1 - a^2}}{(4 - 3a^2)r_h^2 - a^4} = q^{-2}\epsilon_{obs}. \tag{6.16}$$

Here the fact was utilized that the denominator of the second fraction equals $2r_h^3\sqrt{1 - a^2}$, which can be inferred after substituting $r_h = 1 + \sqrt{1 - a^2}$. If one wants to estimate the position of the asymptote of b_-, an expansion of F up to the first order in ϵ_h leads to the same result as for ϵ_A, i.e., $q^{-2}\epsilon_{obs}$. Hence, to show that ϵ_A is larger than the asymptote position and thus that the point where b_-

intersects with b_+ lies beyond the asymptote of either b_- or b_+, it is necessary to proceed one order higher in ϵ_{obs}.

In the other limit, when $r_{obs} \gg 1$, one gets

$$\Gamma_{obs} \simeq 1, \quad \Omega_{obs} = O(u_{obs}^3). \tag{6.17}$$

When also $r \sim r_{obs}$, one gets

$$f_+ \simeq 1, \quad \mathcal{P} \simeq r_{obs}^2 u^2. \tag{6.18}$$

All these values lead to the conclusion that the bracket term in (6.11) for large r_{obs} (far from the horizon) yields

$$1 - q^2 \Gamma_{obs}^2 f_+ \mathcal{P} \simeq 1 - q^2 r_{obs}^2 u^2. \tag{6.19}$$

Hence, in the (r, b)-plane there is also a neck, of an outer edge aimed towards the horizon down to $r_B = q r_{obs}$.

Besides the limiting values r_A and r_B, there are special choices of r_{obs} which cause the neck to formally shrink to a point. The position of this point can be derived from the requirement that not only the bracket term of (6.11) equals zero, but also its first derivative with respect to the radial coordinate vanishes. These two conditions return two equations which have to be solved, namely

$$1 = q^2 \Gamma_{obs}^2 f_+ \mathcal{P}, \tag{6.20}$$

$$(f_+ \mathcal{P})' \propto (1 - a\Omega_{obs})^2 u (3 + r_c^2 u^2) - (r_c^2 - a^2)\Omega_{obs}^2 - 1 = 0. \tag{6.21}$$

The second equation is a cubic equation for u. To solve this problem completely, one has to apply the formula for corresponding solutions (Cardano's formula) as a function of Ω_{obs} and combine that with a numerical approach in order to find two pairs of values (r_{obs}, r). The corresponding solutions for the choice of parameters used in Fig. 5.4 are $(\rho_{obsA}, \rho_A) = (1.726, 2.176)$ and $(\rho_{obsB}, \rho_B) = (6.769, 3.080)$.

The analysis performed above of the neck occurrence in the two limiting regimes for r_{obs} (close and far from the horizon) indicates that the neck connects the forbidden regions if $r_{obs} < \rho_{obsA}$ and also when $r_{obs} > \rho_{obsB}$. It follows that r_{obs} chosen within the interval $(\rho_{obsA}, \rho_{obsB})$ returns two separate forbidden regions without any neck. Furthermore, the interval (ρ_A, ρ_B) is situated completely inside the interval $(\rho_{obsA}, \rho_{obsB})$. Due to this, the relations $\epsilon_A = q^{-2}\epsilon_{obs} > \epsilon_{obs}$ and $r_B = q r_{obs} < r_{obs}$ revealed at $r_{obs} \sim r_h$ and $r_{obs} \gg 1$, respectively, hold over the whole range of r_{obs} chosen between r_h and ρ_{obsA} and further from ρ_{obsB} to infinity. The verification of this conclusion can be performed numerically, as the bracket term of (6.11) is a cubic expression for r and applying Cardano's formula allows one to express r_A and r_B as functions of r_{obs}.

6.4 Allowed Regions in the (r_{obs}, b)-plane

Although the idea of identifying the allowed regions in the (r_{obs}, b)-plane is the same as in the (r, b)-plane, there are some technical differences which should be treated separately. In this section these aspects are analyzed for the rays detected by LNRF observers. The task is still the same, i.e., to find the functions limiting

the impact parameters, but in this case such that $B_\pm = b_\pm(r_{obs})$. In order to complete this task, one has to redefine F presented in (5.9), taking into account that the unknown radial variable is now solely r_{obs}, i.e.,

$$\mathcal{F}_{obs} = F_{obs}u_{obs}^2 = \mathcal{A}_{obs} - 4au_{obs}^3 b - f_{obs}u_{obs}^2 b^2 - \mathcal{D}_{obs}\zeta_{obs}^2, \tag{6.22}$$

where ζ_{obs} is given by relation (5.21).[1] Moreover, because $\mathcal{P}|_{r=r_{obs}} = 1$, the formula for ζ_{obs} is simplified in comparison with the original form (5.21) to

$$\zeta_{obs}^2 = q^2\Gamma_{obs}^2(1-\Omega_{obs}b)^2 = q^2\frac{\mathcal{A}_{obs}}{\mathcal{D}_{obs}}(1-\Omega_{obs}b)^2. \tag{6.23}$$

Substituting this expression in (6.22) and applying identity (5.6) returns

$$\mathcal{F}_{obs} = (1-q^2)\mathcal{A}_{obs}(1-\Omega_{obs}b)^2 - \frac{\mathcal{D}_{obs}}{\mathcal{A}_{obs}}u_{obs}^2 b^2. \tag{6.24}$$

This expression corresponds to the equivalent formula for vacuum with the substitution $\mathcal{D}_{obs} \to \mathcal{D}_{obs}(1-q^2)^{-1}$. Setting $\mathcal{F}_{obs} = 0$, one finds the solutions

$$B_\pm = \frac{\mathcal{A}_{obs}r_{obs}^2}{2ar_{obs}^{-1} \pm \sqrt{\mathcal{D}_{obs}(1-q^2)^{-1}}r_{obs}}. \tag{6.25}$$

The asymptotes of $B_\pm$ at $r_{obs} \gg 1$ are $\pm\sqrt{1-q^2}r_{obs}$. For large b, $\mathcal{F}_{obs}$ can be expressed as

$$\mathcal{F}_{obs} = \left[(1-q^2)\mathcal{A}_{obs}\Omega_{obs}^2 - \frac{\mathcal{D}_{obs}}{r_{obs}^2\mathcal{A}_{obs}}\right]b^2 \propto \left[1-q^2-\frac{\mathcal{D}_{obs}}{4a^2}r_{obs}^4\right]b^2. \tag{6.26}$$

Thus, the asymptote position of the function B_- can be found from the condition $\sqrt{\mathcal{D}_{obs}}r_{obs}^2 = 2a\sqrt{1-q^2}$. For the parameter values used in Fig. 5.4 the asymptote occurs at radius $r_{obs} = 1.874$.

In order to construct the curves $\mathcal{B}_\pm$ in the (r_{obs}, b)-plane, it is necessary to define the interval $(\rho_{obsA}, \rho_{obsB})$, in which a neck does not occur. For r_{obs} from this interval one has to calculate the maximum and minimum impact parameters of the lower and upper forbidden regions in the (r, b)-plane, respectively. A sequence of these points drawn in the (r_{obs}, b)-plane leads to the desired $\mathcal{B}_\pm$ curves. The two lines $\mathcal{B}_-$ and $\mathcal{B}_+$ are separated inside $(\rho_{obsA}, \rho_{obsB})$, but they intersect at the boundaries of this interval. Thus, these two curves form a closed loop in the (r_{obs}, b)-plane as shown in Fig. 5.4. This loop hence forms the boundary of the region $\mathcal{O}_{h+i}$, which is situated inside and the corresponding rays can reach the observer from both sides, i.e., from the horizon as well as from infinity. On the contrary, the rays on the boundary, lying either on $\mathcal{B}_+$ or $\mathcal{B}_-$, arrive at the observer's position from one side only. The rays originating either on the horizon

[1] The vacuum part of (6.22) originally given by (5.8) can be treated with identity (5.6), but notice that the same form can be directly derived when a 2D metric is defined, namely

$$ds_2^2 = -\frac{\mathcal{D}}{\mathcal{A}}dt^2 + \mathcal{A}r^2 d\tilde{\varphi}^2,$$

where $d\tilde{\varphi} = d\varphi - \Omega dt$. Then, the corresponding formula can be obtained from $\mathcal{F}_{vac} = -\omega_0^{-2}\mathcal{D}g^{AB}\tilde{k}_A\tilde{k}_B$, assuming that $\tilde{k}_A = \omega_0(-1+\Omega b, b)$.

or at infinity can be distinguished on the curves $\mathcal{B}_+$ and $\mathcal{B}_-$ due to the points $P_\pm$ which divide the boundary of $\mathcal{O}_{h+i}$ into two parts. The positions of the points $P_\pm$ and the lines $B_\pm$ and $\mathcal{B}_\pm$ in their vicinity are discussed further in detail.

Along with the change of r_{obs} between ρ_{obsA} also ρ_{obsB}, the minima of b_+ and the maxima of b_- also vary, from ρ_A to ρ_B. In general, $\rho_A > \rho_{obsA}$ and $\rho_B < \rho_{obsB}$, and at some r_{obs} the observer's position equals the radius at which the considered limiting value of either b_+ or b_- appears. Hence, these values of r_{obs} correspond to the positions of the points $P_\pm$ in the (r_{obs}, b)-plane. The functions $B_+(r_{obs})$ and $\mathcal{B}_+(r_{obs})$ intersect at r_{obs} which corresponds to the radius of minimum b_+ and similarly $B_-(r_{obs})$ and $\mathcal{B}_-(r_{obs})$ coincide at the position of maximum b_-. The positions of the extreme values in the (r, b)-plane can be found from the condition $\partial_r b_\pm(r_{obs}, r) = 0$ or, equivalently, from the equation $\partial_r F(r_{obs}, r, b)\big|_{b=b_\pm(r_{obs},r)} = 0$. Then, in order to find the corresponding r_{obs} in the (r_{obs}, b)-plane, one has to solve

$$\partial_r F(r_{obs}, r_{obs}, b)\Big|_{b=B_\pm(r_{obs})} = 0. \tag{6.27}$$

This relation is rather complicated, and to express the substantial dependences concisely, the subscript "*obs*" will now be omitted for a while and left only at its original places. Furthermore, rather than with F itself in this case it is useful to deal with the relation

$$fF = \mathcal{D}r^2 - (fb + 2ar^{-1})^2 - fQ^2(1 - \Omega_{obs}b)^2, \tag{6.28}$$

where the identity (5.6) and Q defined in Section 6.2 were used. Then,

$$\partial_r(fF) \propto \frac{1}{4}(f(\mathcal{D}r^2)'r^2 + a^2) - \left(fb + 2ar^{-1} - \frac{a}{2}\right)^2 - \frac{1}{4}f(fQ^2)'r^2(1 - \Omega_{obs}b)^2. \tag{6.29}$$

The first and third terms can be simplified later by using

$$\frac{1}{2}f(\mathcal{D}r^2)'r^2 = r^3 - 3r^2 + 2r, \tag{6.30}$$

$$\frac{1}{2}f(fQ^2)'r^2 = q^2\Gamma_{obs}^2\mathcal{P}f\left(r^3 - 2r^2 + a^2 - \frac{f\mathcal{D}r^5}{r^2 + r_c^2}\right) \equiv q^2\Gamma_{obs}^2\mathcal{P}f\nu. \tag{6.31}$$

Considering the condition (6.27) and getting rid of Q^2 by applying (6.28), from (6.29) one gets

$$\frac{1}{4}(f(\mathcal{D}r^2)'r^2 + a^2) - \left(fB_\pm + 2ar^{-1} - \frac{a}{2}\right)^2 - \frac{1}{2}\nu\left(1 - \frac{(fB_\pm + 2ar^{-1})^2}{\mathcal{D}r^2}\right) = 0. \tag{6.32}$$

From this equation it is possible to find the values of radii r_{obs} where either b_+ or b_- reach their extreme values. The parameter values chosen in Fig. 5.4 yield 1.965 as the radius where b_+ has its minimum, while b_- reaches its maximum at radius 3.593.

The significance of the points $P_\pm$ is not only being the points of coincidence of the functions $\mathcal{B}_\pm$ and $B_\pm$, but in addition the functions are mutually tangent at these points. It should be recalled here that the corresponding pairs of lines (i.e., either $\mathcal{B}_+$ and B_+ or $\mathcal{B}_-$ and B_-) have exclusively one common point. The same conclusion can be also seen when analysing the functions $\mathcal{B}_\pm(r_{obs})$ and $B_\pm(r_{obs})$

close to their extreme values. This is illustrated for the functions $\mathcal{B}_+$ and B_+. The line $\mathcal{B}_+(r_{obs})$ is defined as the minimum of function $b_+(r_{obs}, r)$, and hence $B_+ > \mathcal{B}_+$ in the vicinity of the position where $b_+(r_{obs}, r)$ is minimal. Thus, for r_{obs} larger than this position the relation

$$\frac{dB_+}{dr_{obs}} \geq \frac{d\mathcal{B}_+}{dr_{obs}} \tag{6.33}$$

has to be satisfied, while at r_{obs} less than the minimal radius,

$$\frac{dB_+}{dr_{obs}} \leq \frac{d\mathcal{B}_+}{dr_{obs}}. \tag{6.34}$$

From these two inequalities one directly sees that exactly at the position r_{obs} of minimal b_+

$$\frac{dB_+}{dr_{obs}} = \frac{d\mathcal{B}_+}{dr_{obs}}, \tag{6.35}$$

and so these two derivatives correspond to each other.

Note that in addition to the minimal radii calculated for particular choices of parameters a, r_c, and q, relation (6.32) is also always fulfilled at $r_{obs} = 2$ regardless of the parameter values. This can be easily seen, since at $r_{obs} = 2$ one gets

$$\frac{1}{2} f(\mathcal{D}r^2)' r^2|_{r=2} = 0, \quad fB_\pm + 2ar^{-1}|_{r=2} = a, \quad \mathcal{D} = a^2 r^{-2} \tag{6.36}$$

and (6.32) reduces to

$$\frac{1}{4}(0 + a^2) - \left(a - \frac{a}{2}\right)^2 - \frac{1}{2}\nu\,(1 - 1) = 0. \tag{6.37}$$

However, this solution is rather pathological and it cannot be interpreted that the functions $\mathcal{B}_\pm(r_{obs})$ and $B_\pm(r_{obs})$ merge twice for the same r_{obs}, i.e., at the static limit $r_{obs} = 2$ (inside $(\rho_{obsA}, \rho_{obsB})$) and outside the interval $(\rho_{obsA}, \rho_{obsB})$. The pathology occurs because the expressions used for deriving (6.32) were based on calculating fF, not F only, and the relation $\partial_r F$ includes the additional factor f^{-2} which has to appear also when substituting in (6.32). Then, the correct equation which has to vanish is (6.32) multiplied by f^{-2} evaluated at r_{obs}. When $r_{obs} \sim 2$, $f_{obs} = \epsilon_{obs}/2$ and (6.32) is $O(\epsilon^2_{obs})$, where $\epsilon_{obs} = r_{obs} - 2$. Due to this, the corresponding equation does not generally have a solution at $r_{obs} = 2$. Just for completeness, the coefficient of the term $\propto \epsilon^2_{obs}$ in (6.32) is

$$\left(1 + \frac{a^2}{2}\right)\left[\frac{1}{2} + \frac{4}{(4 + r_c^2)} - 2\left(1 + \frac{a^2}{2}\right) a^{-2} q^{-2}\right] k_\pm + \frac{3}{2} + \frac{a^2}{8}, \tag{6.38}$$

where

$$k_\pm = \frac{\sqrt{(1 - q^2)^{-1}} \mp 1}{\sqrt{(1 - q^2)^{-1}} \pm 1}. \tag{6.39}$$

For $a \sim 0$, the factors (6.38) are negative, reaching the order $\propto -a^{-2}$, but while the negative branch remains less than zero even for a close to 1, the factor with k_+ crosses 0 at some $a_{crit} < 1$. This is true if one assumes that q is not too close to 1. For the parameter values used in Fig. 5.4 one gets $a_{crit} = 0.784$.

The behaviour of (6.38) at the horizon and for $r_{obs} \gg 1$ suggests that zero is intersected at $r_{obs} > 2$ like an increasing function from below and at $r_{obs} < 2$ as decreasing from above. From this I conclude that the radius where b_- reaches its maximum is always larger than 2 for arbitrary a, while the radius of minimal b_+ is larger than 2 only for $a < a_{crit}$. In Fig. 5.4 it was chosen $a = 0.8$, which is greater than a_{crit} and, hence, point P_+ is shifted slightly to the left of $r_{obs} = 2$.

In order to perform a proper derivative of $B_\pm$ and $\mathcal{B}_\pm$ at r_{obs}, one has to realize that the observer's position is present in F only through the additional plasma term introduced in (5.9). Hence, its derivative with respect to r_{obs} in the case of the LNRF observer is

$$(\partial_{r_{obs}} F)|_{r=r_{obs}} = -2Q_{obs}^2 Y(1 - \Omega_{obs} b), \tag{6.40}$$

where

$$Y = \left(\frac{r_{obs} - a^2 r_{obs}^{-2}}{\mathcal{A}_{obs} r_{obs}^2} - \frac{r_{obs} - 1}{\mathcal{D}_{obs} r_{obs}^2} + \frac{r_{obs}}{r_{obs}^2 + r_c^2} \right) (1 - \Omega_{obs} b) + \frac{2a(3r_{obs}^2 + a^2)b}{(\mathcal{A}_{obs} r_{obs}^3)^2}. \tag{6.41}$$

The corresponding derivatives are then found by setting $b = B_\pm$. As seen in Fig. 5.4, it might seem that these derivatives are zero. However, they are only close to zero. Indeed, with the parameter values used in Fig. 5.4, the values of r_{obs} where $Y = 0$ return 1.944 and 3.580 for minimal b_+ and maximal b_-, respectively. Comparing these with the values obtained using equation (6.32), one sees that they are *close* to each other, not identical. If one calculates

$$\partial_b F_{obs} = -2(f_{obs} b + 2a r_{obs}^{-1} - Q_{obs}^2 \Omega_{obs}(1 - \Omega_{obs} b)) \tag{6.42}$$

and associates it with (6.40), one finds that

$$\frac{d\mathcal{B}}{dr_{obs}} = -0.0794 \quad \text{and} \quad \frac{d\mathcal{B}}{dr_{obs}} = 0.0074 \tag{6.43}$$

at r_{obs} corresponding to the minimum of b_+ and the maximum of b_-, respectively.

6.5 Special Features for a Freely Falling Observer

The allowed regions detected by freely falling observers are studied in the (r_{obs}, b)-plane. To describe them, it is useful to define the function $\mathcal{F}_{obs}$ analogously as in the previous section by (6.22), but with ζ known from (5.22). Due to this, a new term appears in the plasma part, so that one gets

$$\zeta^2 = q^2 \hat{\Gamma}_{obs}^2 \mathcal{P}(1 - \Omega_{obs} b - \xi_{obs} \eta_{obs})^2. \tag{6.44}$$

In order to compare the relations obtained for LNRF and for freely falling observers, the corresponding relations should be as similar as possible. It is thus reasonable to introduce an "effective LNRF parameter" defined by

$$q_{NR} = q \frac{\hat{\Gamma}_{obs}}{\Gamma_{obs}} = q \Gamma_{obs}, \tag{6.45}$$

which can be used in (6.44) to get

$$\zeta^2 = q_{NR}^2 \Gamma_{obs}^2 \mathcal{P}(1 - \Omega_{obs} b - \xi_{obs}\eta_{obs})^2. \tag{6.46}$$

A substantial difference between the LNRF and freely falling observers is that in the latter case

$$\mathcal{F}_{obs} = \eta_{obs}^2. \tag{6.47}$$

Note that in the case of the LNRF observer $\mathcal{F}_{obs} = 0$. For this reason, the solutions for η_{obs} have to be found first. Hence, one can write an additional quadratic equation for finding $\eta_{obs}^{(\pm)}$ rather than $b_\pm$, namely

$$\begin{aligned} -\mathcal{F}_{vac}|_{r=r_{obs}} + q_{NR}^2 \mathcal{A}_{obs}(1 - \Omega_{obs} b)^2 \\ -2q_{NR}^2 \mathcal{A}_{obs}\xi_{obs}(1 - \Omega_{obs} b)\eta_{obs} + (1 + q_{NR}^2 \mathcal{A}_{obs}\xi_{obs}^2)\eta_{obs}^2 = 0. \end{aligned} \tag{6.48}$$

It is worth mentioning that the coefficient in front of η_{obs}^2 can be also written as $1 + q_{NR}^2(1 - \Gamma_{obs}^{-2})$.

In order for the rays to reach the observer, the discriminant of (6.48) must be non-negative. One can thus write

$$\begin{aligned} \mathcal{F}_{vac}|_{r=r_{obs}}(1 + q_{NR}^2 \mathcal{A}_{obs}\xi_{obs}^2) - q_{NR}^2 \mathcal{A}_{obs}(1 - \Omega_{obs} b)^2 \\ \propto \mathcal{F}_{vac}|_{r=r_{obs}} - \tilde{q}_{NR}^2 \mathcal{A}_{obs}(1 - \Omega_{obs} b)^2 \geq 0, \end{aligned} \tag{6.49}$$

where

$$\tilde{q}_{NR}^2 = q_{NR}^2(1 + q_{NR}^2 \mathcal{A}_{obs}\xi_{obs}^2)^{-1} \tag{6.50}$$

can be viewed as a "modified effective LNRF parameter". Only rays satisfying (6.49) can reach a freely falling observer at r_{obs}. Moreover, analogously to the previous section, $\tilde{q}_{NR} < 1$ is required for rays of the corresponding frequency. The boundary impact parameters for the allowed regions of the rays are then given by $\tilde{B}_\pm = B_\pm(q \to \tilde{q}_{NR})$ (cf. (6.25)). The impact parameters b for rays which can reach the observer at r_{obs} vary as a function of this radius and the asymptote of $\tilde{B}_-$. For sufficiently large r_{obs} (greater than the asymptote radius) the ray impact parameters have to satisfy $\tilde{B}_- < b < \tilde{B}_+$, while for observer positions below the asymptote either $b < \tilde{B}_+$ or $b > \tilde{B}_-$. This leads to the same shapes of the allowed regions in the (r_{obs}, b)-plane as for the LNRF observers. There are two separate allowed regions for the rays. The region $\mathcal{O}_I$ extends over such r_{obs}, where $\tilde{B}_- < b < \tilde{B}_+$ and r_{obs} is larger than the asymptote of $\tilde{B}_-$, while for smaller r_{obs} it includes regions where $b < \tilde{B}_+$. The region $\mathcal{O}_{II}$ is located only at radii smaller than the asymptote where $b > \tilde{B}_-$.

The turning points of the rays are not situated at the boundaries of $\mathcal{O}_I$ and $\mathcal{O}_{II}$ as it was shown in the case of the LNRF observer. On the contrary, the radial velocity of the ray $\eta_{obs} < 0$ at the boundary of $\mathcal{O}_I$, while $\eta_{obs} > 0$ at the boundary of $\mathcal{O}_{II}$. Within $\mathcal{O}_I$ and $\mathcal{O}_{II}$ the radial velocity η_{obs} attains two values at each point, with either the same sign as at the boundary or the opposite. Of the same sign are the values $\eta_{obs}^{(-)}$ in $\mathcal{O}_I$ and $\eta_{obs}^{(+)}$ in $\mathcal{O}_{II}$, while $\eta_{obs}^{(+)}$ in $\mathcal{O}_I$ and $\eta_{obs}^{(-)}$ in $\mathcal{O}_{II}$ have the opposite sign. The sign of the given η_{obs} changes at the curves $B_\pm$ which are calculated from the assumption that the solution of (6.48) is zero. This leads to solving the equation

$$\mathcal{A}_{obs} - 4au_{obs}^3 b - f_{obs}u_{obs}^2 b^2 - q_{NR}^2 \mathcal{A}_{obs}(1 - \Omega_{obs} b)^2 = 0. \tag{6.51}$$

As r_{obs} approaches the horizon, the function Γ_{obs} increases from 1 to infinity, which causes also $\tilde{q}_{NR}$ to increase towards 1, since

$$\tilde{q}_{NR} = \frac{q_{NR}}{\sqrt{1 + q_{NR}^2 \mathcal{A}_{obs} \xi_{obs}^2}} = \frac{q_{NR}}{\sqrt{1 + q_{NR}^2 (1 - \Gamma_{obs}^{-2})}} = \frac{q}{\sqrt{(1-q^2)\Gamma_{obs}^{-2} + q^2}}. \quad (6.52)$$

Note that $\tilde{q}_{NR}$ is limited from below by q. For a fixed q the shapes of the regions $\mathcal{O}_I$ and $\mathcal{O}_{II}$ look different close to the horizon than in the case with a LNRF observer. While they meet at a given $b = b_h$ on the horizon for the LNRF observer, in the case of the freely falling observer they are separated by a gap limited by

$$b_{h\pm} = \frac{b_h}{1 \pm q b_h \sqrt{(1-q^2)^{-1}}}. \quad (6.53)$$

With the parameter values used in Fig. 5.5 one gets $b_{h+} = 1.045$ and $b_{h-} = -2.188$. The gap is thus located completely under the meeting point $b_h = 4$.

To maintain the formal correspondence of the regions $\mathcal{O}_I$ and $\mathcal{O}_{II}$ with those obtained for LNRF observers, it is suitable to fix $\tilde{q}_{NR}$ rather than q. Then, q decreases from $\tilde{q}_{NR}$ to 0 as r_{obs} heads from infinity to the horizon[2]. In comparison, q_{NR} increases as r_{obs} comes from infinity to the horizon, ranging between $\tilde{q}_{NR}$ and $\tilde{q}_{NR}(1 - \tilde{q}_{NR}^2)^{-1/2}$. The latter limit is larger than 1 for $\tilde{q}_{NR} > 1/\sqrt{2}$. Then, also q_{NR} exceeds 1 at some point above the horizon and the functions $B_\pm$ are thus defined only for r_{obs} above this limit. As a result, η_{obs} does not change its sign at positions between the horizon and the limiting radius. However, with $\tilde{q}_{NR} = 2/3$ chosen in Fig. 5.5 the functions $B_\pm$ are defined over the whole range of r_{obs}.

The main goal of analyzing the allowed regions in the (r_{obs}, b)-plane is to find the boundaries of the regions $\mathcal{O}_{h+i}$, $\mathcal{O}'_h$, $\mathcal{O}'_i$. In the case of an LNRF observer, the functions $\mathcal{B}_\pm$ were found for a given r_{obs} as the minimum of b_+ and the maximum of b_- in the (r, b)-plane, respectively. This is effectively performed by calculating $\mathcal{F}(r, r_{obs}, b) = 0$, which is a quadratic equation in b and can be solved analytically. In the case of a freely falling observer the task is more complicated because there are two classes of rays, given by $\eta_{obs}^{(+)}$ in class I and $\eta_{obs}^{(-)}$ in class II. Hence, there are also two functions $\mathcal{F}^{(\pm)}$ which have to be considered, i.e.,

$$\mathcal{F}^{(\pm)} = \mathcal{F}|_{\eta_{obs}=\eta_{obs}^{(\pm)}} = \mathcal{F}_{vac} - \tilde{q}_{NR}^2 \Gamma_{obs}^2 \mathcal{D}\mathcal{P} \left[\frac{1 - q_{NR}^2(1 - \Gamma_{obs}^{-2})}{1 + q_{NR}^2(1 - \Gamma_{obs}^{-2})} (1 - \Omega_{obs} b)^2 \right. \quad (6.54)$$
$$\left. + \xi_{obs}^2 \mathcal{F}_{vac}|_{r=r_{obs}} \mp 2\xi_{obs} \frac{(\mathcal{F}_{vac}|_{r=r_{obs}} - \tilde{q}_{NR}^2 \mathcal{A}_{obs}(1 - \Omega_{obs} b)^2)^{1/2}}{(1 + q_{NR}^2(1 - \Gamma_{obs}^{-2}))^{1/2}} (1 - \Omega_0 b) \right].$$

However, the corresponding impact parameters solving $\mathcal{F}^{(\pm)} = 0$ have to satisfy the equation $\mathcal{F}^{(+)}\mathcal{F}^{(-)} = 0$ which is quartic in b. In principle, an analytical solution of this expression could be calculated, but it is not much helpful for determining $\mathcal{B}_\pm$. Thus, the values of these functions are found here as the points where $\mathcal{F}^{(+)}$ and $\mathcal{F}^{(-)}$ cross zero at a given r_{obs}, if these exist.

In the case of an LNRF observer, the discussed curves are just segments along the boundary of $\mathcal{O}_{h+i}$ divided by the positions of $P_\pm$. Here, although they are still

[2]Recall that

$$q = \frac{\tilde{q}_{NR}}{\sqrt{(1 - \tilde{q}_{NR}^2)\Gamma_0^2 + \tilde{q}_{NR}^2}}.$$

parts of this boundary, they are separated by whole segments of the curves $\tilde{B}_{\pm}$ rather than only by points. On the curve $\tilde{B}_{+}$ the limiting points of these segments are P_{A+}, P_{B+}, while on $\tilde{B}_{-}$ the points are P_{A-}, P_{B-}. Moreover, at P_{A+} and P_{B+} the value of b is maximal and at P_{A-}, P_{B-} it is minimal out of all rays which can reach the observer with the given frequency. In addition, the rays at $P_{A\pm}$ originate at the peak of the boundary between the forbidden regions in the (r, b)-plane, while those situated at $P_{B\pm}$ terminate there. Hence, the radial positions of the corresponding peaks between the allowed and forbidden regions are different than the positions of the observers at these points. The observer positions are lower at $P_{A\pm}$ and larger at $P_{B\pm}$. The positions of these points for the parameter values used in Fig. 5.5 are $(r_{obsA+}, r_{A+}) = (1.708, 1.900)$, $(r_{obsB+}, r_{B+}) = (2.405, 1.919)$, $(r_{obsA-}, r_{A-}) = (2.859, 3.644)$, and $(r_{obsB-}, r_{B-}) = (4.548, 3.624)$.

As for the LNRF observer, for which $\mathcal{B}_{\pm}$ curves are tangent to the lines $B_{\pm}$, the same relationship can be identified also for functions discussed in the case of a freely falling observer. Thus, $\mathcal{B}_{+}^{(\pm)}$ are tangent to $\tilde{B}_{+}$ and $\mathcal{B}_{-}^{(\pm)}$ to $\tilde{B}_{-}$, i.e., to the boundaries of $\mathcal{O}_I$. Note that $\mathcal{B}_{+}^{(+)}$ lies on the upper border of $\mathcal{O}_{h+i}^{(+)}$, close to the arc $P_{A+}P_{B+}$, while $\mathcal{B}_{-}^{(+)}$ is situated on the lower border of $\mathcal{O}_{h+i}^{(+)}$, close to the arc $P_{A-}P_{B-}$. Similarly, $\mathcal{B}_{\pm}^{(-)}$ define the boundaries of the region $\mathcal{O}_{h+i}^{(-)}$.

The tangency of the curves can be demonstrated in the vicinity of P_{B+} for rays of class I (left panel of Fig. 5.5). Close to this point, the boundary of $\mathcal{O}_{h+i}$ is crossed three times at a given $r_{obs} = const.$ and there is an additional forbidden region confined from both sides. While the rays with $b = \tilde{B}_{+}$ at positions r_{obs} larger than P_{B+} bounce back once they reach the observer, those at r_{obs} less than P_{B+} reach the upper border of the additional forbidden region. In accordance with the previous case, one gets

$$\frac{dB_{+}}{dr_{obs}} \geq \frac{d\mathcal{B}_{+}{}^{(-)}}{dr_{obs}} \quad \text{and} \quad \frac{dB_{+}}{dr_{obs}} \leq \frac{d\mathcal{B}_{+}^{(+)}}{dr_{obs}} \tag{6.55}$$

for r_{obs} larger and r_{obs} lower than P_{B+}, respectively. This leads to the appearance of a new feature. While for an LNRF observer the forbidden region shifts to the left without any deformation as r_{obs} passes P_{+} from larger radii, here, after crossing P_{B+} from the right, the forbidden region shrinks to a point before forming a new forbidden region. From numerical calculations we infer that the transition from the upper forbidden region to the new region is smooth and $d\mathcal{B}/dr_{obs}$ is thus continuous.

As demonstrated in Fig. 5.5, the regions $\mathcal{O}_{h+i}$ are significantly different for rays of classes I and II. In comparison with the previous case, they touch the forbidden regions not only at one point, but along a finite part of their mutual boundary. The region $\mathcal{O}_{h+i}$ shrinks to a point at $Q_{\pm}$ located on $B_{\pm}$ for rays of class I, and it directly reaches the horizon over a finite range of b for rays of class II.

It can also be seen from Fig. 5.5 that the boundary of $\mathcal{O}_{h+i}^{(-)}$ is formed by the arcs $P_{A+}P_{A-}$ and $P_{B+}P_{B-}$ which intersect at the points $Q_{\pm}$. In the (r, b)-plane there are two forbidden regions in the neighbourhood of Q_{-}: the upper region and the additional one discussed above. These two areas are detached and after r_{obs} crosses Q_{-} (here at 3.494) the new region diminishes to a point before expanding again with an opposite direction than before.

In the right neighbourhood of Q_+, the lower forbidden corner and the additional forbidden region are situated. They touch as r_{obs} passes through Q_+ (here at 2.159) and at smaller radial distances only the forbidden corner remains. The central part of $\mathcal{O}^{(+)}_{h+i}$ has its left border at larger radii than Q_+. In this region $\rho^{(+)}_{obsA} = \rho^{(+)}_A$, which furthermore corresponds to the position of Q_+. Besides that, numerical calculations yield the values of the maximal radii $(\rho^{(+)}_{obsB}, \rho^{(+)}_B) = (3.966, 3.161)$.

Finally, we investigate the limiting values of b where $\mathcal{O}^{(-)}_{h+i}$ reaches the horizon. First, let me rewrite the additional term present in $\mathcal{F}^{(-)}$ due to the presence of a plasma as (cf. (6.54))

$$-q^2_{NR}\Gamma^2_{obs}\mathcal{DP}(1-\Omega_{obs}b-\xi_{obs}\eta_{obs})^2 = -q^2_{NR}\Gamma^2_{obs}\mathcal{DP} \tag{6.56}$$
$$\times\left[\frac{1-\Omega_{obs}b+\xi_{obs}((1+q^2_{NR}\mathcal{A}_{obs}\xi^2_{obs})\mathcal{F}_{vac}|_{r=r_{obs}} - q^2_{NR}\mathcal{A}_{obs}(1-\Omega_{obs}b)^2)^{1/2}}{1+q^2_{NR}\mathcal{A}_{obs}\xi^2_{obs}}\right]^2.$$

The term in the square root can be rearranged with the help of the identities (5.6) and (6.52) as follows

$$(1+q^2_{NR}\mathcal{A}_{obs}\xi^2_{obs})\left[(1-\tilde{q}^2_{NR})\mathcal{A}_{obs}(1-\Omega_{obs}b)^2 - \frac{\mathcal{D}_{obs}}{\mathcal{A}_{obs}}u^2_{obs}b^2\right]. \tag{6.57}$$

Notice that the relation in the square brackets in (6.57) formally corresponds to (6.24) with replacement $q \to \tilde{q}_{NR}$. The obtained expressions now have to be evaluated at $r_{obs} = r_h$. Because $\mathcal{D} = 0$ at the horizon, in this limit one gets

$$\xi|_{r_{obs}=r_h} = -\mathcal{A}_h^{-1/2}, \quad q_{NR}|_{r_{obs}=r_h} = \frac{\tilde{q}_{NR}}{\sqrt{1-\tilde{q}^2_{NR}}}, \tag{6.58}$$

which further leads to

$$(1+q^2_{NR}\mathcal{A}_{obs}\xi^2_{obs})\Big|_{r_{obs}=r_h} = 1+q^2_{NR} = \frac{1}{1-\tilde{q}^2_{NR}}. \tag{6.59}$$

Substituting all these relations in (6.56) shows that at $r_{obs} = r_h$ this term

$$\propto 1-\Omega_{obs}b-|1-\Omega_{obs}b|. \tag{6.60}$$

Thus, one can see that at the horizon the plasma term in $\mathcal{F}^{(-)}$ completely drops out and the function $\mathcal{F}^{(-)}(r, r_{obs}, b)$ then reduces to $\mathcal{F}_{vac}(r, b)$. Due to this, at $r_{obs} = r_h$ also $\mathcal{B}_\pm(r_{obs})$ reduce to the vacuum solutions $\mathring{b}_\pm$. Recall that $\mathcal{B}_\pm(r_{obs})$ are defined with $\mathcal{F}^{(-)}(r, r_{obs}, b) = \partial_r\mathcal{F}^{(-)}(r, r_{obs}, b) = 0$.

The choice $a = 0.8$ used in Fig. 5.5 yields limit values of b seen by an observer at the horizon as $(\mathcal{B}_{h+}, \mathcal{B}_{h-}) = (3.237, -6.662)$. Because $\mathcal{O}^{(-)}_{h+i}$ is directly adjacent to the horizon, the radial distances of rays which can reach the black hole are limited only from above, in Fig. 5.5 by the values $(\rho^{(-)}_{obsB}, \rho^{(-)}_B) = (11.378, 3.067)$.

Conclusion

My thesis focuses on an analytical description of various aspects of light propagation in a medium of dispersive and refractive properties in the vicinity of a gravitating object. Although this topic has been widely studied in the literature, there are several important features which are typically overlooked. The main aim of this work was to contribute to the field with a rigorous analysis of these ignored problems.

The applied formalism is based on the geometrical optics approximation and the approach introduced by Synge [1960], for this purpose a basic description of both is provided in Chapter 1. Their main ideas and principles are usually discussed in many papers related to the subject. Instead, this chapter puts more emphasis on aspects of the formalism that are often not explained appropriately and on providing a broader context for the involved terms. At the end of the chapter, a brief review of recently published relevant work is given. Although the presented overview cannot cover the full range of works published in the field, it was included to help clarify the limits of current applications and indicate possible directions of future research.

General formulae obtained for an axially symmetric stationary spacetime immersed in a medium, possibly but not necessarily limited to a cold plasma, are presented in Chapter 2. These expressions include the generalized Carter constant, the photon region, the black hole shadow, and the deflection angle. Note that in order to find the Carter constant, the functions describing both the spacetime and the medium have to satisfy several simple algebraic conditions. These are based on the separability requirement of the Hamilton-Jacobi equation. Such general conditions are also stated in this chapter, providing a simple way how to decide whether a solution exists or not. Moreover, it is shown that the conditions set on the medium (plasma) and on the gravitating objects are independent.

In order to demonstrate the utility of the obtained relations, the general formulae presented in Chapter 2 are applied to specific settings in Chapter 3. For several axially symmetric spacetimes the separability conditions revealed whether the Carter constant exists or not. In those cases where it exists, the Carter constant is calculated and analytical forms of both the photon region and the shadow are derived. The deflection angle around an object characterised by the Hartle-Thorne metric in the weak-field approximation is derived and compared with the solution given by a general formula introduced in Chapter 2. Moreover, ray tracing in a plasma and in vacuum is compared for objects described by both the Kerr and Hartle-Thorne metrics. It is demonstrated that the light deflection in plasma is smaller than in vacuum.

A slightly different setting is studied in Chapter 4. In comparison with the previous chapters, a spherically symmetric spacetime is considered here and a general moving medium is assumed. This assumption requires going beyond the cold plasma approximation and, hence, a more general form of the refractive index is studied. Deflection angles are calculated for the cases of radially falling and rotating media. Furthermore, a perturbative approach to the whole problem is presented. Two perturbative schemes were assumed in this work, namely that *any* kind of plasma represents a small deviation from vacuum and the perturbation

from the cold plasma case. In the former case the zeroth-order term corresponds to the vacuum results, while in the latter the zeroth-order term is the cold plasma deflection angle previously obtained in the literature [e.g., Tsupko, 2021].

Chapters 5, 6 provide a non-standard approach to the topic. Taking the cold plasma approximation characterised as a nonsingular isothermal sphere surrounding a Kerr black hole, the allowed regions for rays are studied. The rays are described by their impact parameters and various aspects of the accessible regions are studied for two classes of observers, locally nonrotating and freely falling. This approach serves as a complementary description to the previous chapters and since it is not commonly applied, it provides unique and useful insights.

The topic of ray propagation in refractive and dispersive media around a relativistic compact object is a broad field. Within the scope of this thesis, it was not possible to capture all of its aspects. There are more effects which should be further included in the description, such as absorption or scattering by the medium and the presence of a magnetic field generated by the plasma. While a proper analysis of some of them lies beyond the geometrical optics approximation, others should be more straightforward to explore in future studies.

Although the presented results may appear to be simple in some sense, a basic understanding of the problems outlined here can still be very valuable. Particularly desirable is the distinction between the effects caused by the medium and those due to gravity. Several additional findings have been already obtained in this regard, and prospective astrophysical applications are among the topics that are next in line.

Bibliography

A. B. Aazami, C. R. Keeton, and A. O. Petters. Lensing by Kerr black holes. II: Analytical study of quasi-equatorial lensing observables. *J. Math. Phys.*, 52 (10), 2011.

A. M. Anile and P. Pantano. Foundation of geometrical optics in general relativistic dispersive media. *J. Math. Phys.*, 20(1):177–183, 1979.

J. Badía and E. F. Eiroa. Shadows of rotating Einstein-Maxwell-dilaton black holes surrounded by a plasma. *Phys. Rev. D*, 107(12):124028, 2023.

V. Balek, B. Bezděková, and J. Bičák. Radiation in the black hole-plasma system: propagation in equatorial plane. *arXiv:2312.04451*, 2023. (submitted to J. Math. Phys.).

B. Bezděková and J. Bičák. Light deflection in plasma in the Hartle-Thorne metric and in other axisymmetric spacetimes with a quadrupole moment. *Phys. Rev. D*, 108(8):084043, 2023.

B. Bezděková, V. Perlick, and J. Bičák. Light propagation in a plasma on an axially symmetric and stationary spacetime: Separability of the Hamilton–Jacobi equation and shadow. *J. Math. Phys.*, 63(9):092501, 2022.

B. Bezděková, O. Yu. Tsupko, and C. Pfeifer. Deflection of light rays in a moving medium around a spherically symmetric gravitating object. *arXiv:2403.16842*, 2024. (accepted to Phys. Rev. D).

G. S. Bisnovatyi-Kogan and O. Yu. Tsupko. Gravitational radiospectrometer. *Gravit. Cosmol.*, 15(1):20–27, 2009.

G. S. Bisnovatyi-Kogan and O. Yu. Tsupko. Gravitational lensing in a non-uniform plasma. *Mon. Not. R. Astron. Soc.*, 404(4):1790–1800, 2010.

G. S. Bisnovatyi-Kogan and O. Yu. Tsupko. Time delay induced by plasma in strong lens systems. *Mon. Not. R. Astron. Soc.*, 524(2):3060–3067, 2023.

J. Bičák and P. Hadrava. General-relativistic radiative transfer theory in refractive and dispersive media. *Astron. Astrophys.*, 44:389–399, 1975.

J. Bičák and Z. Stuchlík. The fall of the shell of dust on to a rotating black hole. *Mon. Not. R. Astron. Soc.*, 175(2):381–393, 1976.

W. B. Bonnor. Static magnetic fields in general relativity. volume 67, page 225. IOP Publishing, 1954.

R. A. Breuer and J. Ehlers. Propagation of high-frequency electromagnetic waves through a magnetized plasma in curved space-time. I. *Proc. R. Soc. A: Math. Phys. Eng. Sci.*, 370(1742):389–406, 1980.

R. A. Breuer and J. Ehlers. Propagation of high-frequency electromagnetic waves through a magnetized plasma in curved space-time. II. Application of the asymptotic approximation. *Proc. R. Soc. A: Math. Phys. Eng. Sci.*, 374(1756): 65–86, 1981.

G. Briozzo and E. Gallo. Analytical expressions for pulse profile of neutron stars in plasma environments. *Eur. Phys. J. C*, 83(2):165, 2023.

G. Briozzo, E. Gallo, and T. Mädler. Shadows of rotating black holes in plasma environments with aberration effects. *Phys. Rev. D*, 107(12):124004, 2023.

A. Broderick and R. Blandford. Covariant magnetoionic theory—I. ray propagation. *Mon. Not. R. Astron. Soc.*, 342(4):1280–1290, 2003.

B. Carter. Global structure of the Kerr family of gravitational fields. *Phys. Rev.*, 174(5):1559, 1968.

G. Crisnejo, E. Gallo, and K. Jusufi. Higher order corrections to deflection angle of massive particles and light rays in plasma media for stationary spacetimes using the Gauss-Bonnet theorem. *Phys. Rev. D*, 100(10):104045, 2019.

X. Er and S. Mao. Effects of plasma on gravitational lensing. *Mon. Not. R. Astron. Soc.*, 437(3):2180–2186, 2014.

X. Er and S. Mao. The effects of plasma on the magnification and time delay of strongly lensed fast radio bursts. *Mon. Not. R. Astron. Soc.*, 516(2):2218–2222, 2022.

F. J. Ernst. Black holes in a magnetic universe. *J. Math. Phys.*, 17(1):54–56, 1976.

F. J. Ernst and W. J. Wild. Kerr black holes in a magnetic universe. *J. Math. Phys.*, 17:182, 1976.

K. Glampedakis and S. Babak. Mapping spacetimes with LISA: inspiral of a test body in a 'quasi-Kerr'field. *Class. Quantum Grav.*, 23(12):4167, 2006.

J. B. Hartle and K. S. Thorne. Slowly rotating relativistic stars. II. Models for neutron stars and supermassive stars. *Astrophys. J.*, 153:807, 1968.

S. U. Islam and S. G. Ghosh. Strong field gravitational lensing by hairy Kerr black holes. *Phys. Rev. D*, 103(12):124052, 2021.

S. V. Iyer and E. C. Hansen. Strong and weak deflection of light in the equatorial plane of a Kerr black hole. *arXiv preprint arXiv:0908.0085*, 2009.

T. Kimpson, K. Wu, and S. Zane. Spatial dispersion of light rays propagating through a plasma in Kerr space–time. *Mon. Not. R. Astron. Soc.*, 484(2): 2411–2419, 2019a.

T. Kimpson, K. Wu, and S. Zane. Pulsar timing in extreme mass ratio binaries: a general relativistic approach. *Mon. Not. R. Astron. Soc.*, 486(1):360–377, 2019b.

K. Kobialko, I. Bogush, and D. Gal'tsov. Black hole shadows of massive particles and photons in plasma. *Phys. Rev. D*, 109(2):024060, 2024.

R. Kulsrud and A. Loeb. Dynamics and gravitational interaction of waves in nonuniform media. *Phys. Rev. D*, 45(2):525–531, 1992. doi: 10.1103/PhysRevD.45.525.

D. Läänemets, M. Hohmann, and C. Pfeifer. Observables from spherically symmetric modified dispersion relations. *Int. J. Geom. Methods Mod. Phys.*, 19 (10):2250155, 2022.

H. Lima Jr., P. Cunha, C. Herdeiro, and L. Crispino. Shadows and lensing of black holes immersed in strong magnetic fields. *Phys. Rev. D*, 104(4):044018, 2021.

C.-Q. Liu, C.-K. Ding, and J.-L. Jing. Effects of homogeneous plasma on strong gravitational lensing of Kerr black holes. *Chin. Phys. Lett.*, 34(9):090401, 2017.

K. Matsuno. Light deflection by squashed Kaluza-Klein black holes in a plasma medium. *Phys. Rev. D*, 103(4):044008, 2021.

M. A. Melvin. Pure magnetic and electric geons. *Phys. Lett.*, 8(1):65–68, 1964.

M. A. Melvin and J. S. Wallingford. Orbits in a magnetic universe. *J. Math. Phys.*, 7(2):333–340, 1966.

Ch. W. Misner, K. S. Thorne, and J. A. Wheeler. *Gravitation*. Macmillan, XXX, 1973.

V. S. Morozova, B. J. Ahmedov, and A. A. Tursunov. Gravitational lensing by a rotating massive object in a plasma. *Astrophys. Space Sci.*, 346(2):513–520, 2013.

P. G. Nedkova, V. K. Tinchev, and S. S. Yazadjiev. Shadow of a rotating traversable wormhole. *Phys. Rev. D*, 88(12):124019, 2013.

V. Perlick. *Ray optics, Fermat's principle, and applications to general relativity*, volume 61. Springer Science & Business Media, 2000.

V. Perlick and O. Yu. Tsupko. Light propagation in a plasma on Kerr spacetime: Separation of the Hamilton-Jacobi equation and calculation of the shadow. *Phys. Rev. D*, 95(10):104003, 2017.

V. Perlick and O. Yu. Tsupko. Calculating black hole shadows: Review of analytical studies. *Phys. Rep.*, 947:1–39, 2022.

V. Perlick and O. Yu. Tsupko. Light propagation in a plasma on Kerr spacetime. II. Plasma imprint on photon orbits. *Phys. Rev. D*, 109(6):064063, 2024.

V. Perlick, O. Yu. Tsupko, and G. S. Bisnovatyi-Kogan. Influence of a plasma on the shadow of a spherically symmetric black hole. *Phys. Rev. D*, 92(10): 104031, 2015.

A. Rogers. Frequency-dependent effects of gravitational lensing within plasma. *Mon. Notices Royal Astron. Soc.*, 451(1):17–25, 2015.

A. Rogers. Escape and trapping of low-frequency gravitationally lensed rays by compact objects within plasma. *Mon. Notices Royal Astron. Soc.*, 465:2151–2159, 2017a.

A. Rogers. Gravitational lensing of rays through the levitating atmospheres of compact objects. *Universe*, 3(1):3, 2017b.

M. Sárený and V. Balek. Effect of black hole–plasma system on light beams. *Gen. Relativ. Gravit.*, 51(11):141, 2019.

P. Schneider, J. Ehlers, and E. E. Falco. *Gravitational Lenses*. Springer, Berlin, 1992.

K. Schulze-Koops, V. Perlick, and D. J. Schwarz. Sachs equations for light bundles in a cold plasma. *Class. Quantum Grav.*, 34(21):215006, 2017.

J. Sun, X. Er, and O. Yu. Tsupko. Binary microlensing with plasma environment – star and planet. *Mon. Not. R. Astron. Soc.*, 520(1):994–1004, 2023.

J. L. Synge. *Relativity: The General Theory*. North-Holland Publishing Company, Amsterdam, 1960.

E. Teo. Rotating traversable wormholes. *Phys. Rev. D*, 58(2):024014, 1998.

O. Yu. Tsupko. Deflection of light rays by a spherically symmetric black hole in a dispersive medium. *Phys. Rev. D*, 103(10):104019, 2021.

O. Yu. Tsupko and G. S. Bisnovatyi-Kogan. Gravitational lensing in plasma: Relativistic images at homogeneous plasma. *Phys. Rev. D*, 87(12):124009, 2013.

O. Yu. Tsupko and G. S. Bisnovatyi-Kogan. Hills and holes in the microlensing light curve due to plasma environment around gravitational lens. *Mon. Not. R. Astron. Soc.*, 491(4):5636–5649, 2020.

M. Wang, S. Chen, and J. Jing. Kerr black hole shadows in Melvin magnetic field with stable photon orbits. *Phys. Rev. D*, 104(8):084021, 2021.

Z. Zhang, H. Yan, M. Guo, and B. Chen. Shadows of Kerr black holes with a Gaussian-distributed plasma in the polar direction. *Phys. Rev. D*, 107(2): 024027, 2023.

Publications related to the thesis topic

A1 B. Bezděková, J. Bičák, and V. Balek. On the Light Rays Propagating in Plasma Medium Around Relativistic Objects, in *WDS'21 Proceedings of Contributed Papers — Physics* (eds. J. Šafránková and J. Pavlů), Prague, Matfyzpress, pp. 13–20, 2021.

A2 B. Bezděková, V. Perlick, and J. Bičák. Light propagation in a plasma on an axially symmetric and stationary spacetime: Separability of the Hamilton–Jacobi equation and shadow. *J. Math. Phys.*, 63(9):092501, 2022.

A3 B. Bezděková and J. Bičák. Light deflection in plasma in the Hartle-Thorne metric and in other axisymmetric spacetimes with a quadrupole moment. *Phys. Rev. D*, 108(8):084043, 2023.

A4 V. Balek, B. Bezděková, and J. Bičák. Radiation in the black hole–plasma system: propagation in equatorial plane, arXiv: 2312.04451, 2023 *(submitted to J. Math. Phys.)*.

A5 B. Bezděková, O. Tsupko, and C. Pfeifer. Deflection of light rays in a moving medium around a spherically symmetric gravitating object. arXiv: 2403.16842, 2024 *(accepted to Phys. Rev. D)*.

Other publications in journals with impact factor

B1 B. Bezděková, F. Němec, M. Parrot, O. Santolík, and O. Kruparova. Magnetospheric Line Radiation: 6.5 Years of Observations by the DEMETER Spacecraft. *J. Geophys. Res. Space Phys.*, 120(11), 9442–9456, 2015.

B2 F. Němec, B. Bezděková, J. Manninen, M. Parrot, O. Santolík, M. Hayosh, and T. Turunen. Conjugate Observations of a Remarkable Quasiperiodic Event by the Low-Altitude DEMETER Spacecraft and Ground-Based Instruments. *J. Geophys. Res. Space Phys.*, 121(9), 8790–8803, 2016.

B3 F. Němec, G. B. Hospodarsky, B. Bezděková, A. G. Demekhov, D. L. Pasmanik, O. Santolík, W. S. Kurth, and C. Kletzing. Quasiperiodic Whistler Mode Emissions Observed by the Van Allen Probes Spacecraft. *J. Geophys. Res. Space Phys.*, 123(11), 8969–8982, 2018.

B4 B. Bezděková, F. Němec, M. Parrot, M. Hajoš, J. Záhlava, and O. Santolík. Dependence of Properties of Magnetospheric Line Radiation and Quasiperiodic Emissions on Solar Wind Parameters and Geomagnetic Activity. *J. Geophys. Res. Space Phys.*, 124(4), 2552–2568, 2019.

B5 B. Bezděková, F. Němec, J. Manninen, G. B. Hospodarsky, O. Santolík, W. S. Kurth, and D. P. Hartley. Conjugate Observations of Quasiperiodic Emissions by the Van Allen Probes Spacecraft and Ground-Based Station Kannuslehto. *J. Geophys. Res. Space Phys.*, 125(6), e2020JA027793, 2020.

B6 B. Bezděková, F. Němec, M. Parrot, O. Kruparova, and V. Krupar. Using Principal Component Analysis to Characterize the Variability of VLF Wave Intensities Measured by a Low-Altitude Spacecraft and Caused by Interplanetary Shocks. *J. Geophys. Res. Space Phys.*, 126(5), e2021JA029158, 2021.

B7 B. Bezděková, F. Němec, and J. Manninen. Ground-Based VLF Wave Intensity Variations Investigated by the Principal Component Analysis. *Earth Planets Space*, 74(30), 2022.

B8 B. Bezděková, F. Němec, J. Manninen, O. Santolík, G. B. Hospodarsky, and W. S. Kurth. Very low frequency whistler mode wave events observed simultaneously by the Kannuslehto station and Van Allen Probes. *J. Geophys. Res. Space Phys.*, 128, e2022JA031078, 2023.

B9 M. Hajoš, F. Němec, A. G. Demekhov, O. Santolík, M. Parrot, T. Raita, and B. Bezděková. Quasiperiodic ELF/VLF Emissions Associated With Corresponding Pulsations of Geomagnetic Field. *J. Geophys. Res. Space Physics*, 128, e2022JA031103, 2023.